2002-03

Development of a Nakagami-Lognormal Model for a cellular CDMA forward

Karagiannis, Ioannis

Monterey, Calif. Naval Postgraduate School

NAVAL POSTGRADUATE SCHOOL
Monterey, California

THESIS

DEVELOPMENT OF A NAKAGAMI-LOGNORMAL MODEL FOR A CELLULAR CDMA FORWARD CHANNEL

by

Ioannis Karagiannis

March 2002

Thesis Advisor:	Tri T. Ha
Thesis Co-Advisor:	Jan E. Tighe
Second Reader:	David C. Jenn
Third Reader:	Jovan Lebaric

Approved for public release; distribution is unlimited

REPORT DOCUMENTATION PAGE			Form Approved OMB No. 0704-0188
Public reporting burden for this collection of information is estimated to average 1 hour per response, including the time for reviewing instruction, searching existing data sources, gathering and maintaining the data needed, and completing and reviewing the collection of information. Send comments regarding this burden estimate or any other aspect of this collection of information, including suggestions for reducing this burden, to Washington headquarters Services, Directorate for Information Operations and Reports, 1215 Jefferson Davis Highway, Suite 1204, Arlington, VA 22202-4302, and to the Office of Management and Budget, Paperwork Reduction Project (0704-0188) Washington DC 20503.			
1. AGENCY USE ONLY ***(Leave blank)***	**2. REPORT DATE** March 2002	**3. REPORT TYPE AND DATES COVERED** Master's Thesis	
4. TITLE AND SUBTITLE: Development of a Nakagami-Lognormal Model for a Cellular CDMA Forward Channel			**5. FUNDING NUMBERS**
6. AUTHOR(S) Ioannis Karagiannis			
7. PERFORMING ORGANIZATION NAME(S) AND ADDRESS(ES) Naval Postgraduate School Monterey, CA 93943-5000			**8. PERFORMING ORGANIZATION REPORT NUMBER**
9. SPONSORING / MONITORING AGENCY NAME(S) AND ADDRESS(ES) N/A			**10. SPONSORING / MONITORING AGENCY REPORT NUMBER**
11. SUPPLEMENTARY NOTES The views expressed in this thesis are those of the author and do not reflect the official policy or position of the Department of Defense or the U.S. Government.			
12a. DISTRIBUTION / AVAILABILITY STATEMENT Approved for public release; distribution is unlimited			**12b. DISTRIBUTION CODE**

13. ABSTRACT ***(maximum 200 words)***

In this thesis, the performance of the forward channel of a DS-CDMA cellular system operating in a Nakagami-fading, Lognormal-shadowing environment is analyzed. Given the upper bound of bit error probability with FEC and including all the appropriate losses and interference terms, the bit error probability in various fading and Lognormal shadowing conditions is computed in two ways; firstly, by setting up a statistical model and secondly, by Monte Carlo simulations. The results predicted by the two methods take into account that the intended user is located at the corner of the hexagon of a seven-cell structure (worst case scenario). Furthermore, in order to obtain more realistic and accurate results, the user's distribution is incorporated in the cell and finally fast power control is applied to overcome the Lognormal shadowing effects.

14. SUBJECT TERMS Nakagami Fading, Lognormal Shadowing, CDMA, Forward Channel Model, Wireless, Performance Analysis, Antenna Sectoring, Sum Distribution, Power Control.			**15. NUMBER OF PAGES** 156
			16. PRICE CODE
17. SECURITY CLASSIFICATION OF REPORT Unclassified	**18. SECURITY CLASSIFICATION OF THIS PAGE** Unclassified	**19. SECURITY CLASSIFICATION OF ABSTRACT** Unclassified	**20. LIMITATION OF ABSTRACT** UL

NSN 7540-01-280-5500 Standard Form 298 (Rev. 2-89)
Prescribed by ANSI Std. 239-18

THIS PAGE INTENTIONALLY LEFT BLANK

Approved for public release; distribution is unlimited

DEVELOPMENT OF A NAKAGAMI-LOGNORMAL MODEL FOR A CELLULAR CDMA FORWARD CHANNEL

Ioannis Karagiannis
Lieutenant, Hellenic Navy
B.S., Hellenic Naval Academy, 1993

Submitted in partial fulfillment of the
requirements for the degrees of

MASTER OF SCIENCE IN ELECTRICAL ENGINEERING
and
MASTER OF SCIENCE IN SYSTEMS ENGINEERING

from the

NAVAL POSTGRADUATE SCHOOL
March 2002

Author: Ioannis Karagiannis

Approved by:
Tri T. Ha
Thesis Advisor

Jan E. Tighe
Thesis Co-Advisor

David C. Jenn
Second Reader

Jovan Lebaric
Third Reader

Dan C. Boger
Chairman, Department of Information Sciences

Jeffrey B. Knorr
Chairman, Department of Electrical and Computer Engineering

THIS PAGE INTENTIONALLY LEFT BLANK

ABSTRACT

In this thesis, the performance of the forward channel of a DS-CDMA cellular system operating in a Nakagami-fading, Lognormal-shadowing environment is analyzed. Given the upper bound of bit error probability with FEC and including all the appropriate losses and interference terms, the bit error probability in various fading and Lognormal shadowing conditions is computed in two ways; firstly, by setting up a statistical model and secondly, by Monte Carlo simulations. The results predicted by the two methods take into account that the intended user is located at the corner of the hexagon of a seven-cell structure (worst case scenario). Furthermore, in order to obtain more realistic and accurate results, the user's distribution is incorporated in the cell and finally fast power control is applied to overcome the Lognormal shadowing effects.

THIS PAGE INTENTIONALLY LEFT BLANK

TABLE OF CONTENTS

LIST OF FIGURES

LIST OF TABLES

THIS PAGE INTENTIONALLY LEFT BLANK

ACKNOWLEDGMENTS

I would like to thank all my thesis advisors for their help in finishing this thesis, especially Professor Tri Ha and Commander Jan Tighe for their valuable contribution and encouragement during my research. I really appreciate Commander Jan Tighe's guidance. Her presence here at NPS during my research was very critical to my success. Finally I would like to thank my wife Eirini Leivadarou for her support during the time at NPS, my parents, my in-laws, and my brother.

THIS PAGE INTENTIONALLY LEFT BLANK

EXECUTIVE SUMMARY

The increasing demand for multimedia interactive services and great mobility led the various communications industries to develop the third generation of service (3G). While the existing second-generation system was originally designed for voice transmissions only, the third generation supports numerous high data rate applications such as full wireless Internet access. The second-generation system can reach up to 10 kbps while the third generation can reach up to 2 mbps. In addition, the third generation wireless system guarantees 144 kbps for faster moving users. The existing systems use different multiple techniques like Time Division Multiple Access (TDMA) and Frequency Division Multiple Access (FDMA), which are bandwidth limited. The next generation of wireless systems (3G) uses Wideband Code Division Multiple Access (W-CDMA). Thus, the system capacity is increased many times compared to the existing systems. This type of multiple access is interference limited. For this reason, W-CDMA systems have to use different types of techniques to overcome intracell and intercell interference as well as the additive white Gaussian noise (AWGN).

Accordingly, a forward channel for a DS-CDMA cellular system is created. The information signal is developed which propagates through the communication channel. The extended Hata model is being used in order to compute the large-scale path loss. Furthermore, since the transmitting signal propagates through different types of terrains, the Nakagami random variable is introduced in order to incorporate small-scale fading conditions. Fluctuations to the received power at points, which have the same distance from the transmitter, are considered also by the use of Lognormal Shadowing. Taking into account all these propagation effects to the information signal, the result is the received signal to the intended mobile user's receiver.

First, the intended user is placed at the corner of the hexagon of the center cell of a seven-cell structure, which is the worst-case scenario. Given an upper bound on the probability of bit error using Forward Error Correction (FEC), the performance of the cellular system is analyzed. A statistical model is created in order to approximate the

sum of d multiplicative Nakagami-square-Lognormal random variables as a multiplicative Nakagami-square-Lognormal random variable. Our model is being tested in different fading and shadowing conditions. Modeled results are compared with those predicted by Monte Carlo simulations.

In order to implement more realistic and accurate results, the user's distribution is incorporated in the cell rather than placing the user at the corner of the hexagon which is the worst-case scenario. Furthermore, fast power control is incorporated in order for the received power by the mobile user to be at a target level and thus eliminating the effect of Lognormal Shadowing.

I. INTRODUCTION

A. BACKGROUND

The increasing demand for multimedia and interactive services led the various communications industries to develop the third generation of service (3G). The existing second-generation system is widely being used mainly for voice transmissions supporting data rates up to 10 kbps. However, many applications like full wireless Internet access demand much higher data rates. The third generation of service can achieve data rates up to 2 mbps and for faster users, up to 144 kbps. This new system employs Code Division Multiple Access (CDMA) and thus is able to increase the system capacity many times compared to the present systems. Japan is the first country in the world, which already uses this new type of wireless communications. Europe and the United States is expected to implement this new technique in 2002, and 2004 respectively.

B. OBJECTIVE

Code division multiple access systems are interference limited. On the other hand, Frequency Division Multiple Access (FDMA) and Time Division Multiple Access (TDMA) systems are bandwidth limited systems. While the transmitted signal from the base station propagates through our communication channel, it is being largely affected by interference as well as by the Additive White Gaussian Noise (AWGN). In addition, and since the signal propagates through different types of terrain, it is undergoing a slow flat fading type. A more general type of fading is Nakagami fading. By varying the Nakagami-*m* parameter, several types of fading such as one-sided Gaussian, Rayleigh and Ricean can be implemented. However, different points located at the same distance from the transmitting base station have vastly different path loss. This phenomenon is called Lognormal Shadowing. Taking into account all the aforementioned facts, the performance of a direct sequence CDMA six-sectored cellular system in a Nakagami fading and Lognormal Shadowing environment is analyzed by computing an upper bound

on the probability of bit error with the use of a statistical model and Monte Carlo simulations. Additionally, by complementing different techniques such as user distribution and fast power control, the performance of the system is enhanced.

C. RELATED WORK

A lot of research on the DS-CDMA channel is on the reverse link, which is in general, different from the forward link. A very analytical work of a DS-CDMA forward channel has been developed in [1]. The analysis in [1] is concerned with Rayleigh fading instead of Nakagami fading. However, many of the concepts are the same, and are very useful for the analysis in this thesis. Furthermore, [2] optimizes power using pilot tone power control in a Rayleigh-Lognormal forward channel.

In summary, it can be concluded that a more general analysis of Nakagami fading including and extending previous research needs to be accomplished.

D. THESIS OUTLINE

In Chapter II, a forward channel for the DS-CDMA cellular system is created. By taking into account all the appropriate losses, interferences and phenomena such as fading and Lognormal Shadowing, the result was a closed formula for the received signal to the intended user.

In Chapter III, the intended user was located in the least optimum position within the center cell, and given the expression for the upper bound on the probability of bit error with the use of Forward Error Correction (FEC) in the form of convolutional encoding with soft-decision decoding, the performance of the cellular system is analyzed. This analysis creates a statistical model in order to approximate the sum of d multiplicative Nakagami-square-Lognormal random variables as a multiplicative Nakagami-square-Lognormal random variable. The model is being tested in various fading and shadowing environments and the Nakagami-m parameter is varied. The

modeled results are compared with the results predicted by 95,000 Monte Carlo trials. The values of the Nakagami-*m* parameter used are: $m = 0.5$, $m = 0.75$, $m = 1$, $m = 1.5$ and $m = 2$.

In Chapter IV, the performance analysis completed in Chapter III is modified by incorporating user distribution within the cell for more realistic results. Furthermore, fast power control is implemented in order to enhance system performance. The analysis is done in different fading environments by varying the Nakagami-*m* parameter.

Finally, in Chapter V, the conclusions are summarized and areas for further research are discussed.

THIS PAGE INTENTIONALLY LEFT BLANK

II. FORWARD CHANNEL MODEL

The forward channel in a Direct Sequence Code Division Multiple Access cellular system is the communication channel, which carries traffic from the base station to mobile users. The reverse channel carries traffic from mobile users to the base station.

In this chapter, a channel model for a DS-CDMA cellular system including fading and shadowing effects will be built. It is known that a mobile user is often surrounded by various obstacles such as buildings, trees and mountains. These cause the presence of phenomena like reflection, diffraction and scattering of the forward transmitted signal from the base station.

The average signal power that a mobile user receives depends on the distance between the transmitting base station and the mobile user, as well as on the type of environment between them [3]. The transmitted base station forward signal arrives at the mobile user's receiver via many paths with different lengths and with various signal powers. The sum of the multiple signals, arriving at the mobile receiver leads to a signal that fluctuates very fast as the mobile and/or environment move(s). Such signal fluctuations are known as fading [4]. The fluctuations that occur over sub-wave lengths scale are known as fast fading or small-scale fading and those occurring over several wavelengths are known as slow fading or large-scale fading [4]. Some large scale and small-scale propagation models, which are used in order to determine the average signal power received, will be discussed later in this chapter.

A. DS-CDMA FORWARD SIGNAL

A basic seven-cell cluster as shown in Figure 2.1 will be used for our analysis. Each cell is represented by a hexagon whose center is the position where the base station of each cell is located. The center cell is the main interest. Let K represent the total number of mobile users or active channels in the center cell, while K_i is the total number of mobile users or active channels in the adjacent cells $i = 1,2\ldots6$.

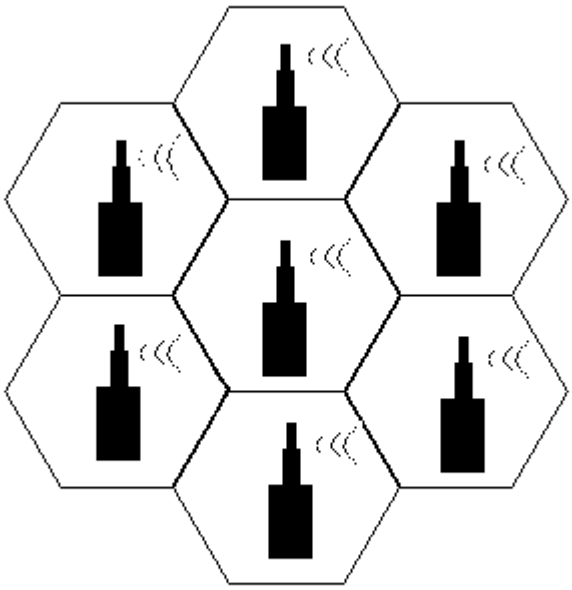

Figure 2.1. Seven -Cell Cluster.

$S_0(t)$ represents the transmitted signal by the base station in each cell which includes the traffic for all active channels in the cell. Due to the DS technique, the power spectrum of these signals has been spread by a factor of *N*. In this analysis, the type of modulation used is BPSK. Suppose that there is a user located at the center cell of Figure 2.1. This mobile user will receive traffic that is intended for other users in his cell, or in our case, the center cell of Figure 2.1. This type of traffic is called intracell interference. In addition to the previous traffic, our user will receive signals $S_i(t)$ transmitted by the base stations of the six adjacent cells. This type of interference is called intercell interference, or co-channel interference.

1. Walsh Functions

Walsh functions are used in DS-CDMA cellular systems in order to spread the traffic over a finite bandwidth and eliminate intracell interference. In the forward link,

the traffic is multiplied with distinct repeating Walsh sequences that are assigned to each channel for the duration of the call. The Walsh sequences (functions) are mutually orthogonal. In that way, in the despreading process, the mobile's user receiver is applying his own unique Walsh function and despreads only the traffic intended for him. All the other traffic from the same cell at the specific receiver goes to zero. However, some intercell interference still occurs due to that fact that multipath and signals from other cells that are not time-aligned with the desired signal are present. To reduce this type of interference, a PN sequence modulation process is used. Thus, it can be stated that the multiple access scheme for the forward link in a DS-CDMA system incorporated the use of orthogonal Walsh sequences (functions) and PN sequences of different purposes.

The Walsh functions of order N can be defined as a set of N time functions as follows: $\{W_j(t);\ t \in (0,T),\ j = 0,1...,N-1\}$ where $W_j(t) \in \{+1,-1\}$, except at the jumping points, where it equals to zero. The quantity $W_j(0) = 1$ for all j while $W_j(t)$ has exactly j sign alternations in the interval $(0,T)$ [5]

$$\int_0^T W_j(t)W_k(t)dt = \begin{cases} 0, & if\ j \neq k \\ T, & if\ j = k \end{cases}$$

In Figure 2.2, a set of Walsh functions of order eight are shown.

$$W_8 = \begin{bmatrix} +1 & +1 & +1 & +1 & +1 & +1 & +1 & +1 \\ +1 & +1 & +1 & +1 & -1 & -1 & -1 & -1 \\ +1 & +1 & -1 & -1 & -1 & -1 & +1 & +1 \\ +1 & +1 & -1 & -1 & +1 & +1 & -1 & -1 \\ +1 & -1 & -1 & +1 & +1 & -1 & -1 & +1 \\ +1 & -1 & -1 & +1 & -1 & +1 & +1 & -1 \\ +1 & -1 & +1 & -1 & -1 & +1 & -1 & +1 \\ +1 & -1 & +1 & -1 & +1 & -1 & +1 & -1 \end{bmatrix}$$

Figure 2.2. Walsh Functions of Order 8.

It is now possible to convert the ± 1 amplitudes of the Walsh functions to a binary logic $\{0,1\}$ representation with the following conversions $+1 \rightarrow "0"$ and $-1 \rightarrow "1"$ [5].

Thus, Table 2.1 is created.

Index integer j	Index sequence	Walsh sequences Of order 8
0	000	$W_0 = 00000000$
1	001	$W_1 = 00001111$
2	010	$W_2 = 00111100$
3	011	$W_3 = 00110011$
4	100	$W_4 = 01100110$
5	101	$W_5 = 01101001$
6	110	$W_6 = 01011010$
7	111	$W_7 = 01010101$

Table 2.1. The Walsh Sequences of Order 8 from [5].

There are many ways that Walsh functions can be generated such as using Rademacher functions and Hadamard matrices.

2. Direct Sequence Spread Spectrum CDMA

A DS-Spread Spectrum technique is used in order to spread the power spectrum of a base band signal over a specified transmission bandwidth [1]. DSSS systems are useful in military applications where a low probability of intercept (LPI), low probability of detection (LPD) and anti-jam protection are required [5]. In third generation cellular systems, DSSS can be used for multiple access applications. Given a finite bandwidth,

each base station located in each cell has to use its own PN spreading signal and Walsh functions for orthogonal covering. Now the mobile receiver despreads only the traffic intended for him using the cell's PN signal and his unique Walsh function.

In order to generate a DSSS signal, it is necessary to multiply the information signal by a spreading signal. Let, as in [1], $b_k(t)$ represents the information signal intended for mobile user k where, $b_k(t) \in \{\pm 1\}\ \boldsymbol{n}T \le t \le (\boldsymbol{n}+1)T$ for $\boldsymbol{n}$ = 0,1,2… with a bit interval T. Each data bit is spread by a factor of N using a spreading signal with chip duration $T_c = \frac{T}{N}$ for all users.

PN sequences are generated from linear feedback shift registers. PN sequences and Walsh functions are used to spread the data signal. Walsh functions eliminate the intracell interference while PN sequences, to a lesser degree, combat the intercell interference. As stated in [1], the application of Walsh function $W_j(t) \in W_N$ alone does not guarantee a spreading factor of N. The PN signal in the center cell is represented as $c(t)$ while PN signals of the adjacent cells are represented as $c_i(t)$ for i = 1,2,…6. Assume that a user is in the center cell. In order for this user to correctly receive the data intended for him, his receiver chipping signal has to be synchronized with the chipping signal $c(t)$ of his cell base station. Since this mobile user, who is in the center cell, is not synchronized with base stations in adjacent cells, the inter-cell traffic remains spread over the bandwidth and minimizes its effect in SNR.

3. Transmitted Signal, *S(t)*

Following the assumption in [1], we get:

k = the mobile user or channel k in the center cell

$b_k(t)$ = the information signal consisting of binary data stream for the k-th user channel in the center cell

$P_{t,k}$ = the average transmit power in the k-th channel

$W_k(t)$ = the Walsh function of the *k*-th user channel in the center cell

$c(t)$ = PN spreading signal for the center cell

f_c = the carrier frequency of the signal

Then, the transmitted signal $S_0(t)$ from the base station of the center cell is given by [1] as follows:

$$S_0(t) = \sum_{k=0}^{K-1} \sqrt{2P_{t,k}} b_k(t) W_k(t) c(t) \cos(2\pi f_c t) \tag{2.1}$$

where *K* is the number of active channels in the center cell.

B. PROPAGATION IN THE MOBILE RADIO CHANNEL

As the transmitted signal travels from the base station to the mobile users it looses power as a function of the distance and the type of environment. This loss in signal power is called path loss, which is represented as *L* in dB.

Propagation measurements in a mobile radio channel have shown that the average received signal power P_r at a distance ***d*** from the transmitter is given as follows:

$$P_r = P_0 \left(\frac{\boldsymbol{d}}{d_0} \right)^{-n} \tag{2.2}$$

where P_0 is a reference power received at distance d_0 from the transmitter, and *n* is the path loss exponent [3]. Table 2.2 shows some values of *n* in different environments.

Environment	**Path Loss Exponent,** n
Free space	2
Urban area cellular radio	2.7 to 3.5
Shadowed urban cellular radio	3 to 5
In building line-of-sight	1.6 to 1.8
Obstructed in building	4 to 6
Obstructed in factories	2 to 3

Table 2.2. Path Loss Exponents in Different Environments from [3].

1. Free Space Propagation Model

The same symbols as in [1] will be used:

P_{fr} = the free space power received

P_t = the transmitted power

G_t = the transmitter antenna gain

G_r = the receiver antenna gain

λ_c = the wavelength of the carrier, $\lambda_c = \frac{c}{f_c}$

$\boldsymbol{d}$ = the separation distance between transmitter and receiver

L_s = the system (hardware) loss factor

f_c = the carrier frequency

Assume for simplicity that $G_t = G_r = L_s = 1$. As seen from Table 2.2 for free space, $n = 2$. Thus, using Equation (2.2) with $n = 2$, it is then possible to calculate P_{fr}

$$P_{fr}(\boldsymbol{d}) = P_{fr}(d_0)\left(\frac{d_0}{\boldsymbol{d}}\right)^2,\ d_0 \le \boldsymbol{d} \tag{2.3}$$

where $P_{fr}(d_0)$ is the free space reference power which can be measured or calculated using the Friis free space equation given by

$$P_{fr} = \frac{P_t G_t G_r \lambda_c^{\,2}}{(4\pi)^2 \boldsymbol{d}^2 L_s} \tag{2.4}$$

The free space propagation model is used when there is an unobstructed line-of-sight path between the transmitting and receiving antenna [1]. However, usually in a mobile environment, many times there is no line-of-sight path so the mobile communication channel cannot be characterized by the use only of the free space propagation model. The Hata model is one of the other large-scale propagation model, which is used to calculate the median path loss.

2. The Hata Model

The Hata Model is the analytical expression of the Okumara empirical model, which is one of the most accurate empirical models in cellular communications [3]. The Hata model computes the median path loss in an urban environment and supplies correction equations in order to be applicable to other situations. The extended Hata model can be used for carrier frequencies from 1500 MHz to 2000 MHz. From [1] and [3] it can be seen that

$$L_{HdB} = 46.3 + 33.9\ \log f_c - 13.82\ \log h_{base} - a\left(h_{mobile}\right) + \left(44.9 - 6.55 \log h_{base}\right)\log \boldsymbol{d} \tag{2.5}$$
$$+ C_M$$

$$a(h_{mobile}) = (1.1 \log f_c - 0.7) h_{mobile} - (1.56 \log f_c - 0.8)(\text{dB}) \tag{2.6}$$

$$C_M = \begin{cases} 0 \text{ dB, for medium sized city and suburban areas} \\ 3 \text{ dB, for metropolitan centers} \end{cases} \tag{2.7}$$

where h_{base} and h_{mobile} are the heights of the base station and mobile antennas, f_c the carrier frequency, $\boldsymbol{d}$ is the distance between the base station and the mobile, C_M is an operating area correction factor. Equations (2.5) and (2.6) are valid when the following units for each parameter are used: f_c in MHz, h_{base} and h_{mobile} in meters and $\boldsymbol{d}$ is measured in kilometers (km). The following restrictions apply in the parameters, which are used in the extended Hata Model:

f_c : 1500 MHz to 2000 MHz

h_{base} : 30m to 200m

h_{mobile} : 1m to 10m

$\boldsymbol{d}$: 1km to 20km

The extended Hata Model is used to predict the median path loss because it better matches with the size and frequency ranges of future cellular systems.

3. Lognormal Shadowing

The average path loss is a function of the path loss exponent *n* and is given in dB as follows: $\overline{L}_{ndB}(\boldsymbol{d}) = \overline{L}_{dB}(d_0) + 10n \log\left(\frac{\boldsymbol{d}}{d_0}\right)$ [1]. Taking into account that the surrounding environment may differ a lot at two separate points, which have the same distance $\boldsymbol{d}$ from the transmitter, it can be stated that the previous equation does not predict with accuracy the path loss at these two different points [3]. These differences can be measured in decibels and they can be represented with a Gaussian random variable. Thus, the path loss with shadowing can be defined as:

$$L_{xdB}(\boldsymbol{d}) = L_{dB}(\boldsymbol{d}) + X_{dB} \tag{2.8}$$

where X_{dB} is a Gaussian random variable, $X_{dB} \sim N(0, \sigma_{dB})$ with zero mean, and standard deviation σ_{dB}, and $L_{dB}(\boldsymbol{d})$ the path loss for distance $\boldsymbol{d}$.

Since X_{dB} is a zero mean Gaussian random variable, L_{xdB} is also a Gaussian random variable $L_{xdB} \sim N(L_{dB}, \sigma_{dB})$ where L_{dB} is the mean and the median value since for a Gaussian random variable the mean value equals the median value. Therefore, in our model, the median path loss predicted by the extended Hata Model will be used as follows:

$$L_{xdB} = L_{HdB} + X_{dB} \tag{2.9}$$

The following equations are from [1]:

$$L_{xdB} = 10 \log L_x$$

$$L_{HdB} = 10 \log L_H$$

$$X_{dB} = 10 \log X$$

$$L_x = L_H X$$

where $X \sim \Lambda(0, \lambda\sigma_{dB})$ is a Lognormal random variable which is the conversion of the Gaussian random variable $X_{dB} \sim N(0, \sigma_{dB})$. The parameters of X are $\mu_x = \lambda\mu_{dB} = 0$ and $\sigma_x = \lambda\sigma_{dB}$ where $\lambda = \ell n 10 / 10$ [2]. L_x is also a Lognormal random variable $L_x \sim \Lambda(\lambda L_{HdB}, \lambda\sigma_{dB})$.

It is known that the received power is given by

$$P_r = \frac{P_t G_t G_r}{L\ L_s} = \frac{P_t}{L} \tag{2.10}$$

since $G_t = G_r = L_s = 1$ have been normalized to one.

However, in our model, it will sometimes be necessary to vary the value of P_t. Thus, by using P_t as our main value of transmitting power at most of our channels, we

can define $P_{t,k}$ as the signal power assigned to each channel *k* using a power factor f_k as follows:

$$P_{t,k} = f_k P_t \tag{2.11}$$

Taking into account our Hata-Lognormal model for path loss, $L = L_H X$, the received power in the *k*-th channel can be converted into a random variable P_k as

$$P_k = \frac{f_k P_t}{L_H(\boldsymbol{d}) X} \tag{2.12}$$

where,

f_k = the power factor used to adjust the power in the *k*-th channel

P_t = the baseline signal power

L_H = the median path loss using the Hata Model

X = the Lognormal random variable $\Lambda\left(0, \lambda\sigma_{dB}\right)$

From [1] it is shown that the inverse of a Lognormal random variable is also a Lognormal random variable. Thus, the power received in the *k*-th channel in Equation (2.12) is a Lognormal random variable, $P_k \sim \Lambda\left(\mu_{p_k}, \lambda\sigma_{dB}\right)$ where $\mu_{p_k} = \ell n\left(f_k P_t / L_H\right)$.

The model that was developed in this Section takes into account large-scale propagation losses and Lognormal shadowing.

4. Small-Scale Fading due to Multipath

The signal fluctuations that occur over sub-wavelengths have already been defined and are known as fast fading or small-scale fading [4], due to the multipath reception of a wireless signal. Many signal copies arrive at the receiver at different time intervals because they follow different propagation paths or because in a wireless environment either transmitter or receiver moves with time. This is why there is a Doppler-shift in the frequency of the transmitted signal. The fact that the receiver will or

will not be able to receive correctly each information data bit or symbol depends on the small-scale fading characteristics of the channel and the signal characteristics itself. In [3], a classification of types of small-scale fading occurs due to two independent facts such as multipath delay spread and Doppler spread. Figure 2.3 shows a tree of the four different types of fading [3].

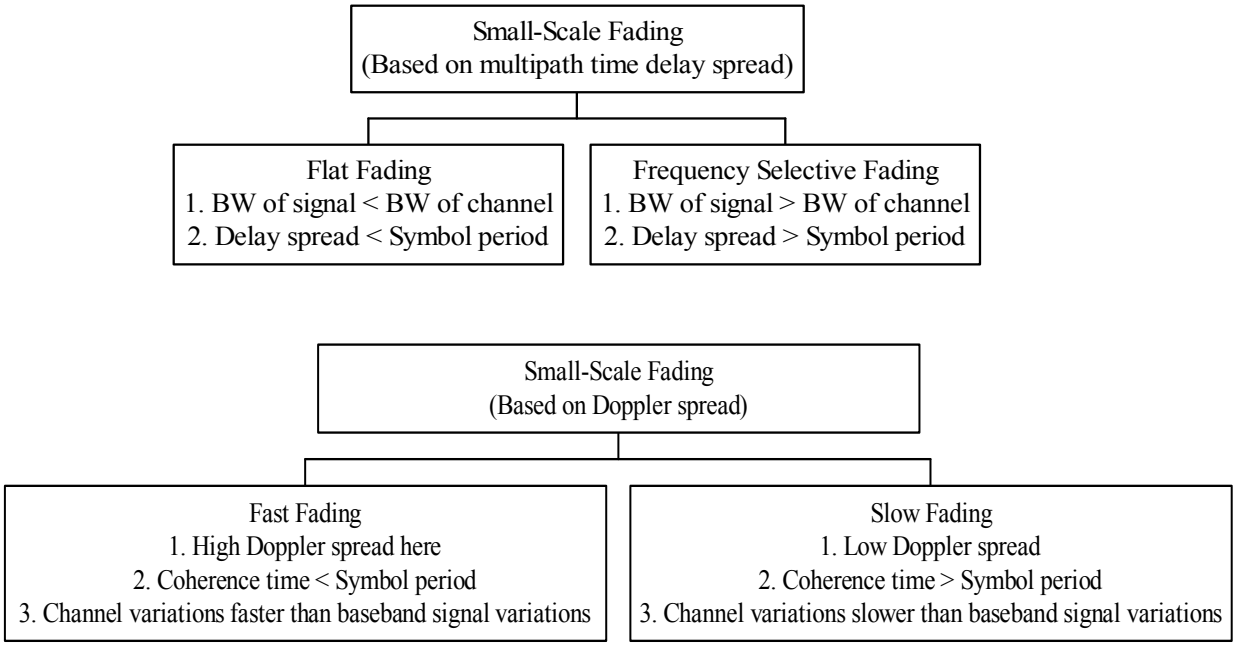

Figure 2.3. Types of Small-Scale Fading from [3].

It can also be mentioned that in reality, fast fading environments have only been observed in communication systems with very low data rates [3]. Since high data rates are going to be used, our model is characterized as slow fading [1]. A general method for modeling the amplitude variations in a flat fading channel is by assuming the amplitudes are distributed as a Nakagami random variable. In the next Section, the effects of large-scale path loss and small scale fading will be taken into account in our channel model and will be defined as the Nakagami-Lognormal channel model.

C. NAKAGAMI-LOGNORMAL CHANNEL MODEL

The Nakagami-Lognormal channel model can be said to be a slow-flat-Nakagami fading channel with Lognormal shadowing and with path loss which are calculated by the extended Hata Model. If the same procedure used in [1] is followed, and the Rayleigh random variable is changed to a Nakagami random variable, we find that in a DS-CDMA cellular system, the received signal by a mobile user in the center cell is given by

$$\begin{aligned} r(t) &= \sum_{k=0}^{k-1} R\sqrt{2P_k}\,b_k(t)W_k(t)c(t)\cos(2\pi f_c t) \\ &+ \sum_{i=1}^{6}\sum_{j=0}^{K_i-1} R_i\sqrt{2P_{ij}}\,b_{ij}\left(t+\tau_i\right)W_{ij}\left(t+\tau_i\right)c_i\left(t+\tau_i\right)\cos\left(2\pi f_c t+\varphi_i\right)+n(t) \end{aligned} \tag{2.13}$$

where as in [1]:

i = the adjacent cells i = 1,2…,6

ij = mobile user or channel j in adjacent cell i

K_i = the number of active channels in adjacent cells i

R_i = Nakagami fading random variable for signals from adjacent cells

P_{ij} = Lognormal random variable representing the average power received from the j-th channel in adjacent cell i

$b_{ij}(t)$ = the information signal for the j-th user channel in adjacent cell i

$W_{ij}(t)$ = Walsh function for the j-th user channel in adjacent cell i

$c_i(t)$ = PN spreading signal for the adjacent cell i

f_c = the carrier frequency of the signal

τ_i = the time delay from adjacent cell i, relative to the time delay from the center cell base station

φ_i = the phase delay from adjacent cell *i*, relative to the phase delay from the center cell base station

The power P_{ij} can be thus defined by consulting Equation (2.12) as follows:

$$P_{ij} = \frac{f_{ij} P_t}{L_H(D_i) X_i} \tag{2.14}$$

where

f_{ij} = the factor used to adjust the power in the *j*-th channel in adjacent cell *i*

$L_H(D_i)$ = the median path loss using the Hata Model at a separation distance D_i

D_i = the distance separating the receiver from the base station in adjacent cell *i*

X_i = Lognormal random variable $\Lambda(0, \sigma_{dB})$

Using the received signal defined by Equation (2.13), the performance of the DS-CDMA system in a Nakagami-fading channel with Lognormal shadowing can be defined.

D. SUMMARY

In this chapter, by taking into account a number of concepts from [1], a Nakagami-Lognormal channel model was developed which incorporates both large-scale and small-scale propagation effects into a single model. The extended Hata Model predicts the median path loss used. Applying this type of channel model to the signal, which is transmitted from the base station, we end up in a formula found in Equation (2.13) that gives the received signal to a mobile user's receiver. This received signal will be used to analyze the performance of the DS-CDMA in the following chapters.

III. DS-CDMA PERFORMANCE IN NAKAGAMI-M-LOGNORMAL FADING CHANNEL

In Chapter II, a Nakagami-*m*-Lognormal channel model was defined, and using the same procedure as in [1], it resulted in the received signal by a mobile user on the forward channel of a DS-CDMA cellular system in a Nakagami-*m*-Lognormal fading environment. In this chapter, by using Forward Error Correction (FEC) Coding to the forward signal (using convolutional codes), the coded probability of error is computed and the variation with different values of the Nakagami-*m* parameter can be seen. As previously mentioned, Nakagami-*m* distribution is a more general distribution for describing fading environments depending on the value of the *m* parameter, which describes the severity of the fading environment.

The analysis which occurred in [1] considered that mobile user one, who is the receiving mobile user, is located in the least optimum position within the cell, which can be any corner of the hexagon as depicted in Figure 3.1.

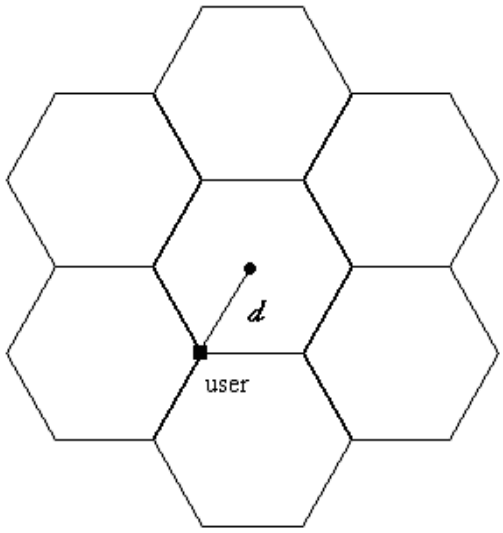

Figure 3.1. Mobile User One in the Seven-Cell Cluster.

The distances from adjacent cell base stations, D_i, to mobile user one for the worst-case distance ***d*** from the base station in the center cell are given in [1] as follows:

$$D_i = \begin{cases} \boldsymbol{d}, & i = 4,5 \\ 2\boldsymbol{d}, & i = 3,6 \\ \sqrt{7}\boldsymbol{d}, & i = 1,2 \end{cases}$$

where ***d*** is the length of each side of the hexagon implying that the hexagon is subdivided into six isosceles triangles. Distances D_i are used in order to compute the Hata median path loss for the transmitted signals from base stations of the *i* cell which was previously mentioned as responsible for the co-channel interference in the received signal. Distance ***d*** is used for computing the median path loss of the information signal transmitted from the center cell's base station.

A. CODED BIT ERROR PROBABILITY

In order to decode our information bit stream the Viterbi algorithm with soft decision decoding was used. It is also assumed that the all zero sequence ($b_1(t) = 1$ for all *t*) was transmitted. The first event error probability will be used in order to compute an upper bound in the coded bit error probability. The first event error probability is the probability where at a node B in the trellis diagram one of the paths that merges with the all-zero path (correct path) for the first time and the merging path has a metric that exceeds the all-zero path metric [1] and [6]. When this situation occurs, the decoder discards the correct path and bit errors ensue. This probability of error in the pair wise comparison of these two paths that differ in *d* bits is from [1], and [6] given by:

$$P_2(d)\Big|_{z_d} = Q\left(\sqrt{\frac{z_d}{\alpha}}\right) \tag{3.1}$$

where, Q denotes the Q function and z_d is the value assumed by the new random variable Z_d, which is the sum of d Nakagami-m square-Lognormal random variables defined as follows:

$$Z_d = \sum_{l=1}^{d} R_l^2 \widetilde{X}_l \tag{3.2}$$

where

R_l^2 = the Nakagami square random variable,

d = distance from the all zero path in the Trellis diagram,

$\widetilde{X}_l = \dfrac{1}{X_l}$ is another Lognormal random variable $\widetilde{X}_l \sim \Lambda\left(0, \lambda\sigma_{dB}\right)$ since X_l is our initial Lognormal random variable, $X_l \sim \Lambda\left(0, \lambda\sigma_{dB}\right)$. The index l in (3.2) runs over the set of d bits in which the two paths differ.

Additionally we have from [1]:

$$\alpha = \frac{\exp\left(\dfrac{\lambda^2\sigma_{dB}^2}{2}\right)}{3N} \sum_{i=1}^{6} \sum_{j=0}^{K_i - 1} \frac{f_{ij}}{f_1} \frac{L_{H(\boldsymbol{d})}}{L_{H(D_i)}} + \frac{N_o}{2E_c} \tag{3.3}$$

It has been assumed that $E_c = \left(k_0 / n_0\right) E_b$ is the coded bit energy, $E_b = f_1 P_t T / L_H(d)$ is a baseline received bit energy with no fading or shadowing and n_0, k_0 are the characteristics of the encoder that is being used. The use of an $\left(k_0, n_0\right)$ encoder means for every k_0 information bits, the encoder produces n_0 coded bits and that the code rate is $R_{cc} = \dfrac{k_0}{n_0}$. In order to keep the same bit rate to the system, the bit duration must be reduced as $T_{cc} = TR_{cc} = T \,{}^{k_0}\!/_{n_0}$ [1].

It can easily be said that if the pdf, $p_{Z_d}(z_d)$ is known, the conditioning of the first-event error probability on the new random variable Z_d can be removed, by integrating across its pdf as follows:

$$\begin{aligned} P_2(d) &= \int_{-\infty}^{\infty} P_2(d)\big|_{Z_d}\, p_{Z_d}(z_d)\, dz_d \\ &= \int_{-\infty}^{\infty} Q\left(\sqrt{\frac{z_d}{\alpha}}\right) p_{Z_d}(z_d)\, dz_d \end{aligned} \tag{3.4}$$

However, in a particular convolutional code there could be a large number of paths with different distances, which could compete, with the all-zero path at node B. That is why it is possible to compute an upper bound on the first-event error probability. One way to calculate an upper bound on the probability of bit error P_e is by using the total number of information bit errors, β_d, which is determined by selecting a path of distance *d* from the all-zero path [6]

$$P_e \le \frac{1}{k} \sum_{d=d_{free}}^{\infty} \beta_d P_2(d) \tag{3.5}$$

Thus, the end result is a formula which makes it possible to calculate the probability of error, P_e, for the coded DS-CDMA cellular system in the Nakagami-*m*-Lognormal channel depending on the distribution of the new random variable Z_d. The calculation of this pdf takes place in the next Section.

B. APPROXIMATING THE SUM OF MULTIPLICATIVE NAKAGAMI-SQUARE-LOGNORMAL RANDOM VARIABLES

Since the new random variable Z_d is defined by Equation (3.2), it would be possible to compute its probability density function if the pdf for one single variable $W = R^2 X$ was known, which represents a Nakagami-*m*-square-Lognormal random variable. Since Z_d is the sum of *d* Nakagami-*m*-square-Lognormal variables, it is thus possible to predict its pdf by convolving $p_W(w)$ with itself *d* times. Additionally, in

order to find the upper bound on the probability of bit error as predicted by Equation (3.5), a series of $P_2(d)$ for $d = d_{free},\ d_{free}+1,\ d_{free}+2,...$ must exist. Using the first five terms we get:

$$P_e \le \frac{1}{k} \sum_{d=d_{free}}^{d_{free}+4} \beta_d P_2(d)$$

In our analysis, which is similar to that occurring in [1], convolutional encoders will be used with $R_{cc} = \frac{1}{2}$ and constraint lengths form 7 to 9, which usually have a d_{free} ranging from 10 to 12.

The sum of Lognormal random variables can be approximated as another Lognormal random variable upon setting up a model with suitable parameters [1]. There are a lot of different ways in order to find the Lognormal model parameters. One of them is the cumulant matching approach in which the model parameters are being computed to make the Cumulative Distribution Function (CDF) of the model Lognormal random variable fit the CDF of the sum of Lognormal random variables (as simulated using Monte Carlo methods). After defining the model parameters by using one of the methods of [7], the approximated distribution is known. The other pdf to determine is the pdf of the sum of *d* Nakagami-*m* square random variables, which will be examined more closely later in this Section. Furthermore, knowing the pdf of the sum of Lognormal variables (approximated as another Lognormal random variable) and the pdf of the sum of *d* Nakagami-*m* square random variables, the sum of *d* Nakagami-*m*-square-Lognormal random variables will be approximated with Z_d as a multiplicative Nakagami-*m*-square-Lognormal random variable.

1. Defining the Model, $\tilde{Z}_d$

It is known that the Nakagami-*m* random variable has a probability density function that is given by:

$$f_{R_l}(r_l) = \begin{cases} \dfrac{2}{\Gamma(m)}\left(\dfrac{m}{\Omega}\right)^m r_l^{2m-1} \exp\left(-\dfrac{mr_l^2}{\Omega}\right), r_l \geq 0 \\ 0 \quad \text{elsewhere} \end{cases} \tag{3.6}$$

where $\Gamma(m)$ is the gamma function, defined by the integral

$$\Gamma(m) = \int_0^\infty x^{m-1} \exp(-x) dx, m > 0$$

and

$$m = \frac{\Omega^2}{\mathrm{Var}\left(R_l^2\right)} \geq \frac{1}{2}$$

$$\Omega = \mathrm{E}\left\{R_l^2\right\}$$

In Appendix III-A it is shown that the probability density function and the characteristic function of a Nakagami-*m* square random variable are given by:

$$f_{R_l^2}\left(r_l^2\right) = \frac{\left(\dfrac{m}{\Omega}\right)^m}{\Gamma(m)} r_l^{2(m-1)} \exp\left(-\frac{mr_l^2}{\Omega}\right), \tag{3.7}$$

$$\Psi_{R_l^2}(\mathrm{j}\omega) = \frac{\left(\dfrac{m}{\Omega}\right)^m}{\left(\dfrac{m}{\Omega} - \mathrm{j}\omega\right)^m}, \tag{3.8}$$

and that the probability density function of the sum of *d* Nakagami-*m* square random variables is given by:

$$f_{Y_{2d}}(y_{2d}) = \left(\frac{m}{\Omega}\right)^{md} \frac{y_{2d}^{md-1}}{\Gamma(md)} \exp\left(-\frac{my_{2d}}{\Omega}\right) \tag{3.9}$$

The model $\tilde{Z}_d$ can now be defined in terms of its two factors, which are defined as follows:

$$\tilde{Z}_d = Y_{2d} X_z$$

where Y_{2d} is a random variable whose pdf is given by Equation (3.9) and it is the sum of d Nakagami-m square random variables, $Y_{2d} = \sum_{l=1}^{d} R_l^2$ and X_z is the lognormal component of $\tilde{Z}_d, X_z \sim \Lambda(\mu_z, \sigma_z)$. The parameters μ_z and σ_z are yet to be specified.

The quantity $\mathrm{E}\{R_l^2\} = \Omega = 1$ has been normalized. For the moments of Y_{2d}:

$$\begin{aligned} \mathrm{E}\{Y_{2d}\} &= dE\{R_l^2\} = d\Omega = d \\ \mathrm{E}\{{Y_{2d}}^2\} &= \Omega^2 d^2 + \Omega^2 \frac{d}{m} = d^2 + \frac{d}{m} \\ \mathrm{Var}\{Y_{2d}\} &= \Omega^2 \frac{d}{m} = \frac{d}{m} \end{aligned} \tag{3.10}$$

Assuming that Y_{2d} and X_z are independent random variables, the expectation for the model is:

$$\mathrm{E}\{\tilde{Z}_d\} = \mathrm{E}\{Y_{2d} X_z\} = \mathrm{E}\{Y_{2d}\}\mathrm{E}\{X_z\} \tag{3.11}$$

From [1], it is known that

$$\mathrm{E}\{X_z\} = \exp\left(\mu_z + \frac{\sigma_z^2}{2}\right) \tag{3.12}$$

Substituting the moments of the two independent random variables Y_{2d} and X_z in Equation (3.11), we get for the expectation of the model:

$$\mathrm{E}\{\tilde{Z}_d\} = \Omega d \exp\left(\mu_z + \sigma_z^2 / 2\right) \tag{3.13}$$

The second moment of $\tilde{Z}_d$ can be defined from the second moments of Y_{2d} and X_z as follows:

$$\mathrm{E}\{\tilde{Z}_d^2\} = \mathrm{E}\{Y_{2d}^2 X_z^2\} = \mathrm{E}\{Y_{2d}^2\}\mathrm{E}\{X_z^2\} \tag{3.14}$$

From [1],

$$\mathrm{E}\{X_z^2\} = \exp\left(2\mu_z + 2\sigma_z^2\right) \tag{3.15}$$

Substituting the values of $\mathrm{E}\left\{Y_{2d}^2\right\}$ and $\mathrm{E}\left\{X_z^2\right\}$ from Equations (3.10) and (3.15) respectively, we get for $\mathrm{E}\left\{\tilde{Z}_d^2\right\}$:

$$\mathrm{E}\left\{\tilde{Z}_d^2\right\} = \Omega^2\left(d^2 + \frac{d}{m}\right)\exp\left(2\mu_z + 2\sigma_z^2\right) \tag{3.16}$$

knowing the first and second moment of $\tilde{Z}_d$ the variance of $\tilde{Z}_d$ can be computed as follows:

$$\mathrm{Var}\left\{\tilde{Z}_d\right\} = \Omega^2\left(d^2 + \frac{d}{m}\right)\exp\left(2\mu_z + 2\sigma_z^2\right) - d^2\exp(2\mu_z + \sigma_z{}^2)\Omega^2 \tag{3.17}$$

However, the parameters μ_z and σ_z^2 for the random variable X_z have not yet been determined in order to approximate Z_d as a Nakagami-*m*-square Lognormal random variable. In order to calculate these two parameters we relate the mean and the variance of the model $\tilde{Z}_d$ defined by Equations (3.13) and (3.17) respectively with a scaled version of mean and variance of the single Nakagami-*m*-square Lognormal random variable R^2X.

The previous analysis is similar to that taking place in [1] in which the random variable *R* is a Rayleigh random variable, special case of the Nakagami-*m* random variable (*m* = 1). As in [1], in simulations it can be seen that the mean of Z_d is proportional to *d* times the mean of the original single Nakagami-*m*-square-Lognormal random variable. Based on that, the mean of $\tilde{Z}_d$ can be equated with *d* times the mean of R^2X scaled by a factor of f_1 as follows:

$$\mathrm{E}\left\{\tilde{Z}_d\right\} = f_1 d\mathrm{E}\left\{R^2X\right\} = f_1 d\mathrm{E}\left\{R^2\right\}\mathrm{E}\left\{X\right\} = f_1 d\Omega\exp\left(\frac{\sigma_x{}^2}{2}\right) = f_1 d\exp\left(\frac{\sigma_x{}^2}{2}\right) \tag{3.18}$$

where $\sigma_x^2 = \lambda^2\sigma_{dB}^2$ is the parameter from the original Lognormal shadowing random variable $X \sim \Lambda\left(0, \sigma_X^2\right)$. Using the Equations (3.13) and (3.18):

$$\mu_z = \frac{\sigma_X^2 - \sigma_z^2}{2} + \ln(f_1) \tag{3.19}$$

The analytical computation for μ_z is given in Appendix III-C. Observing that the variance of Z_d is proportional to d times the variance of the Nagakami-m-square-Lognormal random variable; the variance of the model can be equated with d times the variance of R^2X scaled by a factor of f_2 as follows:

$$\mathrm{Var}\left\{\tilde{Z}_d\right\} = f_2 d \mathrm{Var}\left\{R^2 X\right\} \tag{3.20}$$

The variance of R^2X is calculated in Appendix III-B and it is given as follows:

$$\mathrm{Var}\left\{R^2 X\right\} = \exp\left(\sigma_x^2\right)\left[\Omega^2 \frac{m+1}{m} e^{\sigma_x^2} - \Omega^2\right] \tag{3.21}$$

By using Equations (3.20) and (3.21), σ_Z^2 can be solved as follows:

$$\sigma_Z^2 = \ln\left[\frac{f_2(m+1)}{f_1^2 m} e^{\sigma_X^2} - \frac{f_2}{f_1^2} + d\right] - \ln(1+md) + \ln(m) \tag{3.22}$$

Analytical computation for σ_Z^2 is given in Appendix III-C. The scaling factors f_1 and f_2 vary with the values of σ_{dB} and the Nakagami-m parameter, and have been selected in the way that the CDF of the model $\tilde{Z}_d$ best fits the CDF of Z_d for d = 8,9…,16. The value of $\sigma_{dB} = 7$ will be used to examine the performance of the model $\tilde{Z}_d$ for the following values of the Nakagami-m parameter: m = 0.5, 0.75, 1, 1.5, 2. Each value of m corresponds to a different fading environment. Table 3.1 shows the values of f_1 and f_2 for each value of σ_{dB} as determined by simulation, for m = 0.5.

σ_{dB}	f_1	f_2
2	1	0.9875
3	1	0.937
4	1	0.91
5	1	0.8
6	0.94	0.4775
7	0.908	0.3235
8	0.8625	0.1875
9	0.7875	0.09

Table 3.1. Values of f_1 and f_2 for $\tilde{Z}_d$ for $m = 0.5$.

Table 3.2 shows the values of f_1 and f_2 for each value of σ_{dB} as determined by simulation, for $m = 0.75$.

σ_{dB}	f_1	f_2
2	1	0.9875
3	1	0.9625
4	1	0.8875
5	1	0.7995
6	0.94	0.49
7	0.908	0.3235
8	0.8625	0.1875
9	0.8125	0.1

Table 3.2. Values of f_1 and f_2 for $\tilde{Z}_d$ for $m = 0.75$.

Table 3.3 shows the values of f_1 and f_2 for each value of σ_{dB} for $m = 1$.

σ_{dB}	f_1	f_2
2	1	0.9875
3	1	0.9625
4	1	0.9125
5	1	0.8125
6	0.9375	0.4875
7	0.9125	0.3375
8	0.8625	0.2
9	0.8	0.1

Table 3.3. Values of f_1 and f_2 for $\tilde{Z}_d$ for $m = 1$ from [1].

Table 3.4 shows the values of f_1 and f_2 for each value of σ_{dB} as determined by simulation, for m = 1.5.

σ_{dB}	f_1	f_2
2	1	0.98
3	1	0.97
4	1	0.9225
5	0.9875	0.8025
6	0.9525	0.525
7	0.915	0.3475
8	0.8875	0.223
9	0.8	0.1

Table 3.4. Values of f_1 and f_2 for $\tilde{Z}_d$ for m = 1.5.

Table 3.5 shows the values of f_1 and f_2 for each value of σ_{dB} as determined by simulation, for $m = 2$.

σ_{dB}	f_1	f_2
2	1	0.995
3	1	0.96
4	1	0.925
5	1	0.8375
6	0.955	0.5375
7	0.9275	0.3725
8	0.885	0.224
9	0.835	0.121

Table 3.5. Values of f_1 and f_2 for $\tilde{Z}_d$ for $m = 2$.

The model parameters have been specified, so it is now possible to define the pdf of the model $\tilde{Z}_d$ using the marginal pdfs of its components, which are Y_{2d} and X_z. The quantity $\tilde{Z}_d = Y_{2d} X_z$ has been defined and $X_z = x$ can be fixed so that $\tilde{Z}_d\Big|_x = xy_{2d}$. The conditional pdf of $\tilde{Z}_d\Big|_x$ is given as follows:

$$p_{\tilde{Z}_d|_x}\left(z\middle|x\right) = \frac{1}{|x|} p_{Y_{2d}}\left(\frac{z}{x}\right) \tag{3.23}$$

However, the pdf $p_{Y_{2d}}$ of Y_{2d} is given by Equation (3.9) so (3.23) becomes:

$$\begin{aligned} p_{\tilde{Z}_{d|x}}\left(z\middle|x\right) &= \frac{1}{|x|}\left(\frac{m}{\Omega}\right)^{md} \frac{\left(\frac{z}{x}\right)^{md-1}}{\Gamma(md)} \exp\left(-\frac{m}{\Omega}\frac{z}{x}\right) \\ &= \frac{1}{|x|}\left(\frac{m}{\Omega}\right)^{md} \frac{1}{\Gamma(md)} \frac{z^{md-1}}{x^{md-1}} \exp\left(-\frac{m}{\Omega}\frac{z}{x}\right) \\ &= \frac{\left(\frac{m}{\Omega}\right)^{md}}{\Gamma(md)x^{md}} z^{md-1} \exp\left(-\frac{m}{\Omega}\frac{z}{x}\right), \ \frac{z}{x} \geq 0 \end{aligned} \tag{3.24}$$

The conditional of $\tilde{Z}_d$ on $X_z = x$ can be removed as follows:

$$
\begin{aligned}
p_{\tilde{Z}_d}(z) &= \int_{-\infty}^{\infty} p_{\tilde{Z}_d|x} \quad p_{x_Z}(x)dx \\
&= \int_0^{\infty} \frac{\left(\frac{m}{\Omega}\right)^{md}}{\Gamma(md)x^{md}} z^{md-1} \exp\left(-\frac{m}{\Omega}\frac{z}{x}\right) \frac{1}{x\sqrt{2\pi}\sigma_Z} \\
&\times \exp\left[\frac{-\left(\ln x - \mu_z\right)^2}{2\sigma_z^2}\right] dx \qquad (3.25) \\
&= \frac{\left(\frac{m}{\Omega}\right)^{md} z^{md-1}}{\Gamma(md)\sqrt{2\pi}\sigma_Z} \int_0^{\infty} \frac{1}{x^{md+1}} \exp\left\{\frac{-zm}{x\Omega} - \frac{\left(\ln x - \mu_z\right)^2}{2\sigma_Z^2}\right\} dx, \; z \geq 0
\end{aligned}
$$

where μ_z and σ_Z^2 have been defined by Equations (3.19) and (3.22) respectively.

A distribution for the Nakagami-*m*-square-Lognormal random variable has now been defined, which approximates the distribution of a sum of *d* Nakagami-*m*-square-Lognormal random variables. In the next Section, some examples of the model will be examined and the performance results using the model with the results predicted by the Monte Carlo simulations will be compared.

2. Testing the Model $\tilde{Z}_d$

In this Section, the model's applicability to bit error analysis of DS-CDMA with forward error correction coding will be demonstrated. Using the first five terms of the union bound from Equation (3.5) we will approximate the probability of bit error. The value of lognormal shadowing will be taken to be $\sigma_{dB} = 7$ and a convolutional encoder with a rate of $\frac{1}{2}$ and a constraint length $v = 8$ will be used. The function $P_2(d)$ will be approximated using the model for $d = 10$ through 14 which are critical values of *d* for this type of encoder with constraints lengths 7 and 8. MATLAB is the programming software used to obtain my results. First of all, the model will be checked and compared with the one developed in [1] by giving the Nakagami-*m* parameter the value of $m = 1$ (which is

the Rayleigh fading case), if it reproduces the same results. Figures 3.2 through 3.6 show histograms for Z_d for $\sigma_{dB} = 7$ and Nakagami-*m* parameter $m = 1$ with an over plot of the pdf of our model. The histograms for Z_d were developed by generating d sets of Nakagami-square-Lognormal distributed data consisting of 400,000 independent samples per set and summing over the d sets similar to those in [1]. In these Figures concerning the histograms part, the x axis represents the possible values of the random variable we are trying to model and the y axis is the number of occurrences of the possible values of x within each bin. For the pdf part the y axis is the value of the pdf normalized by the number of samples we generate and the binwidth.

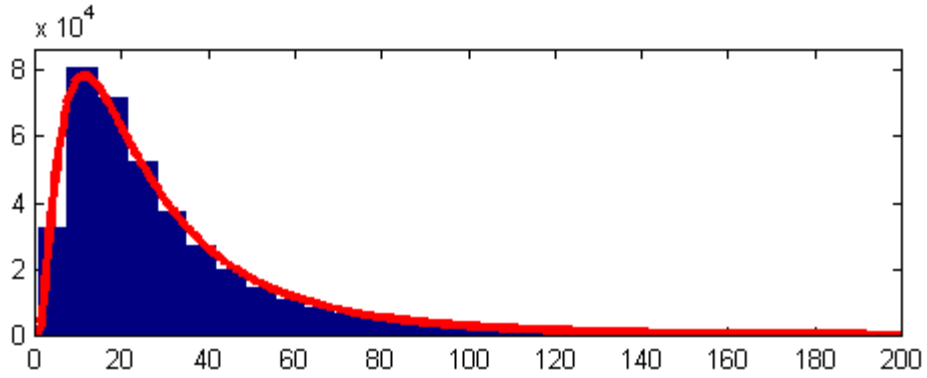

Figure 3.2. Histogram of Z_{10} and the PDF for $\tilde{Z}_{10}$ for $\sigma_{dB} = 7$, $d = 10$ and $m = 1$.

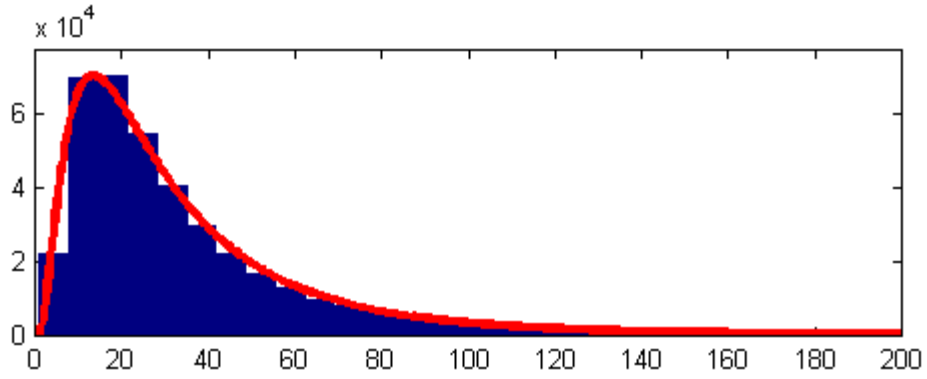

Figure 3.3. Histogram of Z_{11} and the PDF for $\tilde{Z}_{11}$ for $\sigma_{dB} = 7$, $d = 11$ and $m = 1$.

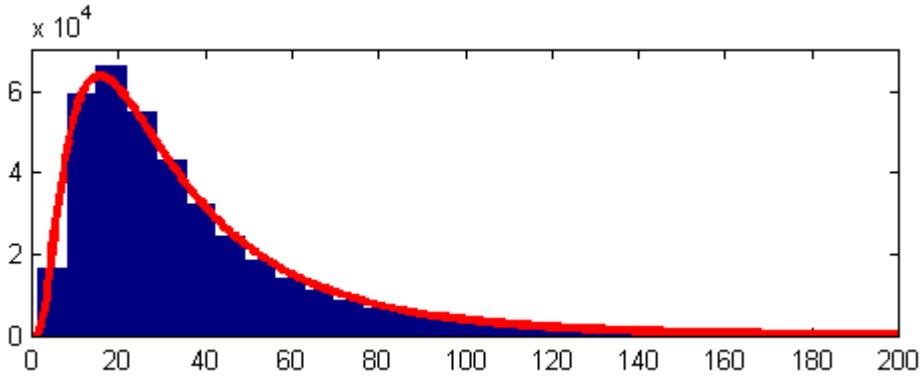

Figure 3.4. Histogram of Z_{12} and the PDF for $\tilde{Z}_{12}$ for $\sigma_{dB} = 7$, $d = 12$ and $m = 1$.

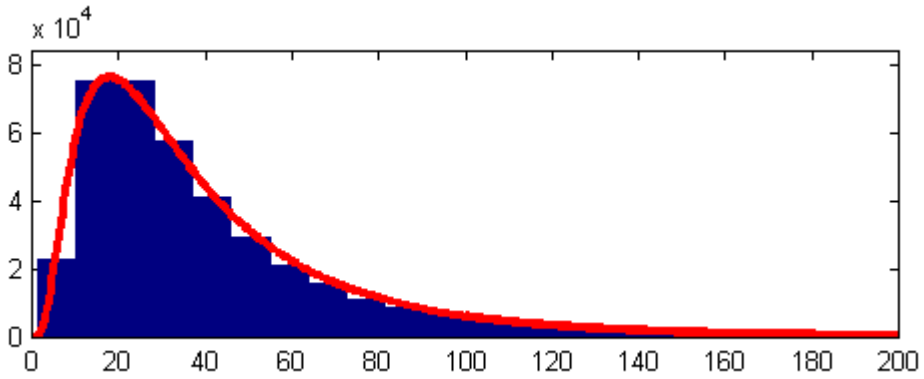

Figure 3.5. Histogram of Z_{13} and the PDF for $\tilde{Z}_{13}$ for $\sigma_{dB} = 7$, $d = 13$ and $m = 1$.

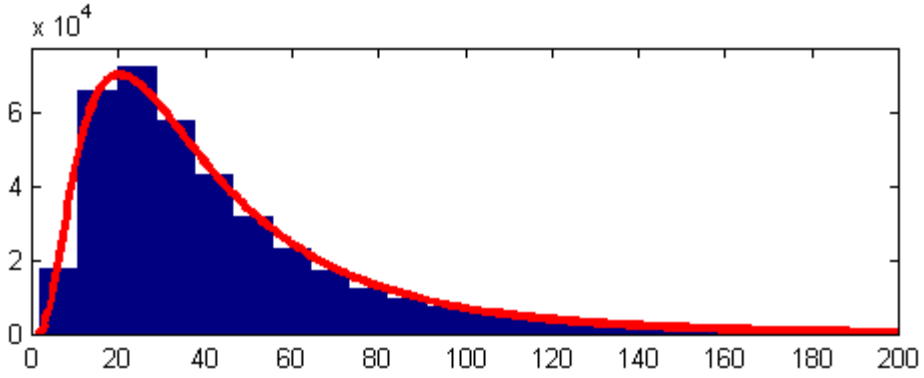

Figure 3.6. Histogram of Z_{14} and the PDF for $\tilde{Z}_{14}$ for $\sigma_{dB} = 7$, $d = 14$ and $m = 1$.

Comparing these results with the corresponding results, which were obtained in [1], it can be seen that the model $\tilde{Z}_d$ has almost the same results as the model in [1] for the Rayleigh case.

Figures 3.7 through 3.11 show the histograms for Z_d for $\sigma_{dB} = 7$ and the pdf of the model $\tilde{Z}_d$ for $m = 0.5$ and for $d = 10$ through $d = 14$.

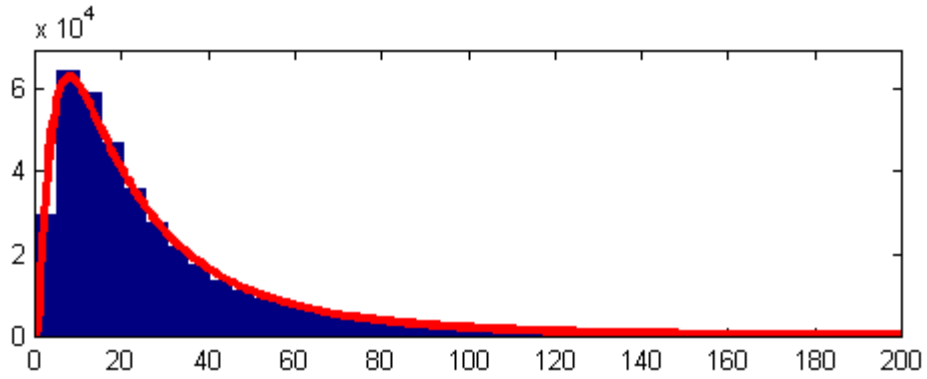

Figure 3.7. Histogram of Z_{10} and the PDF for $\tilde{Z}_{10}$ for $\sigma_{dB} = 7$, $d = 10$ and $m = 0.5$.

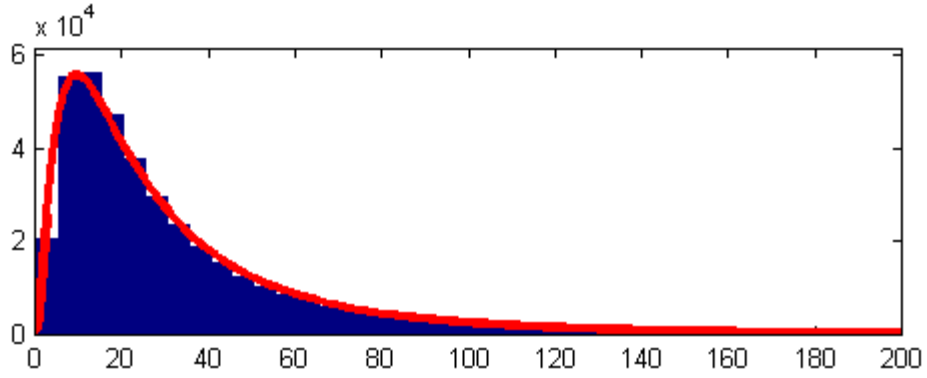

Figure 3.8. Histogram of Z_{11} and the PDF for $\tilde{Z}_{11}$ for $\sigma_{dB} = 7$, $d = 11$ and $m = 0.5$.

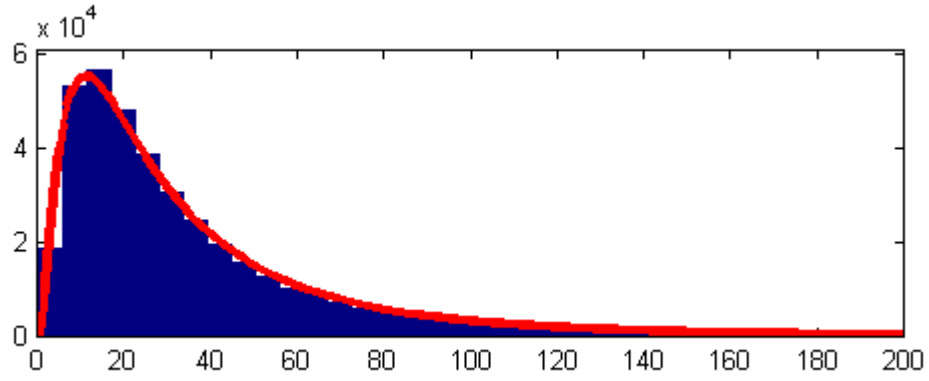

Figure 3.9. Histogram of Z_{12} and the PDF for $\tilde{Z}_{12}$ for $\sigma_{dB} = 7$, $d = 12$ and $m = 0.5$.

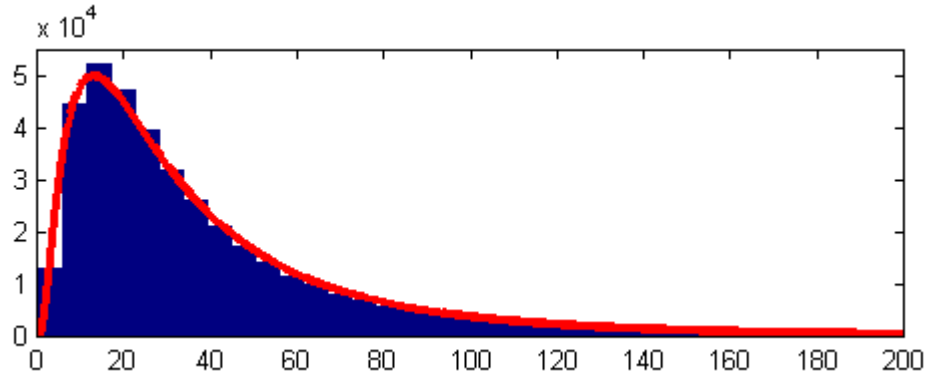

Figure 3.10. Histogram of Z_{13} and the PDF for $\tilde{Z}_{13}$ for $\sigma_{dB} = 7$, $d = 13$ and $m = 0.5$.

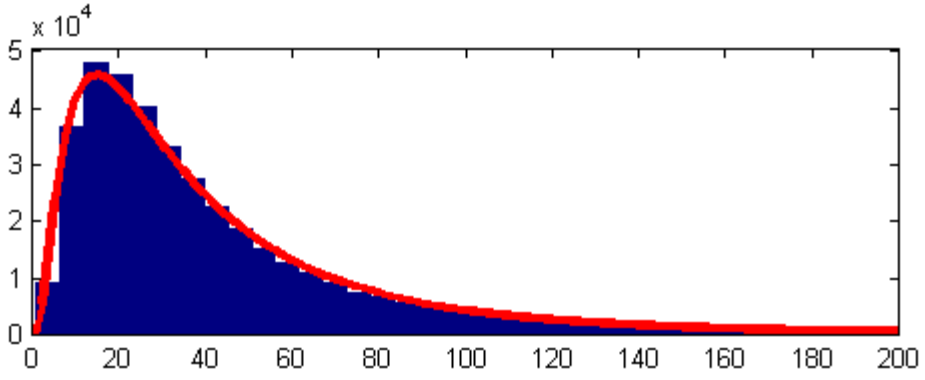

Figure 3.11. Histogram of Z_{14} and the PDF for $\tilde{Z}_{14}$ for $\sigma_{dB} = 7$, $d = 14$ and $m = 0.5$.

Figures 3.12 through 3.16 show histograms for Z_d for $\sigma_{dB} = 7$ and $m = 0.75$ and an over plot of the pdf of our model for $d = 10$ through $d = 14$.

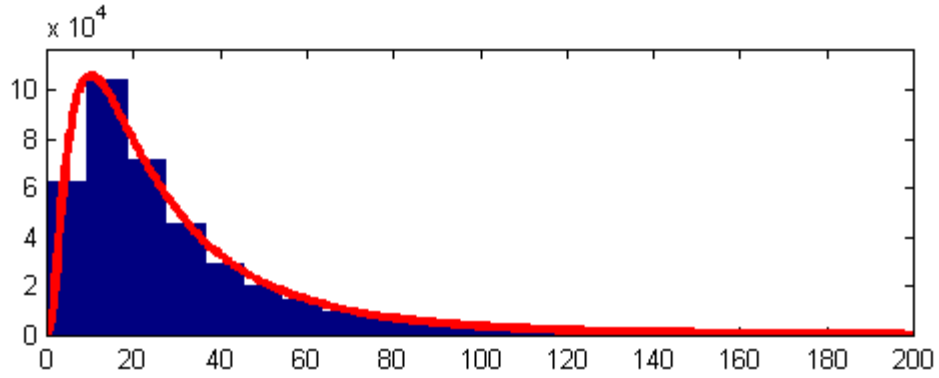

Figure 3.12. Histogram of Z_{10} and the PDF for $\tilde{Z}_{10}$ for $\sigma_{dB} = 7$, $d = 10$ and $m = 0.75$.

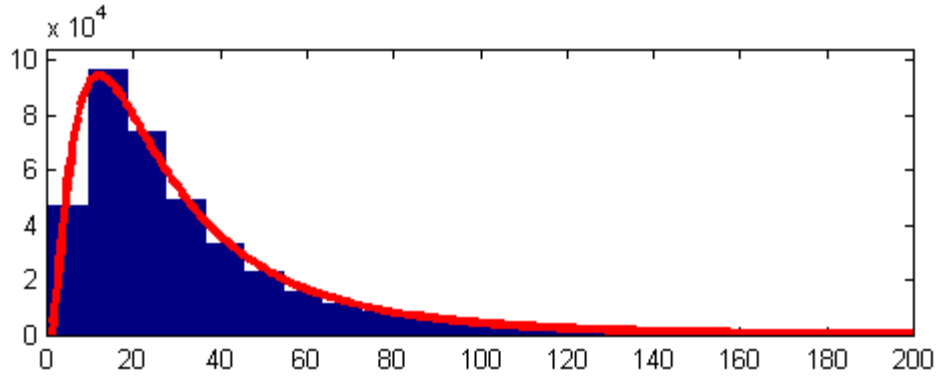

Figure 3.13. Histogram of Z_{11} and the PDF for $\tilde{Z}_{11}$ for $\sigma_{dB} = 7$, $d = 11$ and $m = 0.75$.

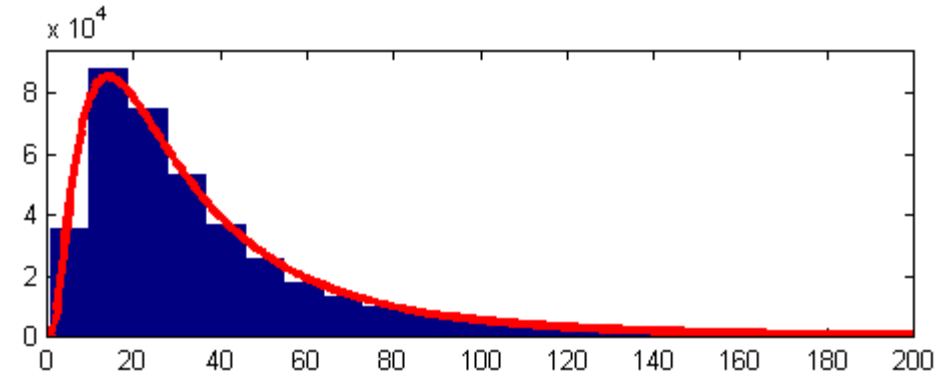

Figure 3.14. Histogram of Z_{12} and the PDF for $\tilde{Z}_{12}$ for $\sigma_{dB} = 7$, $d = 12$ and $m = 0.75$.

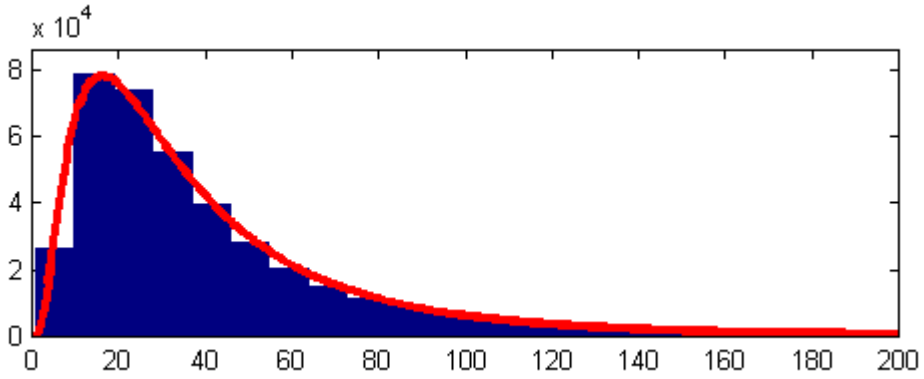

Figure 3.15. Histogram of Z_{13} and the PDF for $\tilde{Z}_{13}$ for $\sigma_{dB} = 7$, $d = 13$ and $m = 0.75$.

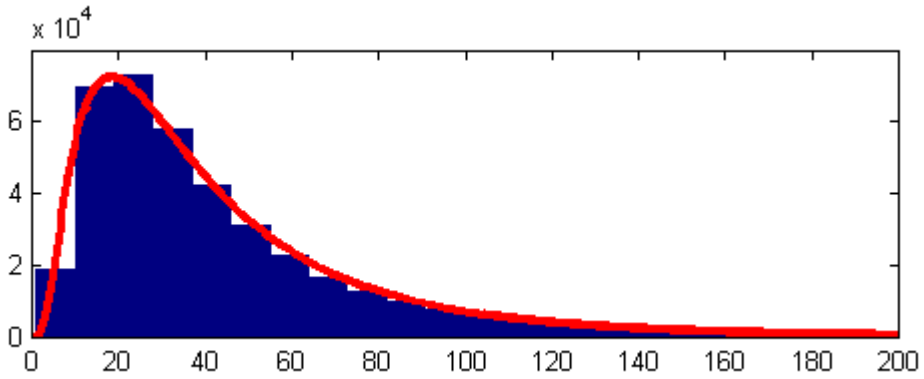

Figure 3.16. Histogram of Z_{14} and the PDF for $\tilde{Z}_{14}$ for $\sigma_{dB} = 7$, $d = 14$ and $m = 0.75$.

Figures 3.17 through 3.21 show histograms for Z_d for $\sigma_{dB} = 7$ and $m = 1.5$ and an over plot of the pdf of our model for $d = 10$ through $d = 14$.

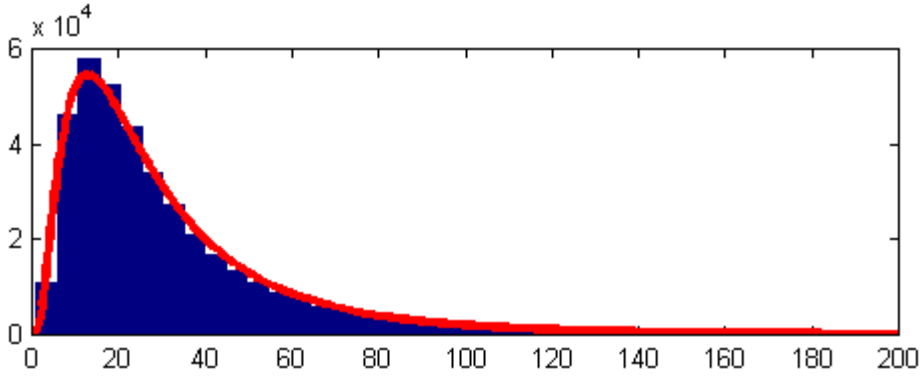

Figure 3.17. Histogram of Z_{10} and the PDF for $\tilde{Z}_{10}$ for $\sigma_{dB} = 7$, $d = 10$ and $m = 1.5$.

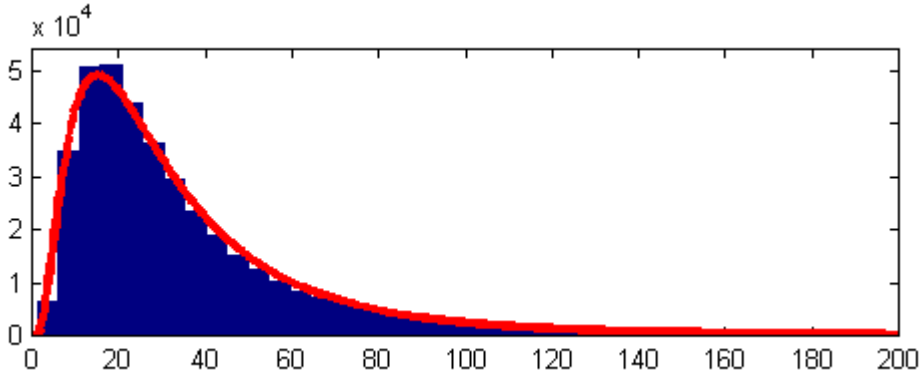

Figure 3.18. Histogram of Z_{11} and the PDF for $\tilde{Z}_{11}$ for $\sigma_{dB} = 7$, $d = 11$ and $m = 1.5$.

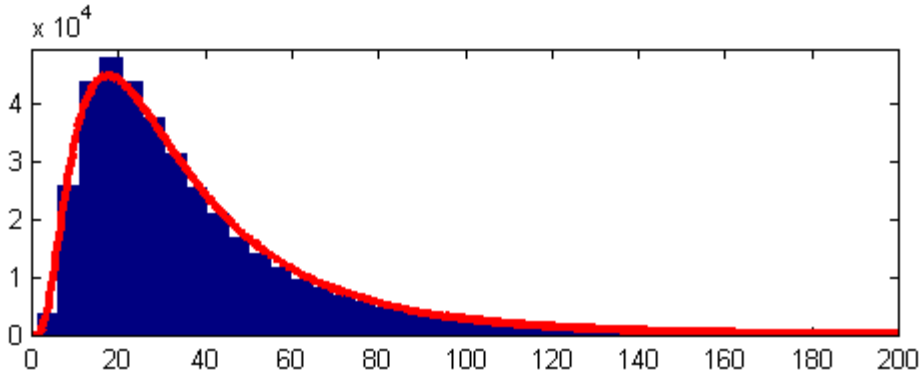

Figure 3.19. Histogram of Z_{12} and the PDF for $\tilde{Z}_{12}$ for $\sigma_{dB} = 7$, $d = 12$ and $m = 1.5$.

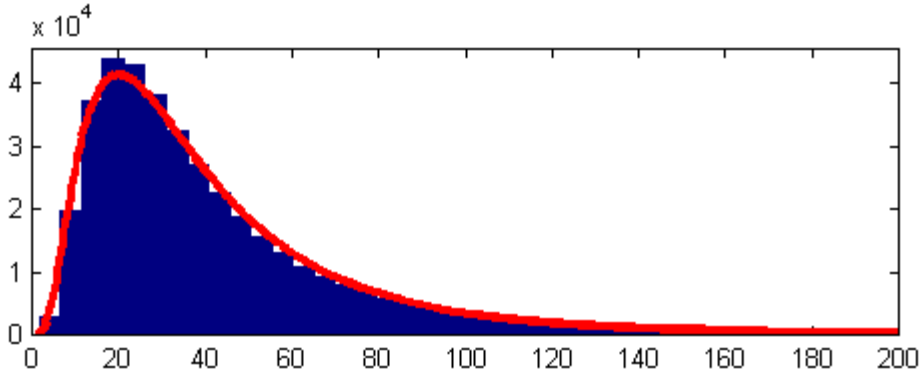

Figure 3.20. Histogram of Z_{13} and the PDF for $\tilde{Z}_{13}$ for $\sigma_{dB} = 7$, $d = 13$ and $m = 1.5$.

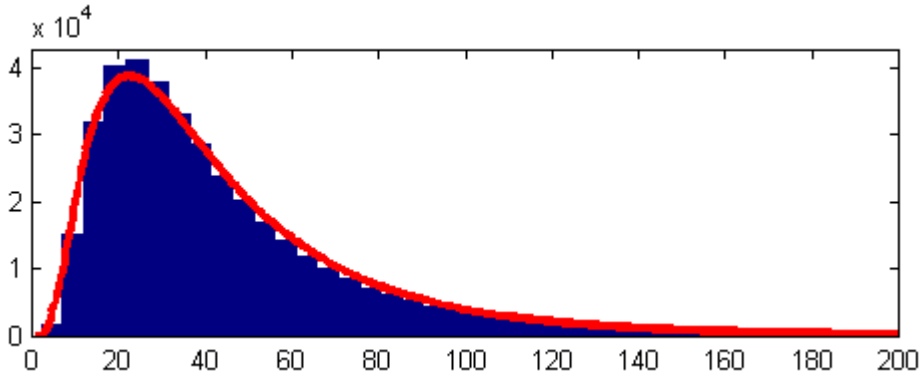

Figure 3.21. Histogram of Z_{14} and the PDF for $\tilde{Z}_{14}$ for $\sigma_{dB} = 7$, $d = 14$ and $m = 1.5$.

Figures 3.22 through 3.26 show histograms for Z_d for $\sigma_{dB} = 7$ and $m = 2$ and an over plot of the pdf of our model for $d = 10$ through $d = 14$.

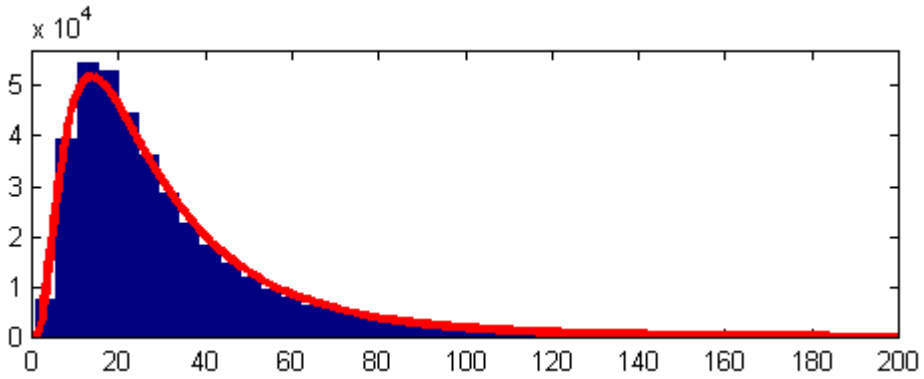

Figure 3.22. Histogram of Z_{10} and the PDF for $\tilde{Z}_{10}$ for $\sigma_{dB} = 7$, $d = 10$ and $m = 2$.

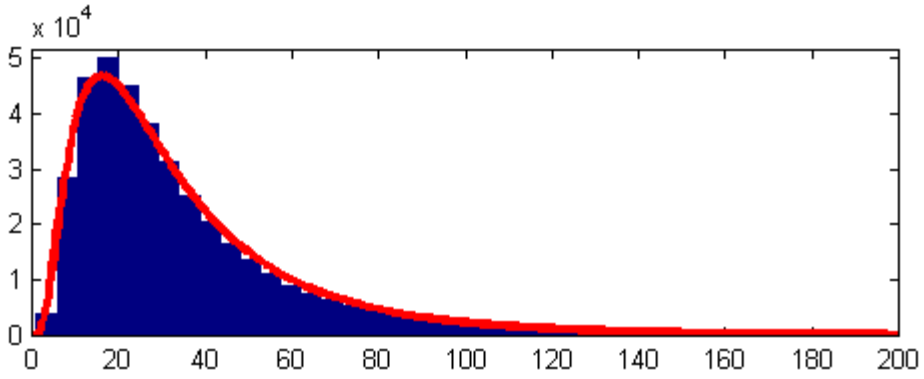

Figure 3.23. Histogram of Z_{11} and the PDF for $\tilde{Z}_{11}$ for $\sigma_{dB} = 7$, $d = 11$ and $m = 2$.

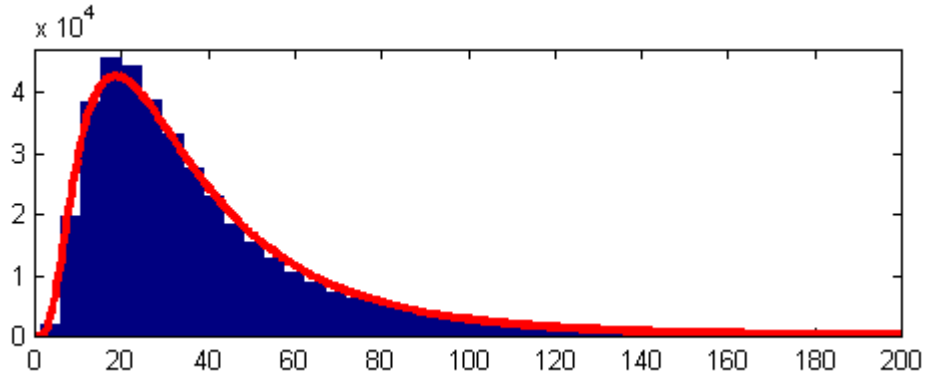

Figure 3.24. Histogram of Z_{12} and the PDF for $\tilde{Z}_{12}$ for $\sigma_{dB} = 7$, $d = 12$ and $m = 2$.

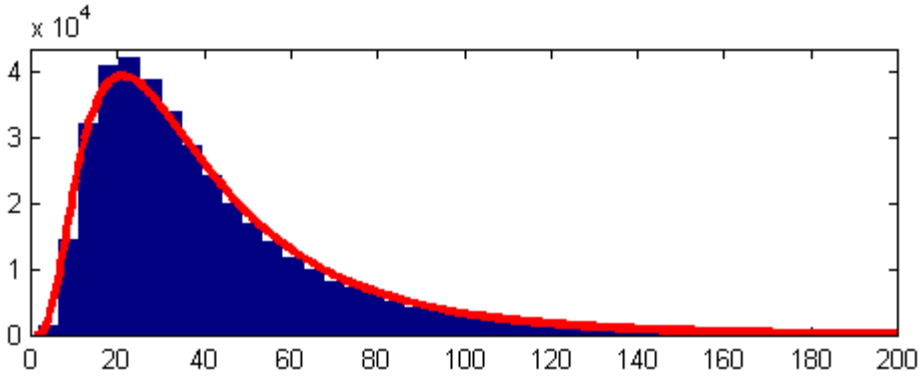

Figure 3.25. Histogram of Z_{13} and the PDF for $\tilde{Z}_{13}$ for $\sigma_{dB} = 7$, $d = 13$ and $m = 2$.

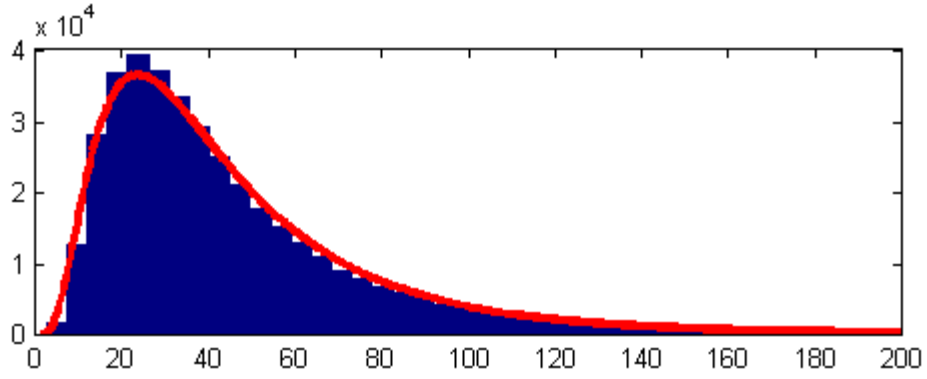

Figure 3.26. Histogram of Z_{14} and the PDF for $\tilde{Z}_{14}$ for $\sigma_{dB} = 7$, $d = 14$ and $m = 2$.

The next question is how well can the model $\tilde{Z}_d$ approximate Z_d in calculating the first-event error probability, which is given by (3.4). This answer will be given by comparing the result predicted by the model $\tilde{Z}_d$ to that one which simulates the integral of (3.4) by generating d independent samples form the Nakagaim-m-square-Lognormal distribution and summing them in order to form one realization for Z_d and one realization, p_1, for $P_2(d)$. This process is repeated 95,000 times and gives our estimation, $\overline{p}_i$, for $P_2(d)$ as follows:

$$\overline{p} = \frac{1}{95,000} \sum_{i=1}^{95,000} p_i \tag{3.26}$$

First of all, by using the following values, an attempt will be made to replicate the results obtained in [1] using the model $\tilde{Z}_d$ as follows: m = 1 (Rayleigh case), $\sigma_{dB} = 7$, number of sectors 6, 60 users per adjacent cell and d = 10 through 13. Figures 3.27 through 3.36 show how well the model $\tilde{Z}_d$ is useful in computing $P_2(d)$ and comparing it to that predicted by Monte Carlo simulations of the integral of (3.4).

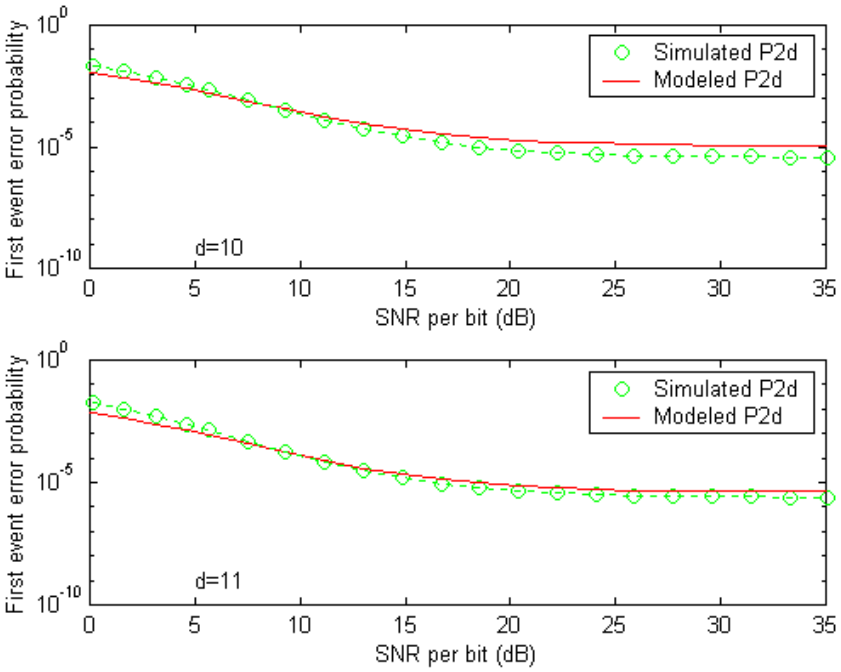

Figure 3.27. First Event Error Probability $P_2(10)$ and $P_2(11)$ with 60 Users Per Cell and 60° Sectoring, for $m = 1$.

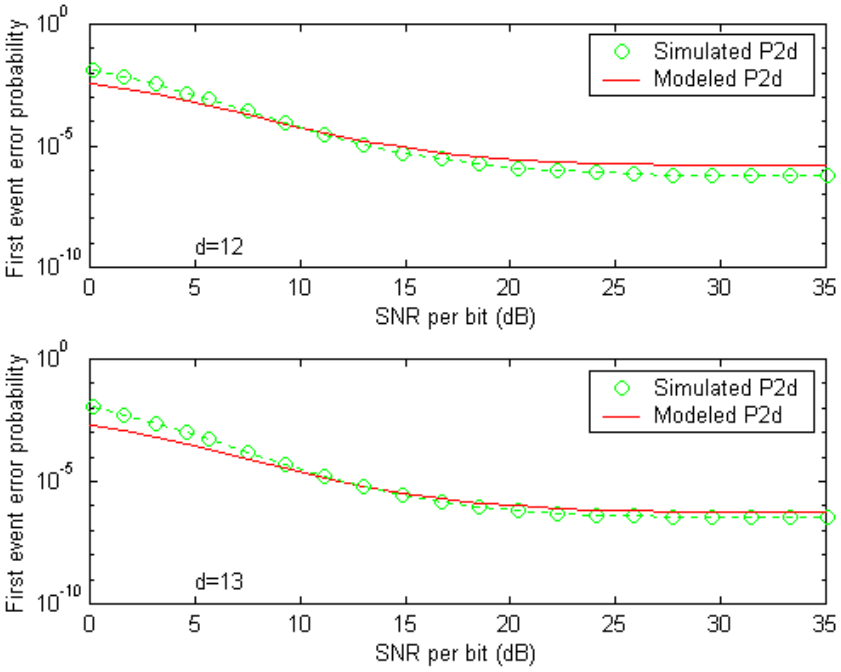

Figure 3.28. First Event Error Probability $P_2(12)$ and $P_2(13)$ with 60 Users Per Cell and 60° Sectoring, for $m = 1$.

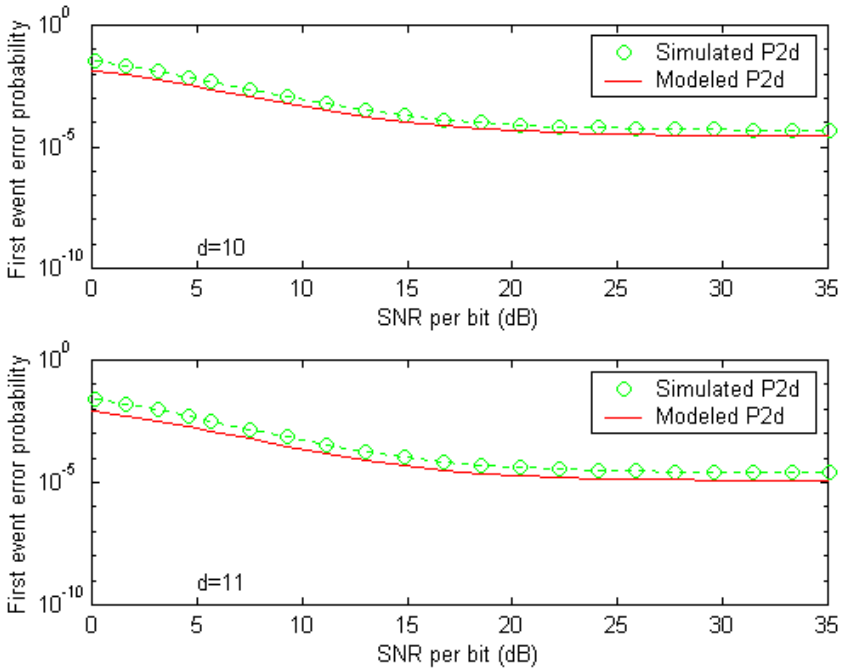

Figure 3.29. First Event Error Probability $P_2(10)$ and $P_2(11)$ with 60 Users Per Cell and 60° Sectoring, for $m = 0.5$.

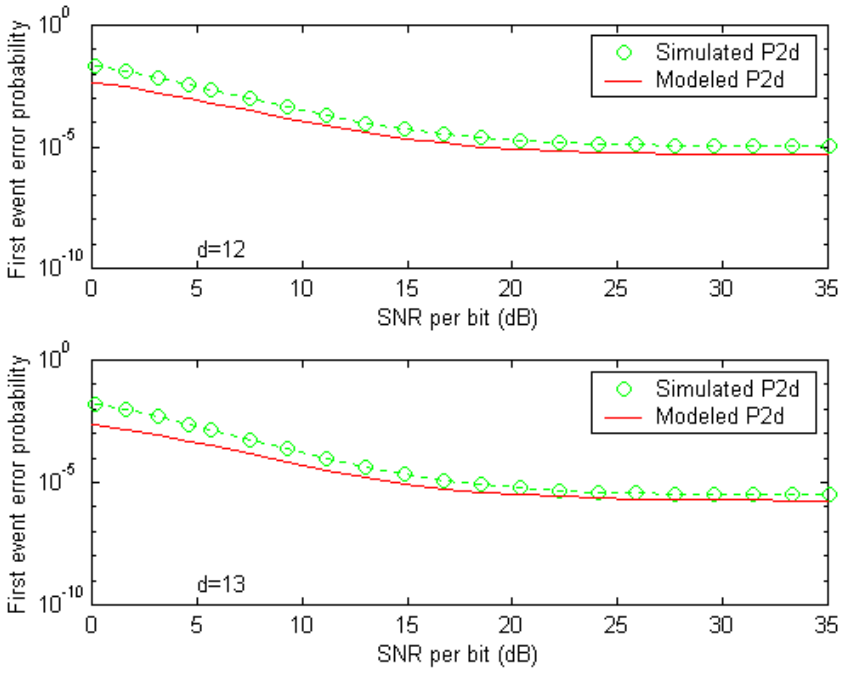

Figure 3.30. First Event Error Probability $P_2(12)$ and $P_2(13)$ with 60 Users Per Cell and 60° Sectoring, for $m = 0.5$.

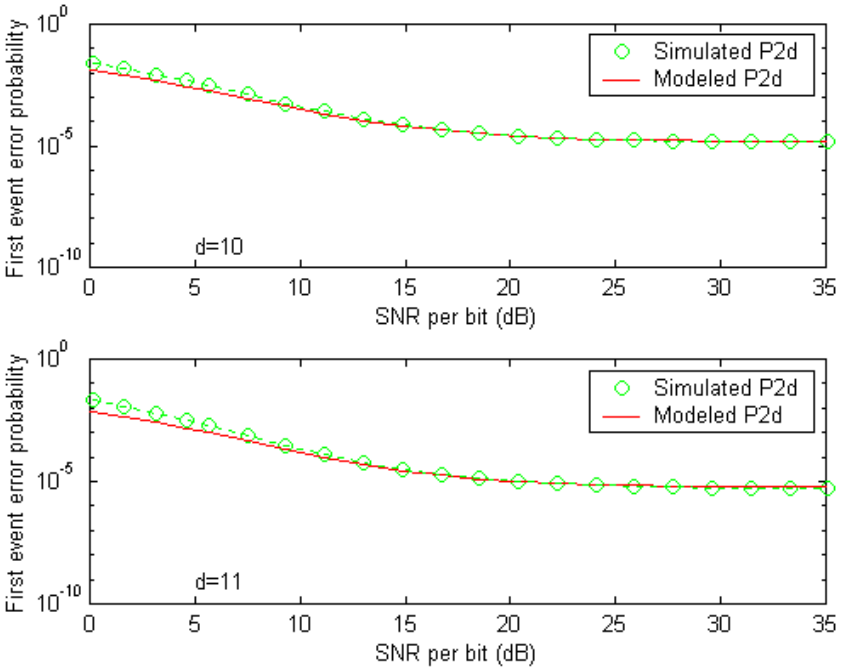

Figure 3.31. First Event Error Probability $P_2(10)$ and $P_2(11)$ with 60 Users Per Cell and 60° Sectoring, for $m = 0.75$.

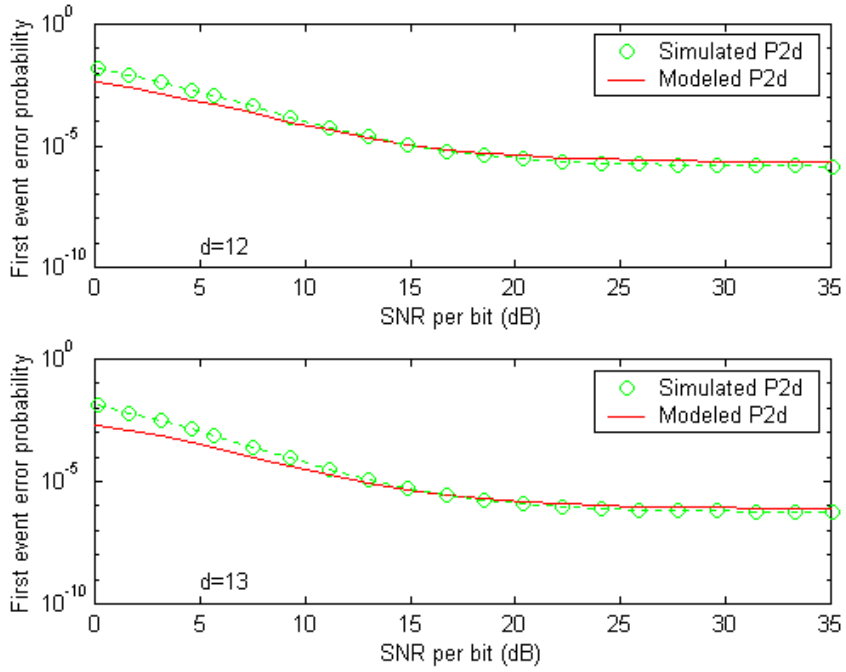

Figure 3.32. First Event Error Probability $P_2(12)$ and $P_2(13)$ with 60 Users Per Cell and 60° Sectoring, for $m = 0.75$.

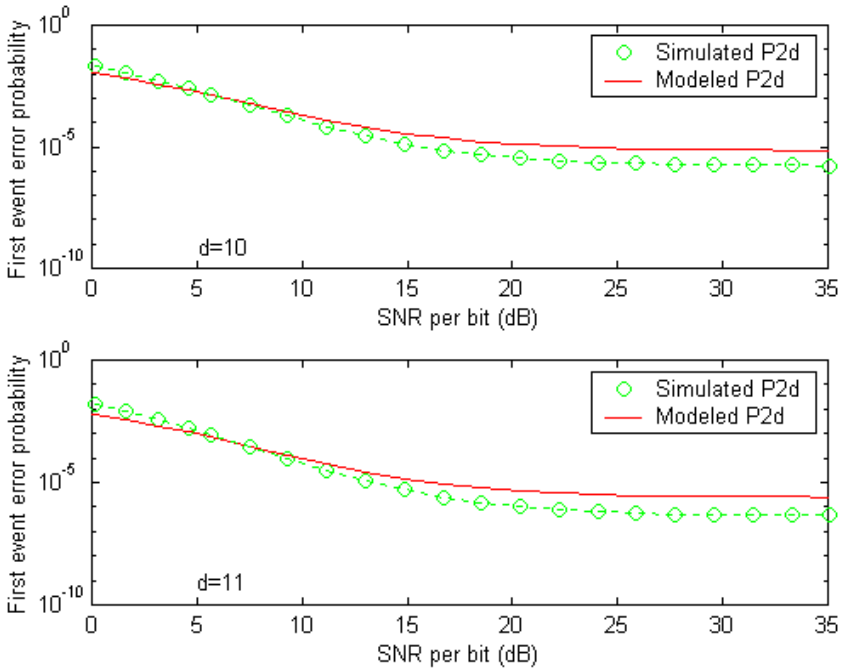

Figure 3.33. First Event Error Probability $P_2(10)$ and $P_2(11)$ with 60 Users Per Cell and 60° Sectoring, for m = 1.5.

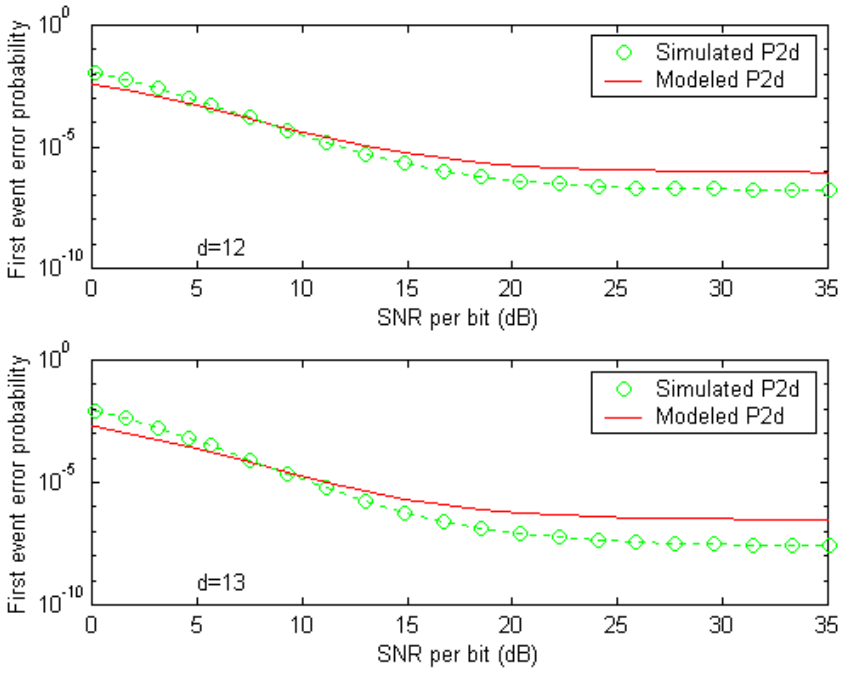

Figure 3.34. First Event Error Probability $P_2(12)$ and $P_2(13)$ with 60 Users Per Cell and 60° Sectoring, for m = 1.5.

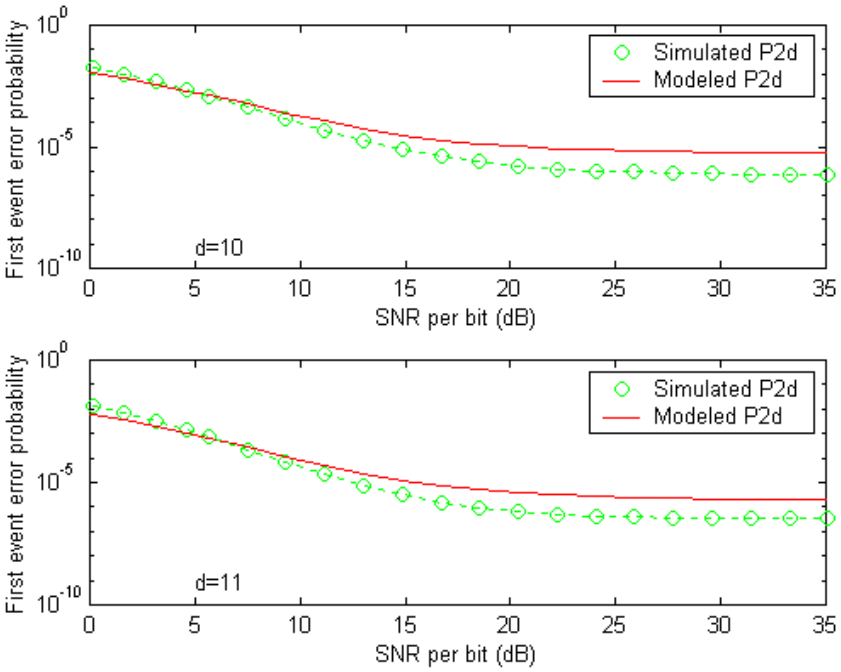

Figure 3.35. First Event Error Probability $P_2(10)$ and $P_2(11)$ with 60 Users Per Cell and 60° Sectoring, for $m = 2$.

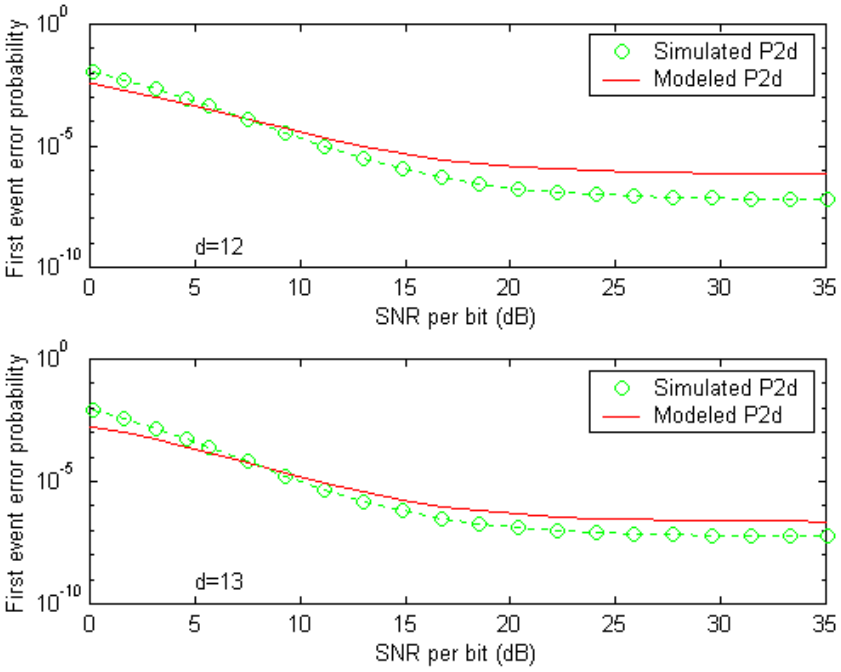

Figure 3.36. First Event Error Probability $P_2(12)$ and $P_2(13)$ with 60 Users Per Cell and 60° Sectoring, for $m = 2$.

Observing Figures 3.27 through 3.36, it can be seen that the model $\tilde{Z}_d$ approximates the simulated results well for $P_2(d)$ for the values of m = 0.5, 0.75, 1.5 and 2. Using these results for $P_2(d)$ and adding them to (3.5), it is possible to compute the modeled probability of bit error for the first five terms in the union bound. Figures 3.37 through 3.41 show the comparison of the modeled and simulated probability of bit error using different values of m. To obtain these results, a rate of ½ convolutional encoder was incorporated with a length of v = 8. The average received SNR per bit for the Nakagami-Lognormal channel is from [1]:

$$\overline{\gamma}_b = \mathrm{E}\left\{\frac{R^2 f_1 P_t T}{N_0 L_H(\boldsymbol{d}) X}\right\} = \mathrm{E}\{R^2\}\mathrm{E}\left\{1/X\right\} = \mathrm{E}\{X\}\frac{E_b}{N_0} \tag{3.27}$$

since $\mathrm{E}\{R^2\} = \Omega = 1$ has been normalized.

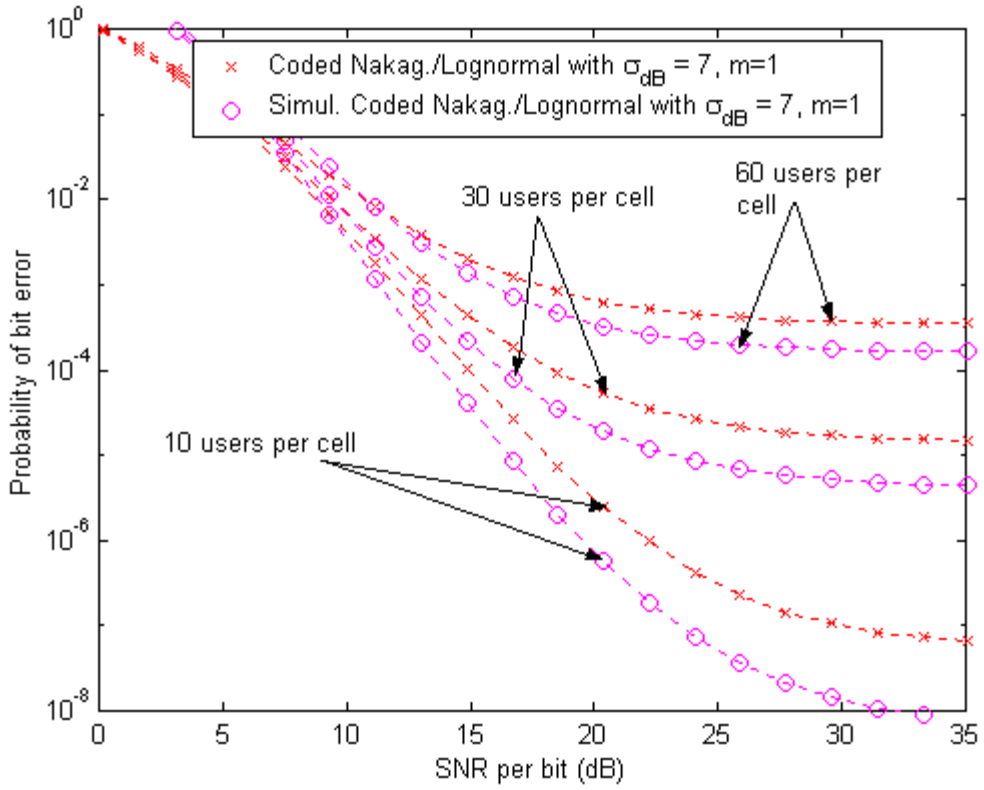

Figure 3.37. Probability of Bit Error for DS-CDMA with Nakagami Fading with m = 1 (Rayleigh Case) and Lognormal Shadowing $(\sigma_{dB} = 7)$ using Six Sectors and a Rate ½ Convolutional Encoder with v = 8.

For the case of v = 8, the modeled and simulated results of $P_2(d)$ were obtained for d =10 through 14 since $d_{free} = 10$ and $\beta_{10} = 2,\ \beta_{11} = 22,\ \beta_{12} = 60,\ \beta_{13} = 148,\ \beta_{14} = 340$ [1]. By selecting the Nakagami parameter to be m = 1, the channel becomes a Rayleigh-Lognormal channel.

Comparing the modeled and simulated probability of bit error, it can be observed that the modeled and simulated results do not differ much. More specifically, at the range 10 to 15 dB (probability of bit error 10^{-3} to 10^{-4}) the differences between the modeled and simulated results are quite small. This particular range of SNR is a practical one in which DS-CDMA cellular systems operate. Differences between the modeled and simulated results become notable when the interference floor is in a range between 10^{-4} and 10^{-7}. The difference in the probability of bit error as the number of users per cell increases from 10 to 60 should also be mentioned. Channel bit error probability becomes worse as the number of users in a cell increases due to co-channel interference.

Figure 3.38 is similar to Figure 3.37, that compares the modeled and simulated probability of bit error but for a different value of m. In this case, the Nakagami parameter m equals to 0.5. This type of fading is more severe than Rayleigh fading. The differences in the fading environment as the value of m varies will be examined later in this chapter. As for the differences in the modeled and simulated results, the same comments from the previous figure apply, but in this case, the probability of bit error is worse when comparing to the previous one for all the range values of SNR.

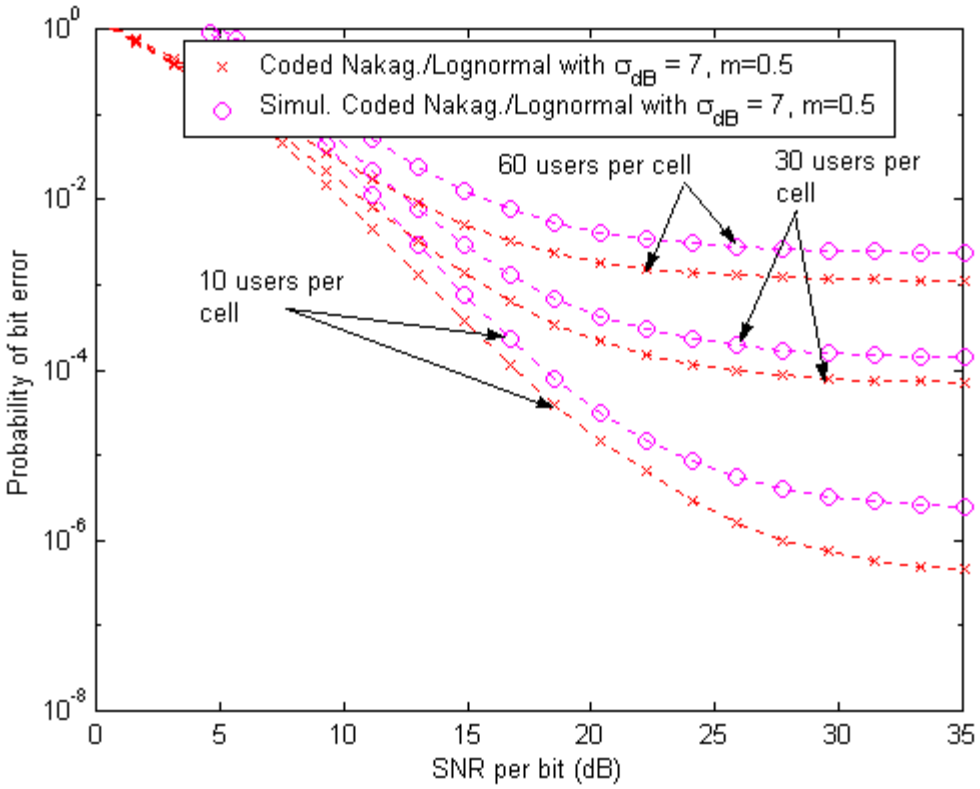

Figure 3.38. Probability of Bit Error for DS-CDMA with Nakagami Fading with m = 0.5 and Lognormal Shadowing $(\sigma_{dB} = 7)$ using Six Sectors and a Rate ½ Convolutional Encoder with v = 8.

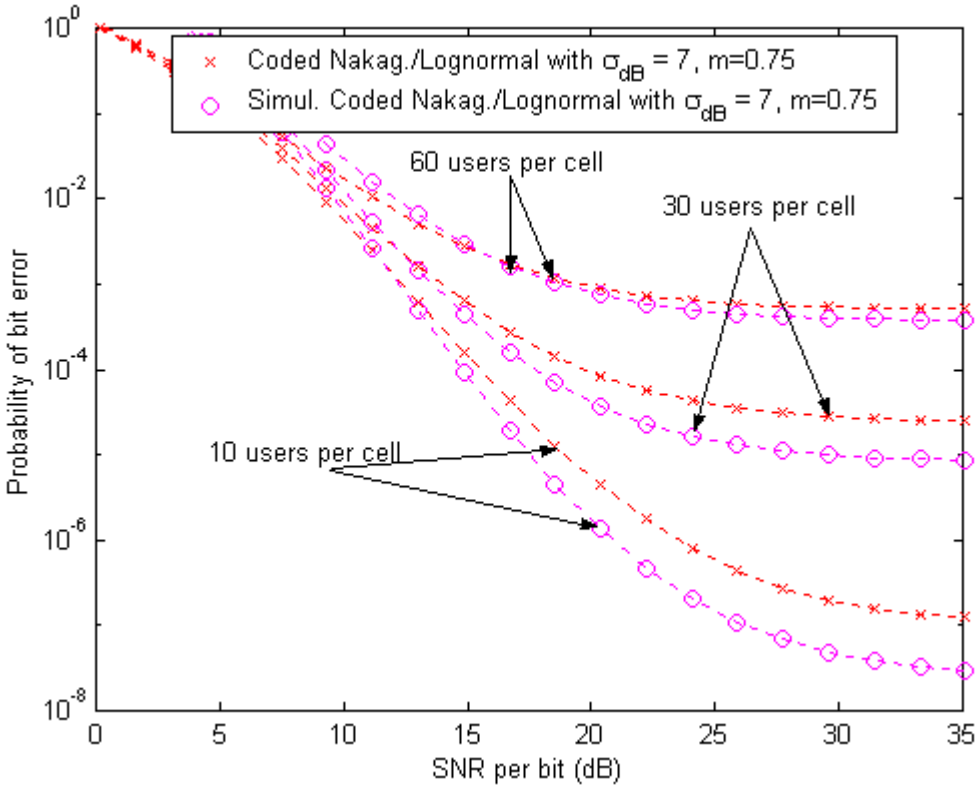

Figure 3.39. Probability of Bit Error for DS-CDMA with Nakagami Fading with m = 0.75 and Lognormal Shadowing $(\sigma_{dB} = 7)$ using Six Sectors and a Rate ½ Convolutional Encoder with v = 8.

In the case of the Nakagami parameter m = 0.75, the modeled and simulated results for the bit error probability are very similar in the range of SNR from 10 to 15 dB.

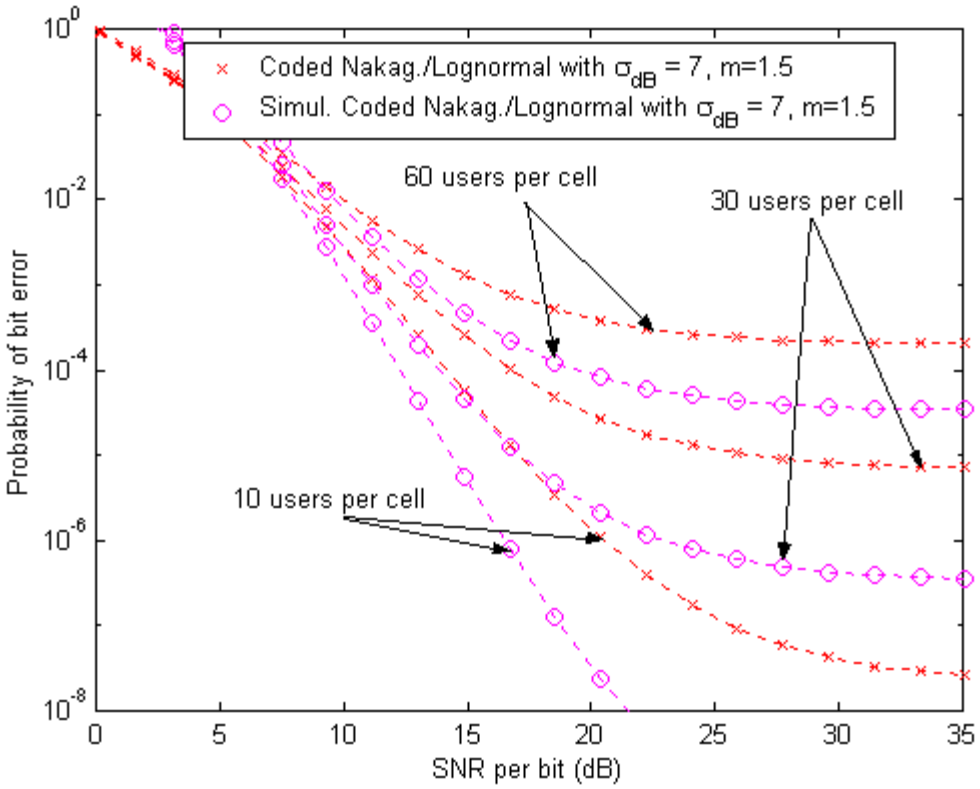

Figure 3.40. Probability of Bit Error for DS-CDMA with Nakagami Fading with m = 1.5 and Lognormal Shadowing $(\sigma_{dB} = 7)$ using Six Sectors and a Rate ½ Convolutional Encoder with v = 8.

In Figure 3.40, it can be seen that the differences between the simulated and modeled probability of error are noteworthy and greater than the previous differences in the SNR range of 20 to 30 dB but they correspond to the interference floor from 10^{-4} to 10^{-7} of bit error probability.

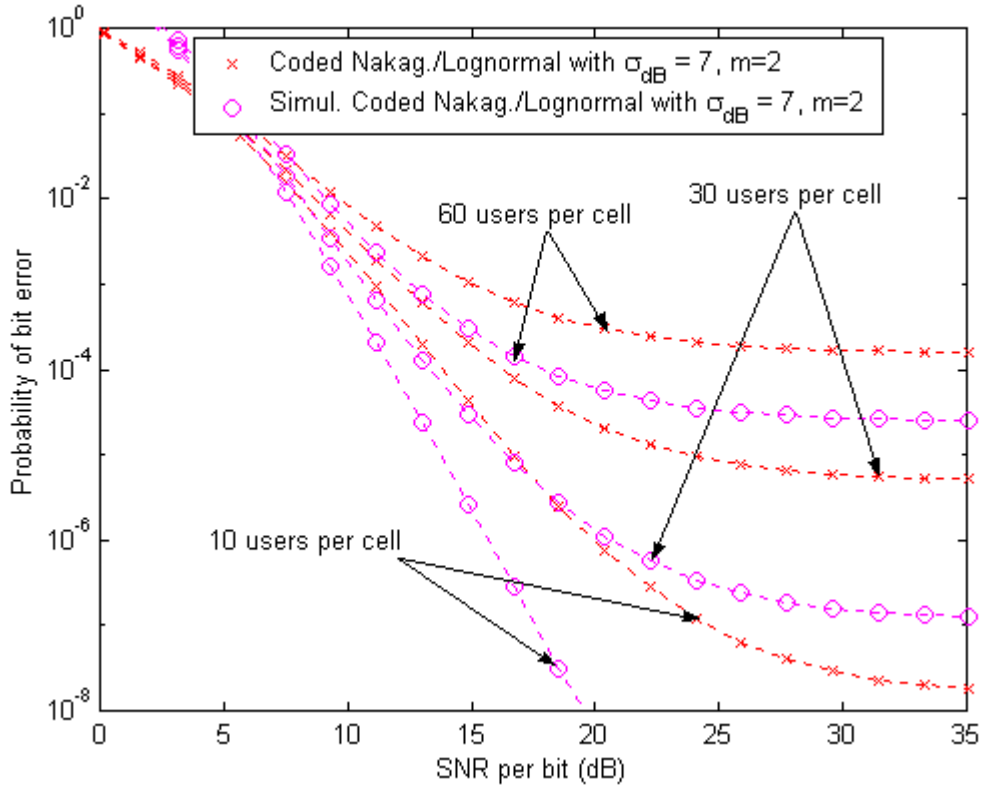

Figure 3.41. Probability of Bit Error for DS-CDMA with Nakagami Fading with $m = 2$ and Lognormal Shadowing $(\sigma_{dB} = 7)$ using Six Sectors and a Rate ½ Convolutional Encoder with $v = 8$.

Figure 3.41 depicts that our modeled and simulated results fit each other in the SNR range 10 to 15 dB in the case of the Nakagami parameter $m = 2$ which corresponds to Ricean fading. There is LOS path between the base station and the mobile user. Appendix III-D shows similar results for $\sigma_{dB} = 4$. The objective of the next Section is to use these results to explore the performance analysis of our system in a Nakagami Fading and Lognormal Shadowing environment.

C. BIT ERROR ANALYSIS OF DS-CDMA WITH FEC

In the previous Section, a model was created which is a useful tool for approximating the distribution for a sum of multiplicative Nakagami square-Lognormal

random variables. In this Section, by using this approximation, the performance of DS-CDMA with FEC will be analyzed for the different values of the Nakagami parameter *m*. Figures 3.42 through 3.47 show these results for 20, 40, and 60 users per adjacent cell respectively for both modeled and Monte Carlo simulated results. In each case, the Nakagami parameter *m* varies for the specific values of $m = 0.5$, $m = 0.75$, $m = 1$, $m = 1.5$ and $m = 2$.

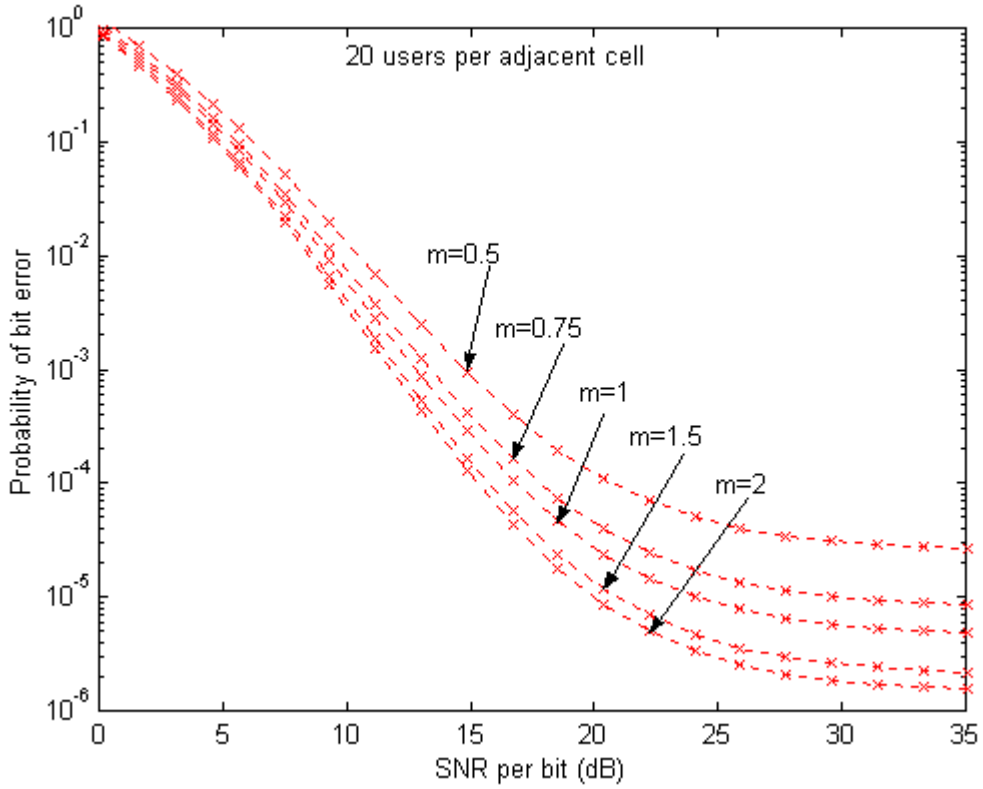

Figure 3.42. Probability of Bit Error for DS-CDMA Predicted by Model with FEC in Various Fading Conditions with 20 Users Per Cell, Employing a 60° Sectoring ($R_{cc} = 1/2$ and $v = 8$) and Lognormal Shadowing of $\sigma_{dB} = 7$.

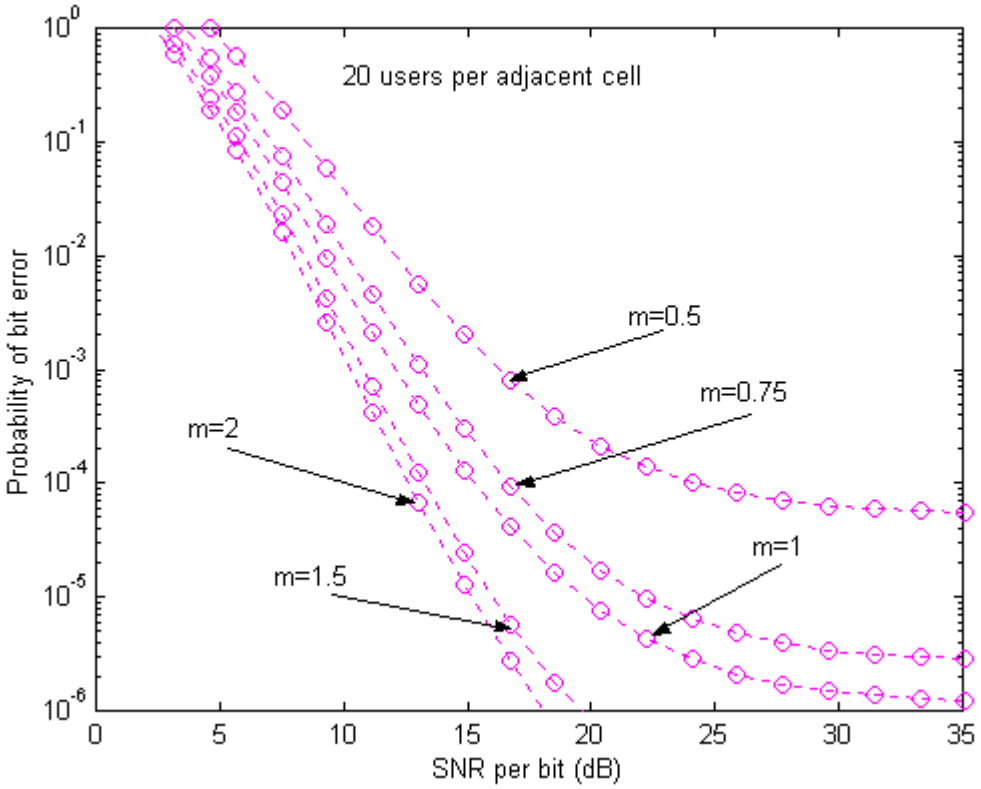

Figure 3.43. Probability of Bit Error for DS-CDMA Predicted by Monte Carlo Simulations with FEC in Various Fading Conditions with 20 Users Per Cell, Employing a 60° Sectoring (R_{cc} = 1/2 and v = 8) and Lognormal Shadowing of $\sigma_{dB} = 7$.

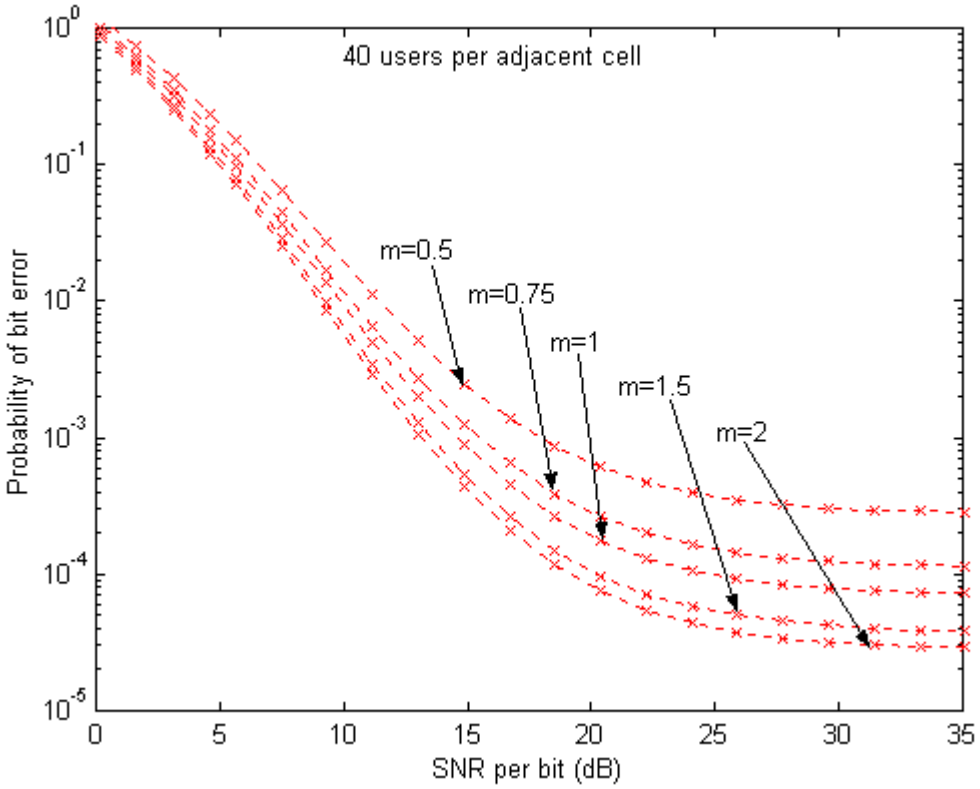

Figure 3.44. Probability of Bit Error for DS-CDMA Predicted by Model with FEC in Various Fading Conditions with 40 Users Per Cell, Employing a 60° Sectoring ($R_{cc} = 1/2$ and $v = 8$) and Lognormal Shadowing of $\sigma_{dB} = 7$.

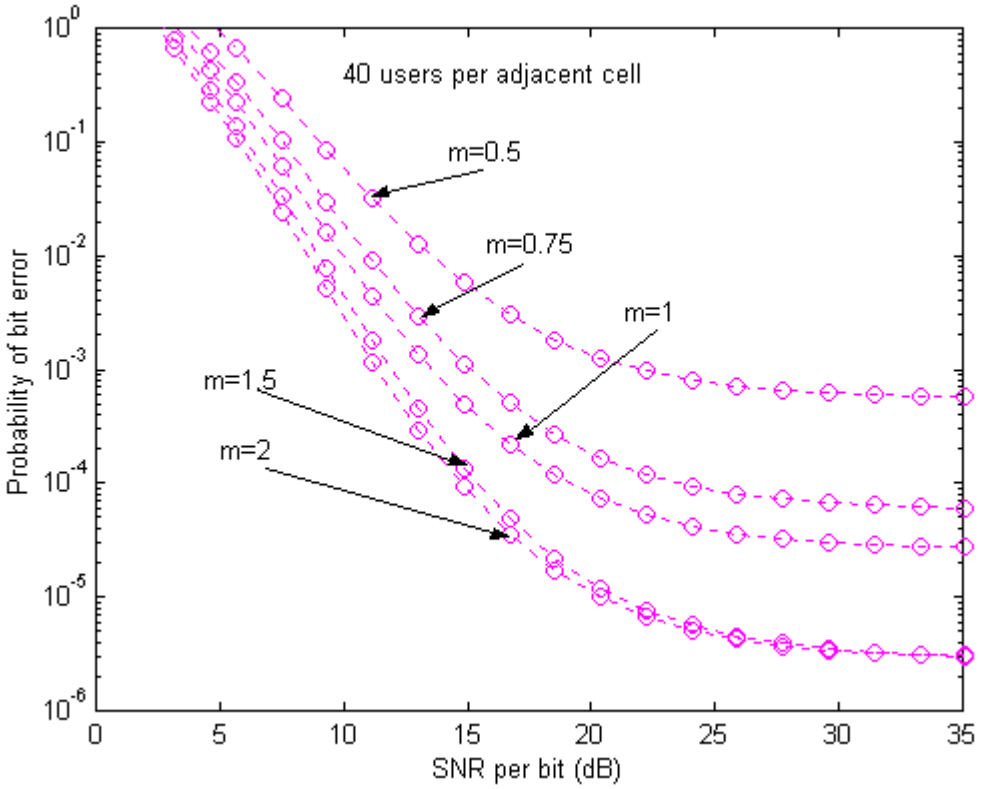

Figure 3.45. Probability of Bit Error for DS-CDMA Predicted by Monte Carlo Simulations with FEC in Various Fading Conditions with 40 Users Per Cell, Employing a 60° Sectoring (R_{cc} = 1/2 and v = 8) and Lognormal Shadowing of $\sigma_{dB} = 7$.

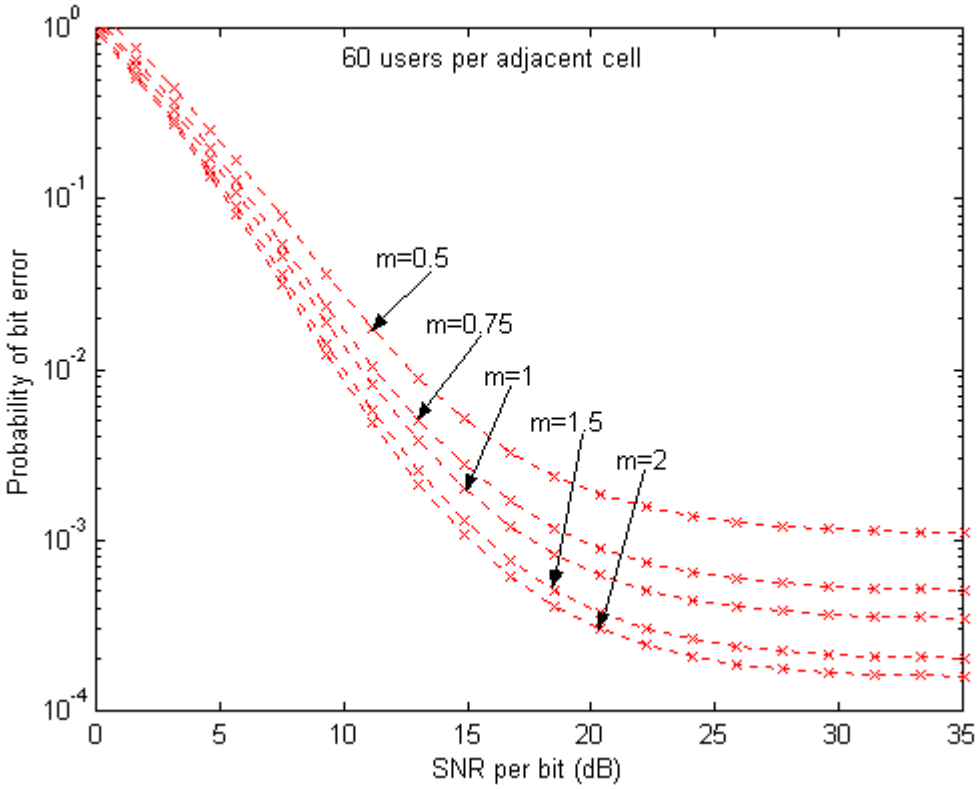

Figure 3.46. Probability of Bit Error for DS-CDMA Predicted by Model with FEC in Various Fading Conditions with 60 Users Per Cell, Employing a 60° Sectoring ($R_{cc} = 1/2$ and $v = 8$) and Lognormal Shadowing of $\sigma_{dB} = 7$.

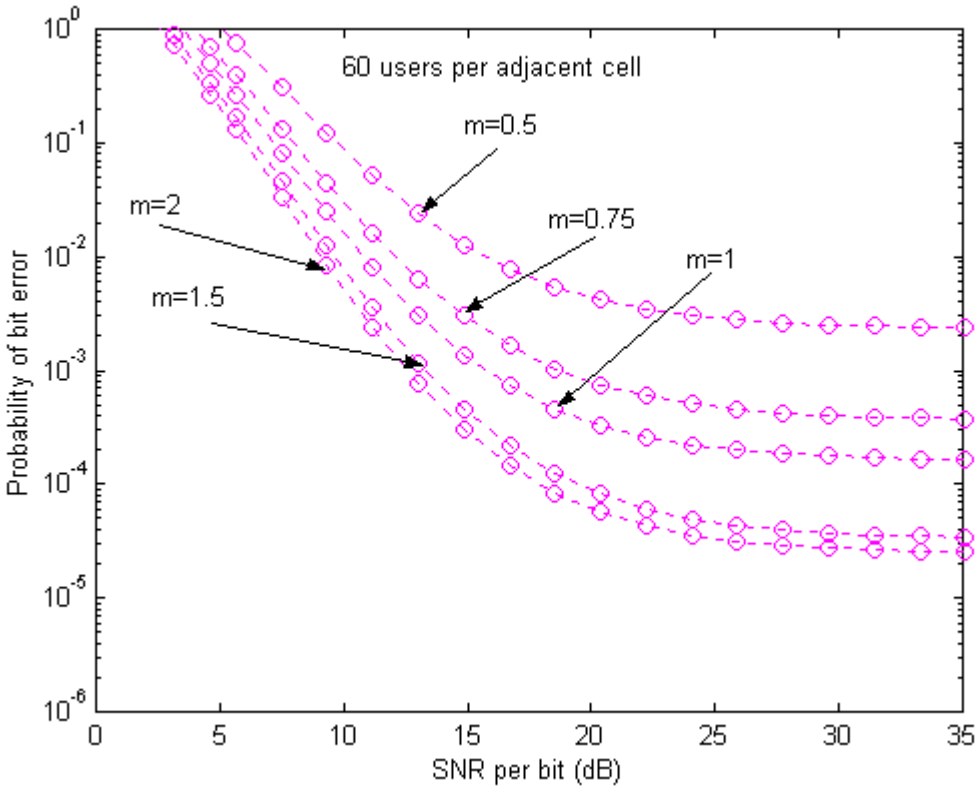

Figure 3.47. Probability of Bit Error for DS-CDMA Predicted by Monte Carlo Simulations with FEC in Various Fading Conditions with 60 Users Per Cell, Employing a 60° Sectoring ($R_{cc} = 1/2$ and $v = 8$) and Lognormal Shadowing of $\sigma_{dB} = 7$.

From Figures 3.42, through 3.47, it can be seen that when our channel operates in a fading environment where m = 0.5, it performs worse than it does for the other four values of m. On the other hand, when m = 2, the case of Ricean Fading, a LOS path occurs and our channel performs better than it does for the other types of fading. An average fading condition between them is the Rayleigh Fading environment where m = 1. There is no great difference in the performance of our system when the value of m goes from 1.5 to 2. It should also be noted how the interference floor varies as the number of users increases per adjacent cell. In the case of Figure 3.42 with 20 users per adjacent cell, the interference floor corresponds to a probability of bit error from 10^{-4} to 10^{-5}. Furthermore, for SNR = 15 dB, our system achieves a probability of bit error from 10^{-3} to 10^{-4} for the five types of fading environment. As the number of users per adjacent cell increases from 20 to 40, as shown in Figure 3.44, the intercell interference increases. The

new level now is above 10^{-4} of bit error probability. For the same value of SNR (15 dB) our system can now achieve a bit error probability of 10^{-3} to 10^{-2} for the different types of fading. Comparing the results from Figures 3.42 and 3.44, our system performs better in Figure 3.42 because of the lesser amount of intercell interference. Additionally, results become worse if the number of users per adjacent cell increases to 60 as seen in Figure 3.46. For SNR =15 dB, a bit error probability of 10^{-3} to 10^{-2} can be achieved and the interference floor is above 10^{-3} to 10^{-4}. Similar figures are obtained in Appendix III-E for $\sigma_{dB} = 4$. If the 60° sectoring directional antennas with constant gain inside the 60° antenna pattern and zero dB gain outside of it, are replaced with 120° antennas or with one antenna (no sectoring case), the amount of intercell interference increases by a factor of 3 and 6 respectively. Figures 3.48 through 3.57 show the results obtained using the model and the Monte Carlo simulations with six sectors, three sectors and one sector.

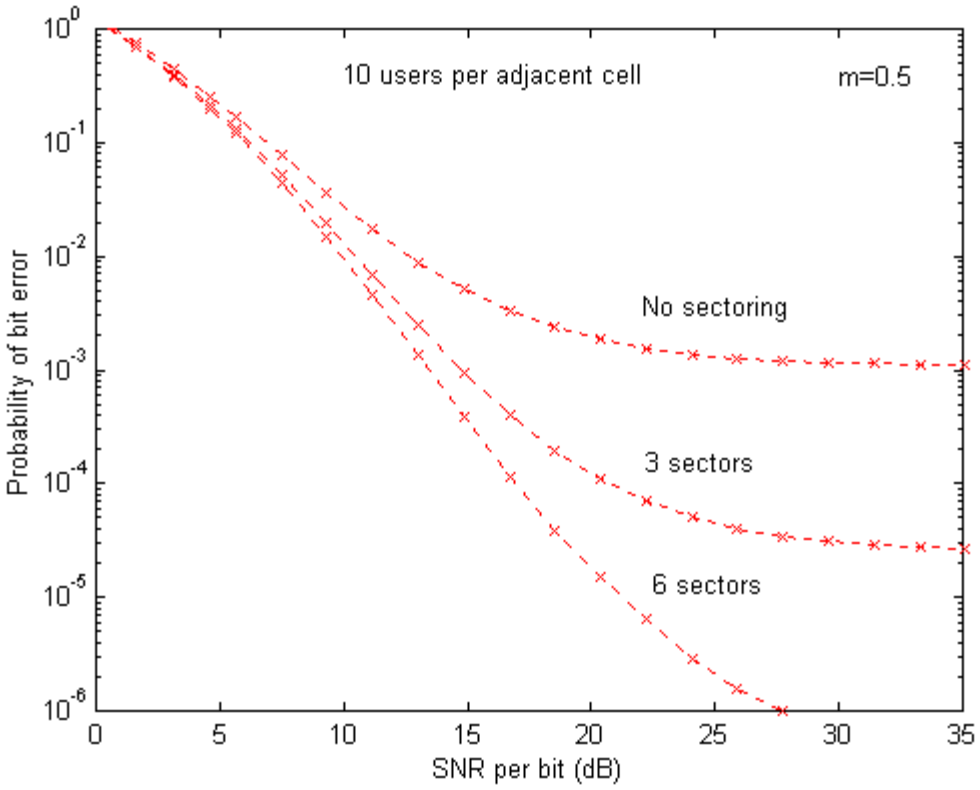

Figure 3.48. Probability of Bit Error for DS-CDMA Predicted by Model Using Sectoring for $m = 0.5$ and $\sigma_{dB} = 7$ ($R_{cc} = 1/2$ and $v = 8$).

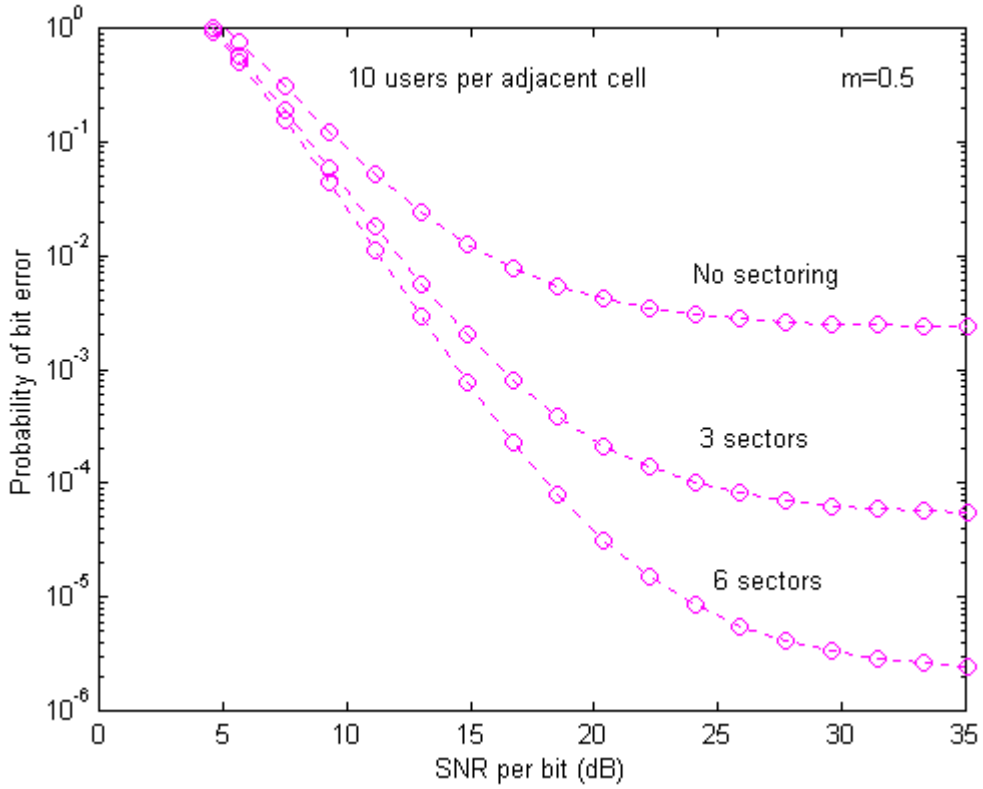

Figure 3.49. Probability of Bit Error for DS-CDMA Predicted by Monte Carlo Simulations Using Sectoring for $m = 0.5$ and $\sigma_{dB} = 7$ ($R_{cc} = 1/2$ and $v = 8$).

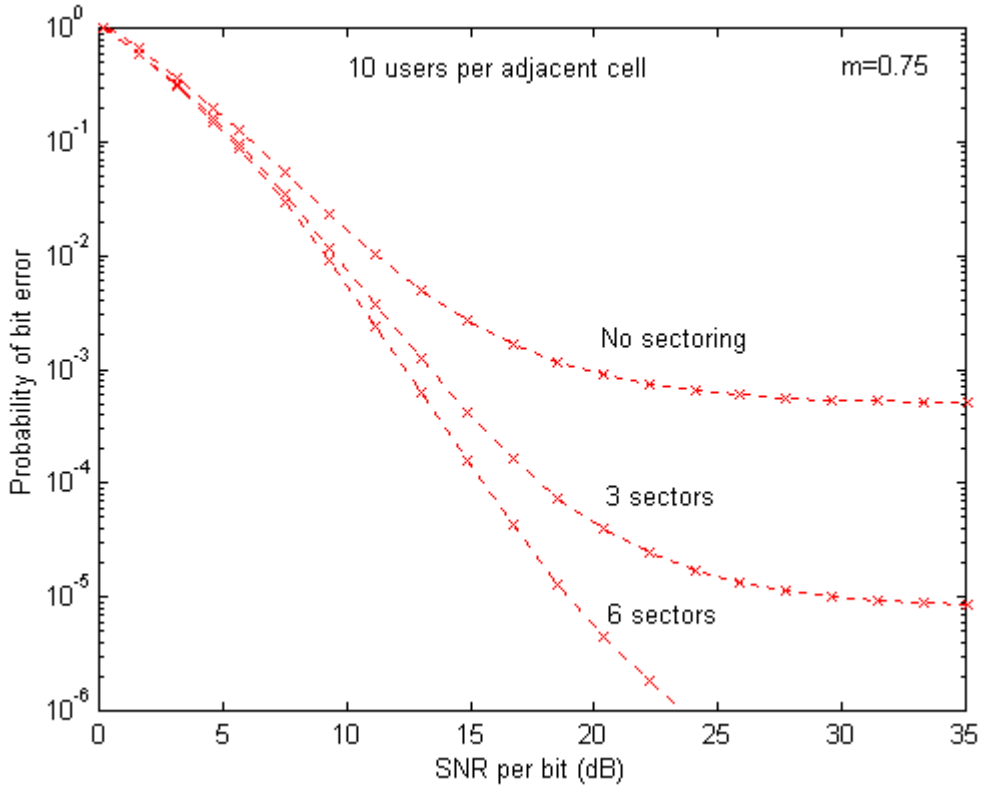

Figure 3.50. Probability of Bit Error for DS-CDMA Predicted by Model Using Sectoring for $m = 0.75$ and $\sigma_{dB} = 7$ ($R_{cc} = 1/2$ and $v = 8$).

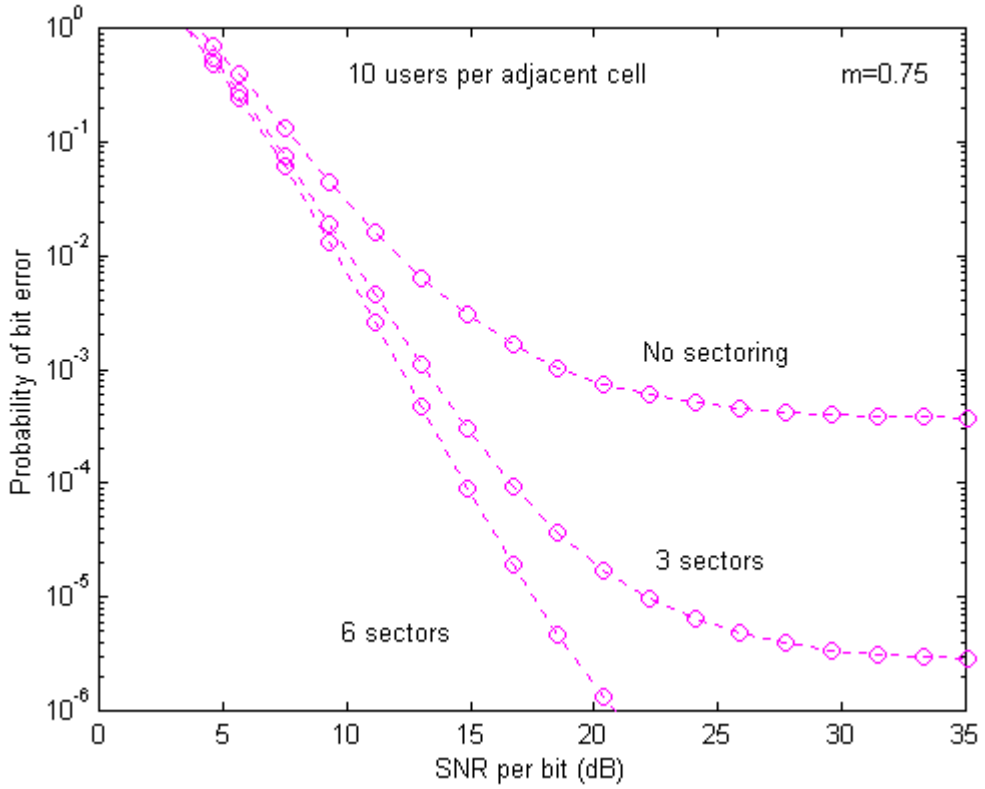

Figure 3.51. Probability of Bit Error for DS-CDMA Predicted by Monte Carlo Simulations Using Sectoring for $m = 0.75$ and $\sigma_{dB} = 7$ ($R_{cc} = 1/2$ and $v = 8$).

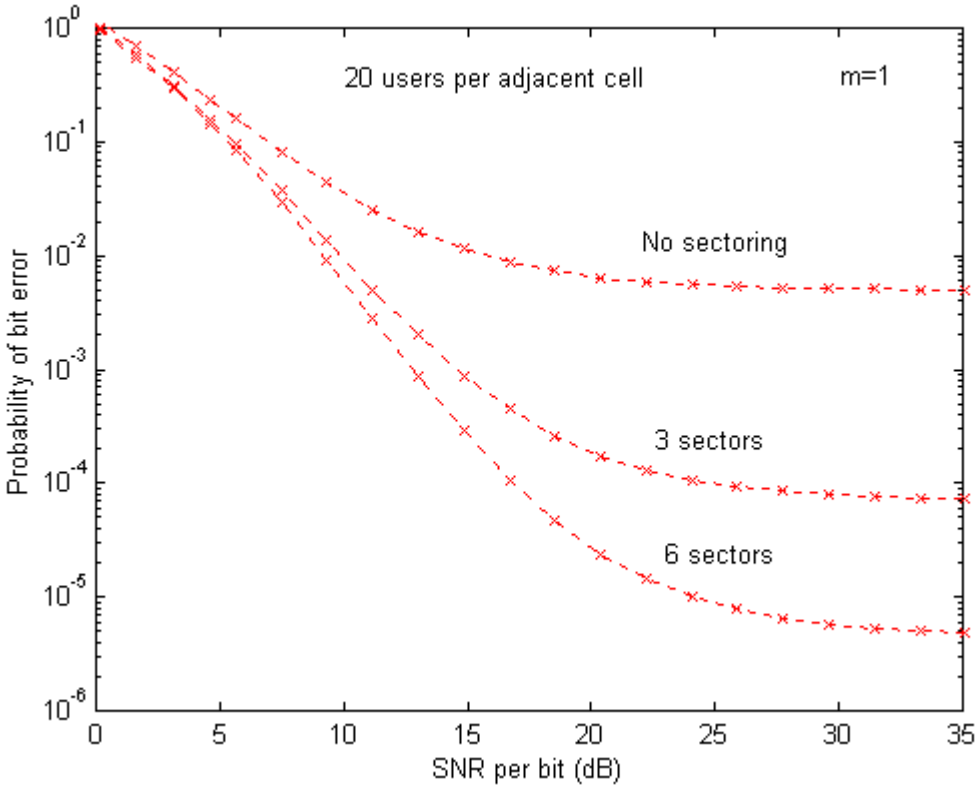

Figure 3.52. Probability of Bit Error for DS-CDMA Predicted by Model Using Sectoring for $m = 1$ and $\sigma_{dB} = 7$ ($R_{cc} = 1/2$ and $v = 8$).

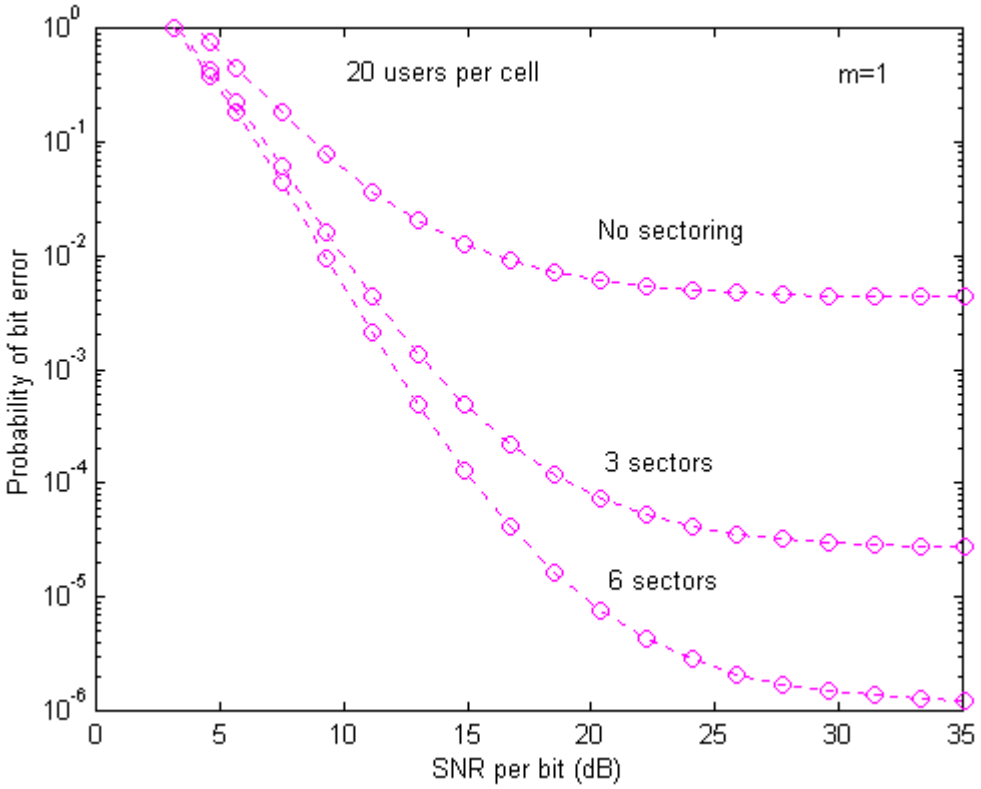

Figure 3.53. Probability of Bit Error for DS-CDMA Predicted by Monte Carlo Simulations Using Sectoring for $m = 1$ and $\sigma_{dB} = 7$ ($R_{cc} = 1/2$ and $v = 8$).

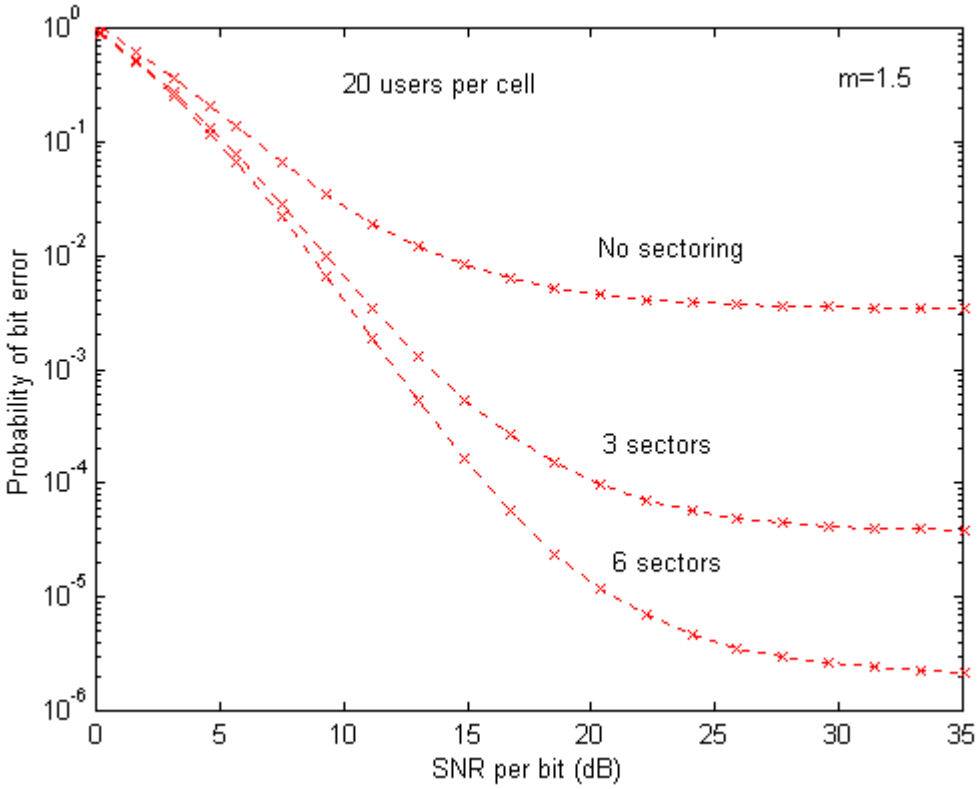

Figure 3.54. Probability of Bit Error for DS-CDMA Predicted by Model Using Sectoring for $m = 1.5$ and $\sigma_{dB} = 7$ ($R_{cc} = 1/2$ and $v = 8$).

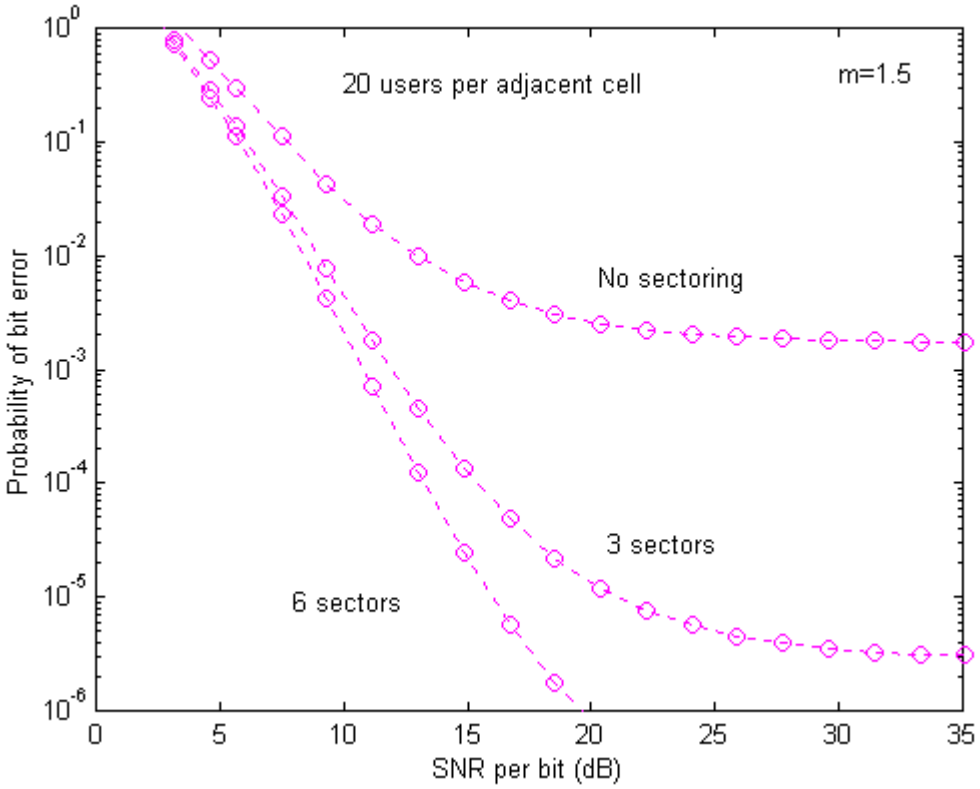

Figure 3.55. Probability of Bit Error for DS-CDMA Predicted by Monte Carlo Simulations Using Sectoring for $m = 1.5$ and $\sigma_{dB} = 7$ ($R_{cc} = 1/2$ and $v = 8$).

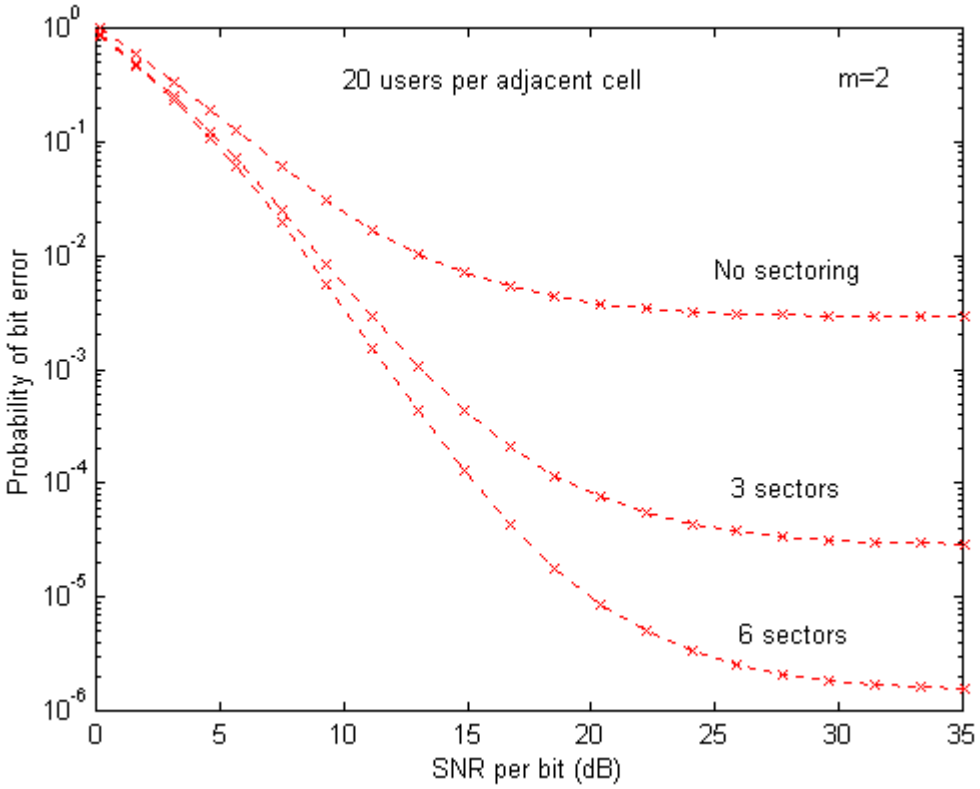

Figure 3.56. Probability of Bit Error for DS-CDMA Predicted by Model Using Sectoring for $m = 2$ and $\sigma_{dB} = 7$ ($R_{cc} = 1/2$ and $v = 8$).

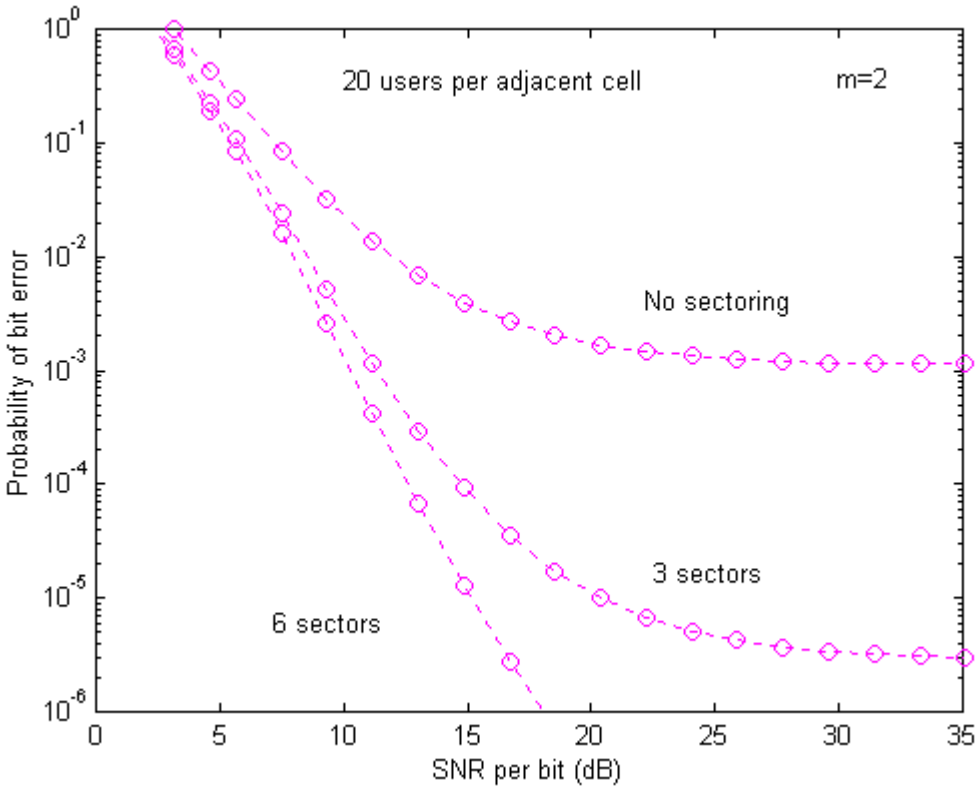

Figure 3.57. Probability of Bit Error for DS-CDMA Predicted by Monte Carlo Simulations Using Sectoring for $m = 2$ and $\sigma_{dB} = 7$ ($R_{cc} = 1/2$ and $v = 8$).

The degradation in performance is obvious when changing to 120° sectoring or no sectoring in all the above cases.

D. SUMMARY

In this chapter, given the expression for the upper bound on the probability of bit error, the performance of the DS-CDMA cellular system operating in a Nakagami-*m*-Lognormal channel was analyzed under various operating conditions. However, in order to be able to analyze the DS-CDMA cellular system performance, the sum of *d* Nakagami-square-Lognormal random variables is approximated as a multiplicative Nakagami-square-Lognormal random variable by the use of the model $\tilde{Z}_d$. Our performance analysis took into account that our intended mobile user was in the worst-

case position at the edge of the center cell shown in Figure 3.1, and that 60° sectoring was employed by using six directional antennas at the base stations. Using this type of antenna at the base station, the number of interferers decreased from 6 to 1 in the first tier assuming a 7-cell reuse pattern. Furthermore, by varying the Nakagami parameter *m*, it was possible to see how our system performed in various severe types of fading. The worst case of system performance was the one-sided Gaussian fading environment, which corresponds to a value of the Nakagami-*m* parameter of 0.5. On the other hand, the less severe fading environment was Ricean Fading ($m = 2$) where there is a LOS path between the transmitting base station and the intended user. The improvement in our system's performance is obvious when changing from $m = 0.5$ to $m = 2$. In the next chapter, more realistic results will be shown by assuming that the mobile user is randomly distributed in the cell.

APPENDIX III-A. DEVELOPMENT OF THE PDF OF THE NAKAGAMI-SQUARE RANDOM VARIABLE AND THE PDF OF THE SUM OF INDEPENDENT NAKAGAMI-SQUARE RANDOM VARIABLES

It is known that the pdf of a Nakagami random variable R_l is given as follows:

$$f_{R_l}(r_l) = \frac{2}{\Gamma(m)}\left(\frac{m}{\Omega}\right)^m r_l^{2m-1} \exp\left(\frac{-mr_l^2}{\Omega}\right) \tag{3.28}$$

Given (3.28), we can compute the pdf of the Nakagami-square random variable R_l^2 using the transformation $Y = R_l^2$. Then for the pdf of R_l^2 we get:

$$f_Y(y) = \frac{1}{2\sqrt{y}}\left[f_{R_l}\left(-\sqrt{y}\right) + f_{R_l}\left(\sqrt{y}\right)\right] \tag{3.29}$$

and since our random variable has only positive values, Equation (3.29) becomes:

$$\begin{aligned} f_Y(y) &= \frac{1}{2\sqrt{y}} f_{R_l}\left(\sqrt{y}\right) \\ &= \frac{1}{\Gamma(m)}\left(\frac{m}{\Omega}\right)^m \sqrt{y}^{2(m-1)} \exp\left(\frac{-my}{\Omega}\right) \end{aligned} \tag{3.30}$$

Substituting Y with R_l^2 we get:

$$f_{R_l^2}(r_l^2) = \frac{1}{\Gamma(m)}\left(\frac{m}{\Omega}\right)^m r_l^{2(m-1)} \exp\left(\frac{-mr_l^2}{\Omega}\right) \tag{3.31}$$

Given the pdf of the Nakagami-square random variable we can compute the characteristic function of the Nakagami-square random variable as follows:

$$\begin{aligned} \Psi_Y(\mathrm{j}\omega) &= \int_{-\infty}^{\infty} f_Y(y) \exp(\mathrm{j}\omega y)\, dy \\ &= \frac{1}{\Gamma(m)}\left(\frac{m}{\Omega}\right)^m \int_0^{\infty} y^{m-1} \exp\left[-\left(\frac{m}{\Omega} - \mathrm{j}\omega\right) y\right] dy \end{aligned} \tag{3.32}$$

By the use of the following identity from [8]:

$$\int_0^\infty \boldsymbol{x}^{\nu-1} \exp\left(-\mu \boldsymbol{x}\right) d\boldsymbol{x} = \frac{\Gamma\left(\nu\right)}{\mu^{\nu}}, \;\; \mathrm{Re}(\mu) > 0, \;\; \mathrm{Re}(\nu) > 0 \tag{3.33}$$

where $\Gamma(\nu)$ is the gamma function defined by:

$$\Gamma\left(\nu\right) = \int_0^\infty \boldsymbol{x}^{\nu-1} \exp(-\boldsymbol{x}) d\boldsymbol{x}, \;\; \nu > 0 \tag{3.34}$$

and make the following substitutions:

$\frac{m}{\Omega} - \mathrm{j}\omega = \mu$ and $\nu = \mu$ we get for the characteristic function of the Nakagami-square random variable the following equation:

$$\begin{aligned} \Psi_Y\left(\mathrm{j}\omega\right) &= \frac{1}{\Gamma\left(m\right)} \left(\frac{m}{\Omega}\right)^m \frac{\Gamma\left(m\right)}{\left(\frac{m}{\Omega} - \mathrm{j}\omega\right)^m} \\ &= \frac{\left(\frac{m}{\Omega}\right)^m}{\left(\frac{m}{\Omega} - \mathrm{j}\omega\right)^m} \end{aligned} \tag{3.35}$$

and thus:

$$\Psi_{R_l^2}\left(\mathrm{j}\omega\right) = \frac{\left(\frac{m}{\Omega}\right)^m}{\left(\frac{m}{\Omega} - \mathrm{j}\omega\right)^m} \tag{3.36}$$

Now since R_l^2 are independent random variables the characteristic function of the random variable $Y_{2d} = \sum_{l=1}^{d} R_l^2$ is given as follows:

$$\Psi_{Y_{2d}}(\mathrm{j}\omega) = \frac{\left(\frac{m}{\Omega}\right)^{md}}{\left(\frac{m}{\Omega} - \mathrm{j}\omega\right)^{md}} \tag{3.37}$$

so the pdf of the sum of d Nakagami-square random variables is given by:

$$f_{Y_{2d}}(y_{2d}) = \frac{1}{2\pi}\int_{-\infty}^{\infty} \frac{\left(\frac{m}{\Omega}\right)^{md}}{\left(\frac{m}{\Omega} - \mathrm{j}\omega\right)^{md}} \exp(-\mathrm{j}\omega y_{2d})\, d\omega \tag{3.38}$$

Substituting $\frac{m}{\Omega} = \alpha_1$ and $md = \alpha_2$, Equation (3.38) becomes:

$$f_{Y_{2d}}(y_{2d}) = \frac{1}{2\pi}\int_{-\infty}^{\infty} \frac{\alpha_1^{\alpha_2}}{(\alpha_1 - \mathrm{j}\omega)^{\alpha_2}} \exp(-\mathrm{j}\omega y_{2d})\, d\omega \tag{3.39}$$

Furthermore we can use the following identity from [8]:

$$\int_{-\infty}^{\infty} \frac{\exp(-\mathrm{j}\rho \boldsymbol{x})}{(\beta - \mathrm{j}\boldsymbol{x})^{\nu}} d\boldsymbol{x} = \frac{2\pi\rho^{\nu-1}\exp(-\beta\rho)}{\Gamma(\nu)}\ ,\ \rho > 0 \tag{3.40}$$

and making the substitutions $\beta = \alpha_1$, $\nu = \alpha_2$ and $\rho = y_{2d}$, we get for $f_{Y_{2d}}$:

$$\begin{aligned} f_{Y_{2d}}(y_{2d}) &= \frac{1}{2\pi}\alpha_1^{\alpha_2}\frac{2\pi y_{2d}^{\alpha_2 - 1}\exp(-\alpha_1 y_{2d})}{\Gamma(\alpha_2)} \\ &= \left(\frac{m}{\Omega}\right)^{md}\frac{y_{2d}^{md-1}}{\Gamma(md)}\exp\left(-\frac{m y_{2d}}{\Omega}\right) \end{aligned} \tag{3.41}$$

THIS PAGE INTENTIONALLY LEFT BLANK

APPENDIX III-B. VARIANCE OF R^2X

The variance of the product of the Nakagami-square random variable and the Lognormal random variable can be computed as follows. Assume that $A = R^2 X$, then

$$\mathrm{E}\left\{A^2\right\} = \mathrm{E}\left\{R^4 X^2\right\} = \mathrm{E}\left\{R^4\right\}\mathrm{E}\left\{X^2\right\} \tag{3.42}$$

$$\mathrm{Var}\left\{R^2 X\right\} = \mathrm{E}\left\{R^4 X^2\right\} - \left[\mathrm{E}\left\{R^2 X\right\}\right]^2 \tag{3.43}$$

The characteristic function of R^2 is as follows:

$$\Psi_{R^2}(\mathrm{j}\omega) = \frac{\left(\frac{m}{\Omega}\right)^m}{\left(\frac{m}{\Omega} - \mathrm{j}\omega\right)^m} \tag{3.44}$$

Taking the derivative of both sides in Equation (3.44) with respect to ω, the following appears:

$$\begin{aligned}\Psi'_{R^2}(\mathrm{j}\omega) &= \frac{-\left(\frac{m}{\Omega}\right)^m m\left(\frac{m}{\Omega} - \mathrm{j}\omega\right)^{m-1}(-\mathrm{j})}{\left(\frac{m}{\Omega} - \mathrm{j}\omega\right)^{2m}} \\ &= \frac{\mathrm{j}\left(\frac{m}{\Omega}\right)^m m}{\left(\frac{m}{\Omega} - \mathrm{j}\omega\right)^{m+1}}\end{aligned} \tag{3.45}$$

The second derivative of the characteristic function is:

$$\Psi''_{R^2}(\mathrm{j}\omega) = \frac{-\mathrm{j}\left(\frac{m}{\Omega}\right)^m (m+1)\left(\frac{m}{\Omega} - \mathrm{j}\omega\right)^m (-\mathrm{j})}{\left(\frac{m}{\Omega} - \mathrm{j}\omega\right)^{2m+2}}$$

$$= -\frac{m\left(\frac{m}{\Omega}\right)^m (m+1)}{\left(\frac{m}{\Omega} - \mathrm{j}\omega\right)^{m+2}} \tag{3.46}$$

It is already assumed that $\mathrm{E}\{R^2\} = \Omega = 1$ and it is known that:

$$\mathrm{E}\left[\{R^2\}^2\right] = \frac{1}{\mathrm{j}^2}\frac{d^2}{d\omega^2}\Psi_{R^2}(\mathrm{j}\omega)\big|_{\omega=0}$$

$$= \frac{m\left(\frac{m}{\Omega}\right)^m (m+1)}{\left(\frac{m}{\Omega}\right)^{m+2}}$$

$$= \frac{(m+1)\Omega^2}{m} \tag{3.47}$$

From [1] it is also given that:

$$\mathrm{E}\{X^2\} = \exp\left(2\sigma_x^2\right) \tag{3.48}$$

Applying Equations (3.47) and (3.48) into (3.42):

$$\mathrm{E}\{A^2\} = \frac{m+1}{m}\Omega^2 \exp\left(2\sigma_x^2\right) \tag{3.49}$$

Since $\mathrm{E}\{R^2 X\} = \mathrm{E}\{R^2\}\mathrm{E}\{X\} = \Omega^2 \exp\left(\sigma_x^2/2\right)$ and $\Omega^2 = 1$, Equation (3.43) becomes:

$$\begin{aligned}\mathrm{Var}\left\{R^2X\right\} &= \frac{m+1}{m}\Omega^2\exp\left(2\sigma_x^2\right)-\Omega^2\exp\left(\sigma_x^2\right)\\ &= \exp\left(\sigma_x^2\right)\Omega^2\left[\frac{m+1}{m}\exp\left(\sigma_x^2\right)-1\right]\\ &= \exp\left(\sigma_x^2\right)\left[\frac{m+1}{m}\exp\left(\sigma_x^2\right)-1\right]\end{aligned} \tag{3.50}$$

THIS PAGE INTENTIONALLY LEFT BLANK

APPENDIX III-C. MEAN AND VARIANCE OF THE MODEL

Equation (3.18) gives that $\mathrm{E}\left\{\tilde{Z}_d\right\} = f_1 d \exp\left(\frac{\sigma_x^2}{2}\right)$. Equation (3.13) gives that $\mathrm{E}\left\{\tilde{Z}_d\right\} = \Omega d \exp\left(\mu_z + \frac{\sigma_z^{\,2}}{2}\right)$. Equating the last two equations we get:

$$\begin{aligned} f_1 d \exp\left(\frac{\sigma_x^2}{2}\right) &= \Omega d \exp\left(\mu_z + \frac{\sigma_z^{\,2}}{2}\right) \Leftrightarrow \\ \exp\left(\frac{\sigma_x^2}{2} - \mu_z - \frac{\sigma_z^2}{2}\right) &= \frac{1}{f_1} \Leftrightarrow \\ \frac{\sigma_x^2 - \sigma_z^2}{2} - \mu_z &= -\ln f_1 \Leftrightarrow \\ \mu_z &= \frac{\sigma_x^2 - \sigma_z^2}{2} + \ln f_1 \end{aligned} \tag{3.51}$$

Equation (3.17) gives:

$$\begin{aligned} \mathrm{Var}\left\{\tilde{Z}_d\right\} = \Omega^2 &\left(d^2 + \frac{d}{m}\right)\exp\left(2\mu_z + 2\sigma_z^2\right) \\ &- d^2 \exp\left(2\mu_z + 2\sigma_z^2\right)\Omega^2 \end{aligned}$$

Equation (3.20) gives:

$$\mathrm{Var}\left\{\tilde{Z}_d\right\} = f_2 d \mathrm{Var}\left\{R^2 X\right\}$$

Equation (3.21) gives:

$$\begin{aligned} \mathrm{Var}\left\{R^2 X^2\right\} &= \Omega^2 \exp\left(\sigma_x^2\right)\left[\frac{m+1}{m}\exp\sigma_x^2 - 1\right] \\ &= \exp\left(\sigma_x^2\right)\left[\frac{m+1}{m}\exp\sigma_x^2 - 1\right] \end{aligned}$$

since $\Omega^2 = 1$.

Equating Equations (3.17) and (3.20) and taking into account Equation (3.21) gives the following:

$$f_2 d \exp\sigma_x^2 \left[\frac{m+1}{m} \exp\sigma_x^2 - 1 \right] = \left(d^2 + \frac{d}{m} \right) \exp\left(2\mu_z + 2\sigma_z^2\right) - d^2 \exp\left(2\mu_z + \sigma_z^2\right) \quad (3.52)$$

Applying (3.51) in (3.52) gives:

$$mf_2 d \left[\frac{m+1}{m} \exp\sigma_x^2 - 1 \right] = \left(d^2 m + d \right) \exp\sigma_z^2 f_1^2 - d^2 f_1^2 m \Leftrightarrow$$

$$mf_2 d \left[\frac{m+1}{m} \exp\sigma_x^2 - 1 \right] + d^2 f_1^2 m = \left(d^2 m + d \right) f_1^2 \exp\sigma_z^2 \Leftrightarrow$$

$$\exp\sigma_z^2 = \frac{1}{\left(d^2 m + d \right) f_1^2} mf_2 d \left[\frac{m+1}{m} \exp\sigma_x^2 - 1 \right] + \frac{d^2 f_1^2 m}{\left(d^2 m + d \right) f_1^2} \Leftrightarrow$$

$$\exp\sigma_z^2 = \frac{mf_2}{dm+1} \left[\frac{m+1}{f_1^2 m} \exp\sigma_x^2 - \frac{1}{f_1^2} \right] + \frac{md}{md+1} \Leftrightarrow$$

$$\exp\sigma_z^2 = \frac{m}{md+1} \left[\frac{f_2 \left(m+1 \right)}{f_1^2 m} \exp\sigma_x^2 - \frac{f_2}{f_1^2} \right] + \frac{md}{md+1} \Leftrightarrow$$

$$\exp\sigma_z^2 = \frac{m}{md+1} \left[\frac{f_2 \left(m+1 \right)}{f_1^2 m} \exp\sigma_x^2 - \frac{f_2}{f_1^2} + d \right] \Leftrightarrow$$

$$\sigma_z^2 = \ln\left[\frac{f_2 \left(m+1 \right)}{f_1^2 m} \exp\sigma_x^2 - \frac{f_2}{f_1^2} + d \right] - \ln\left(md+1 \right) + \ln(m) \quad (3.53)$$

APPENDIX III-D. MODELED AND SIMULATED PROBABILITY OF BIT ERROR FOR THE NAKAGAMI-LOGNORMAL CHANNEL USING 60º ANTENNA SECTORING

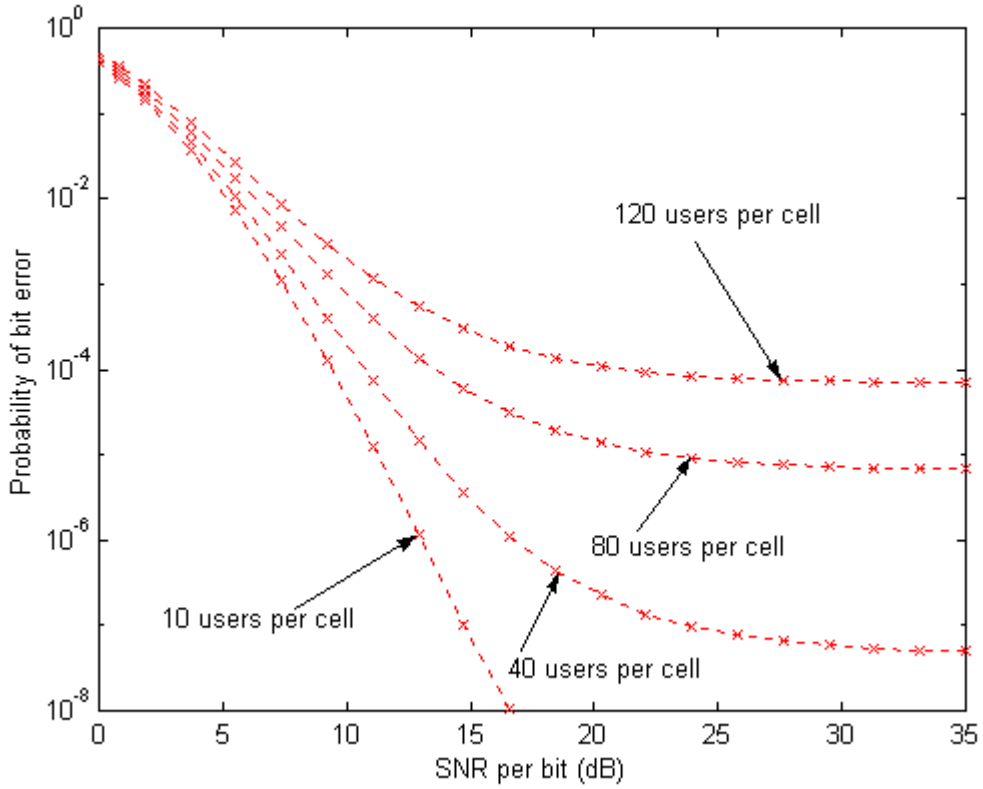

Figure 3.58. Probability of Bit Error for DS-CDMA with Nakagami Fading (m = 0.5) and Lognormal Shadowing $(\sigma_{dB} = 4)$ Using Six Sectors and a Rate 1/2 Convolutional Encoder with v = 8.

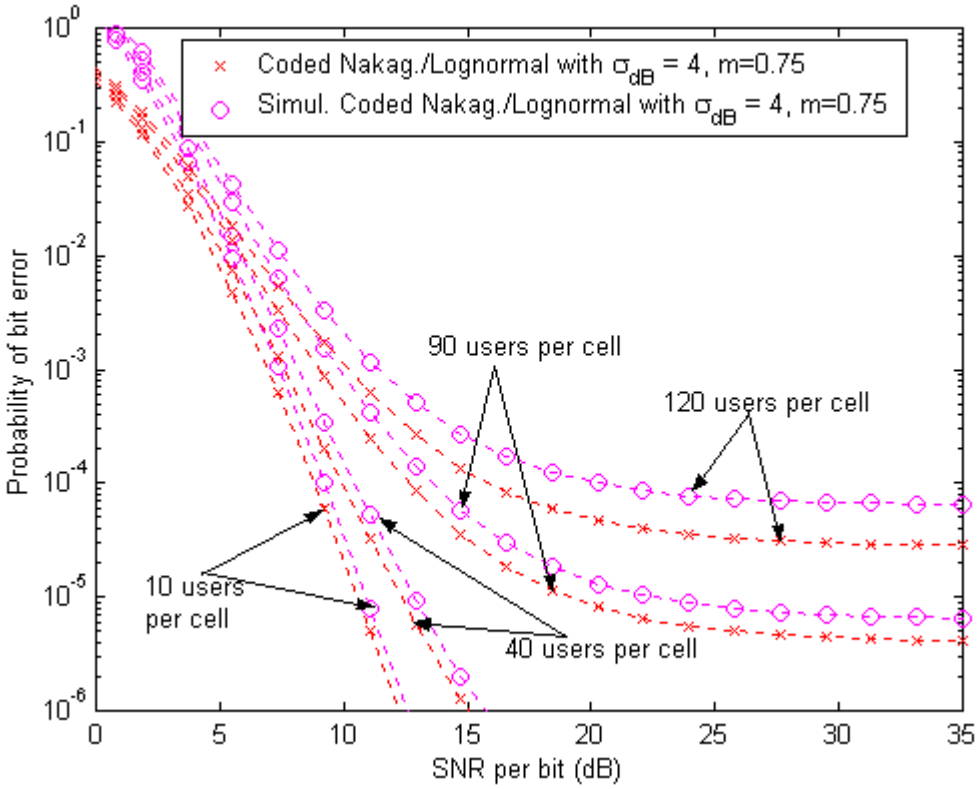

Figure 3.59. Probability of Bit Error for DS-CDMA with Nakagami Fading (m = 0.75) and Lognormal Shadowing $(\sigma_{dB} = 4)$ Using Six Sectors and a Rate 1/2 Convolutional Encoder with v = 8.

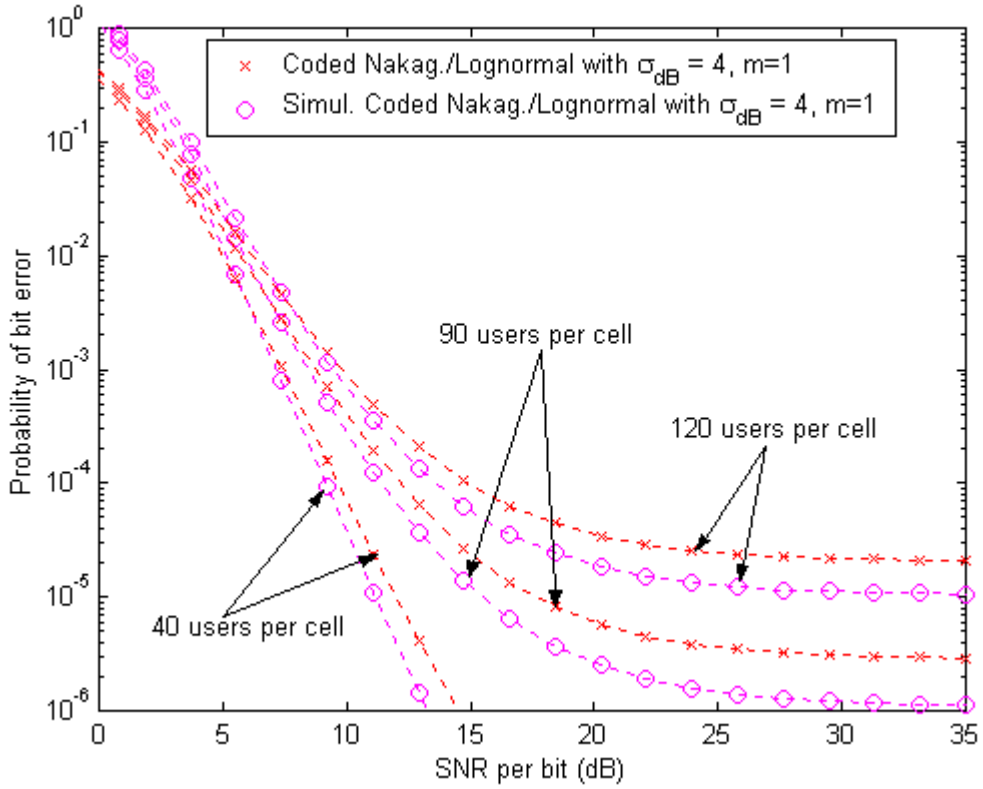

Figure 3.60. Probability of Bit Error for DS-CDMA with Nakagami Fading (m = 1) and Lognormal Shadowing $(\sigma_{dB} = 4)$ Using Six Sectors and a Rate 1/2 Convolutional Encoder with v = 8.

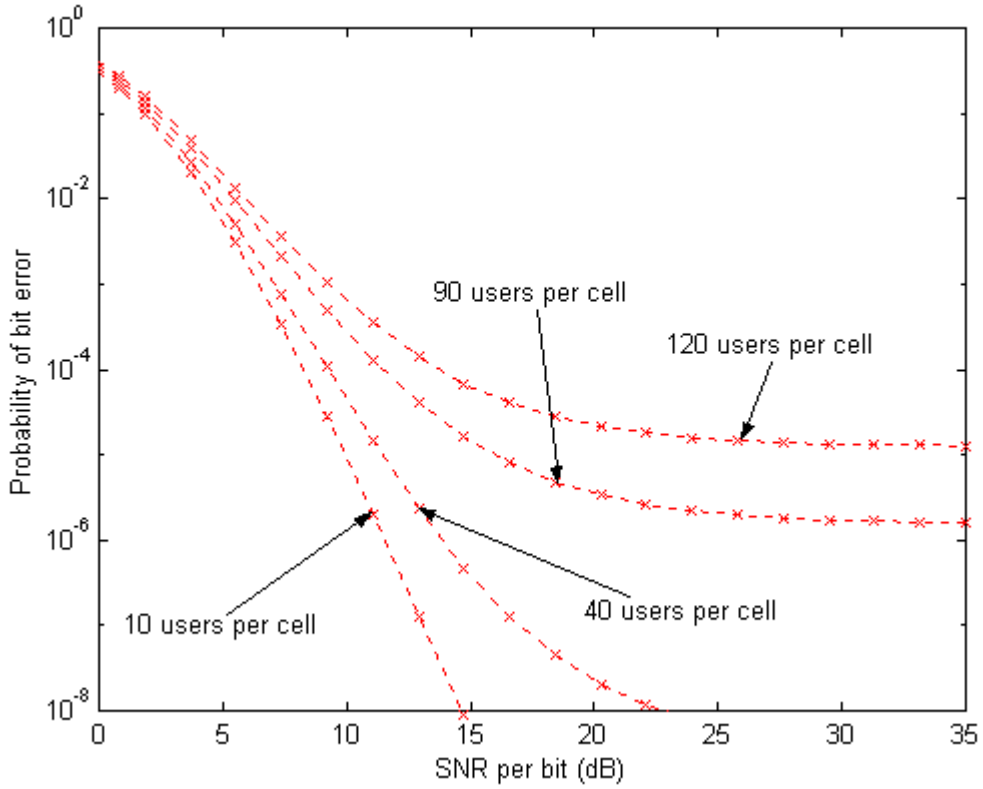

Figure 3.61. Probability of Bit Error for DS-CDMA with Nakagami Fading (m = 1.5) and Lognormal Shadowing $(\sigma_{dB} = 4)$ Using Six Sectors and a Rate 1/2 Convolutional Encoder with v = 8.

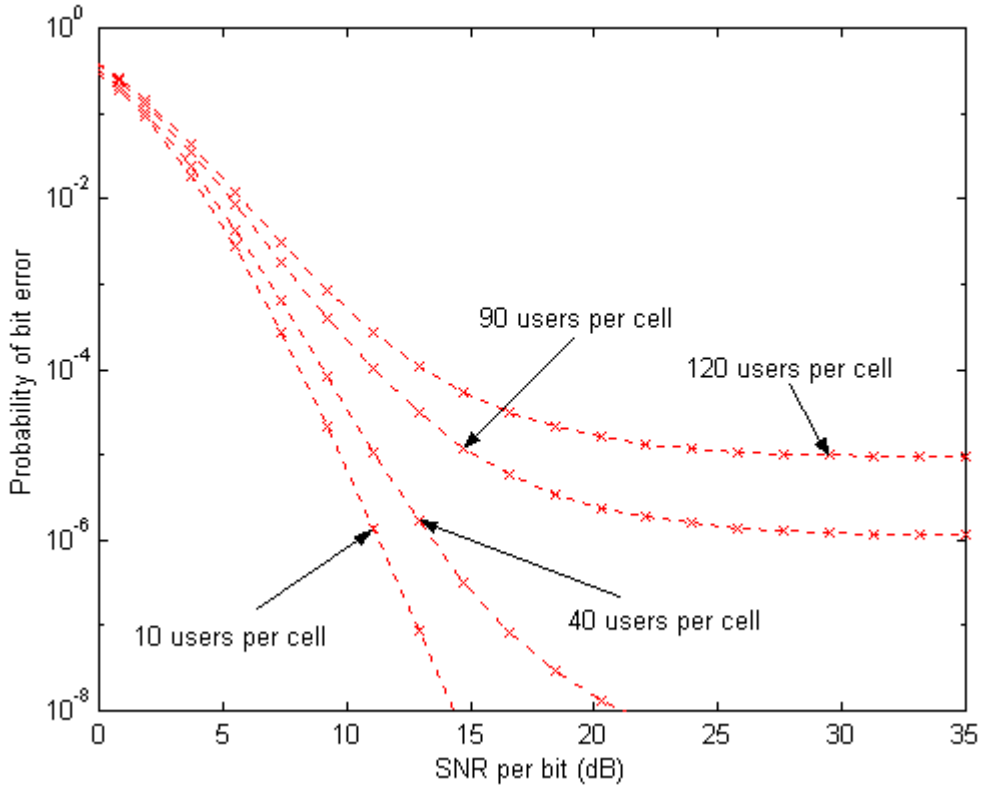

Figure 3.62. Probability of Bit Error for DS-CDMA with Nakagami Fading ($m = 2$) and Lognormal Shadowing $(\sigma_{dB} = 4)$ Using Six Sectors and a Rate 1/2 Convolutional Encoder with $v = 8$.

THIS PAGE INTENTIONALLY LEFT BLANK

APPENDIX III-E. PROBABILITY OF BIT ERROR FOR THE NAKAGAMI-LOGNORMAL CHANNEL KEEPING THE NUMBER OF USERS FIXED AND VARYING THE NAKAGAMI PARAMETER

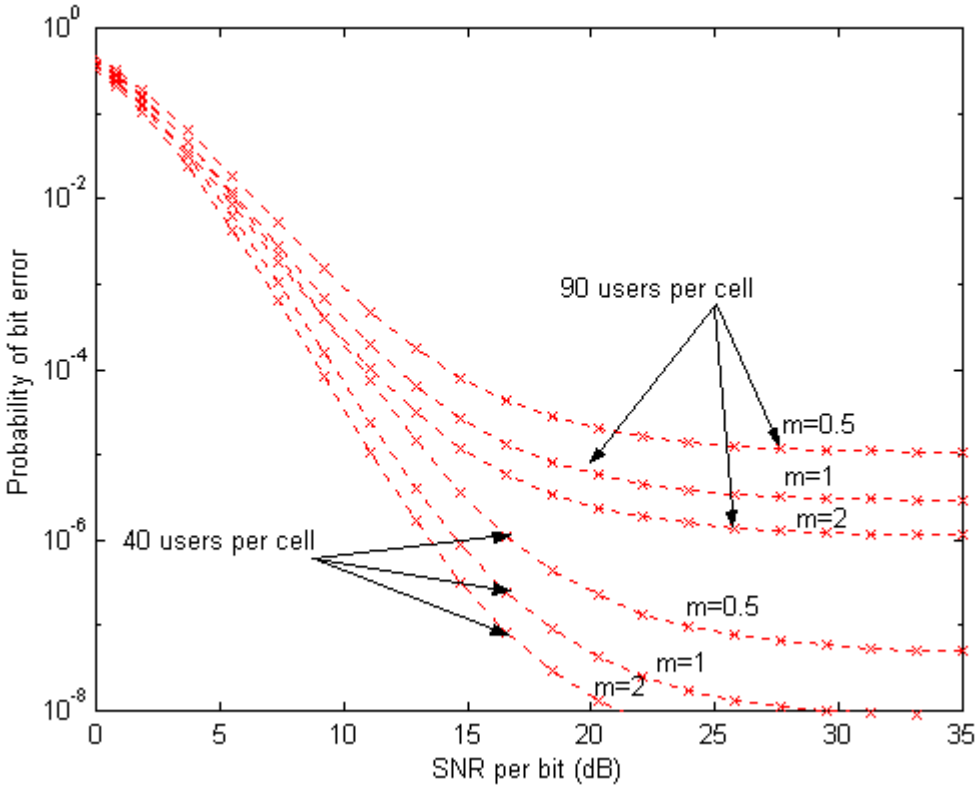

Figure 3.63. Probability of Bit Error for DS-CDMA with FEC in Various Fading Conditions with 40 and 90 Users Per Cell, 60º Sectoring, Lognormal Shadowing $(\sigma_{dB} = 4)$ Using a Rate 1/2 Convolutional Encoder with $v = 8$.

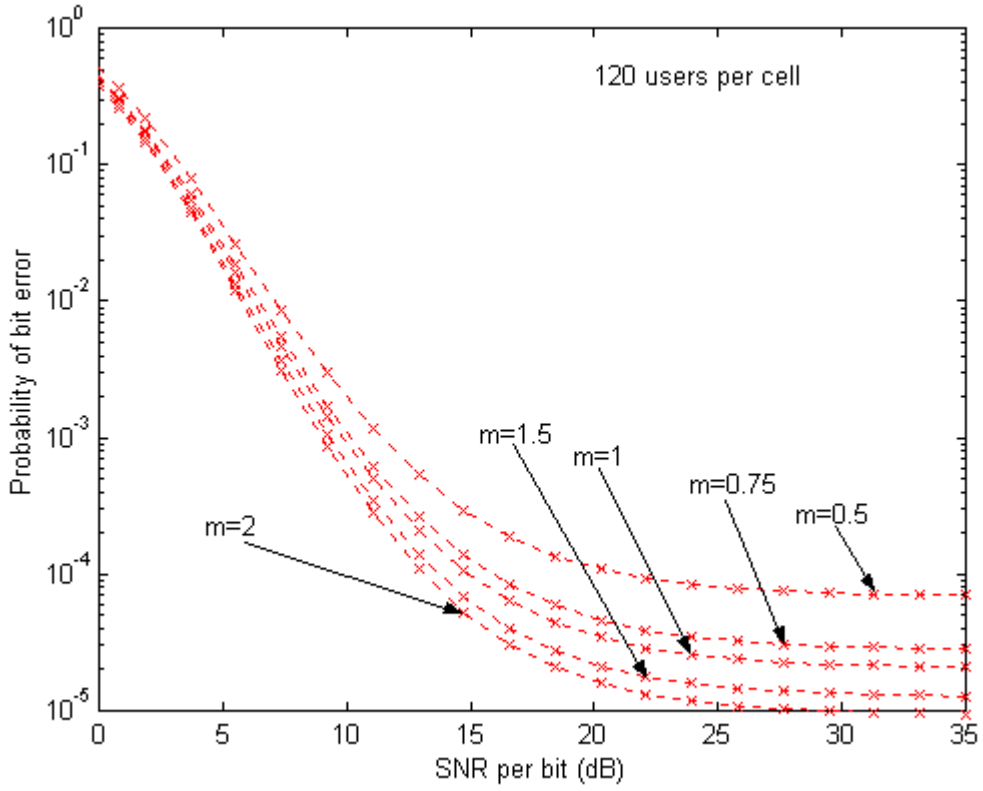

Figure 3.64. Probability of Bit Error for DS-CDMA with FEC in Various Fading Conditions with 120 Users Per Cell, 60º Sectoring, Lognormal Shadowing $(\sigma_{dB} = 4)$ Using a Rate 1/2 Convolutional Encoder with $v = 8$.

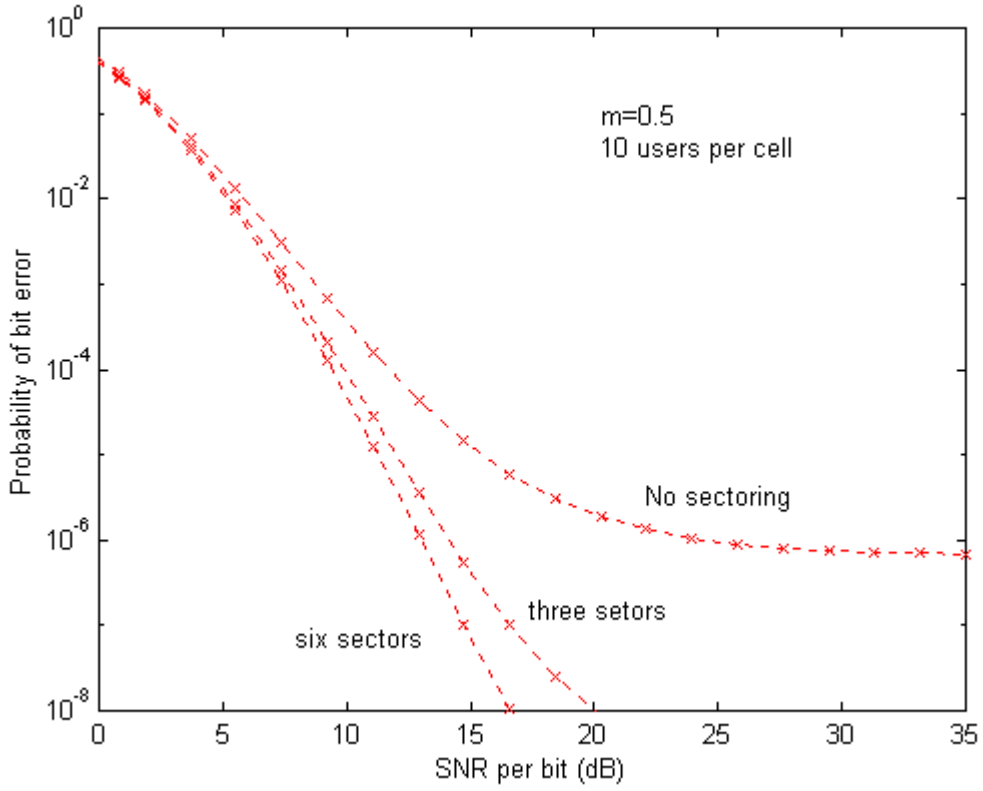

Figure 3.65. Probability of Bit Error for DS-CDMA Using Sectoring for $(\sigma_{dB} = 4)$, m = 0.5 and 10 Users Per Adjacent Cell Using a Rate 1/2 Convolutional Encoder with v = 8.

.

THIS PAGE INTENTIONALLY LEFT BLANK

IV. EFFECT OF USER DISTRIBUTION AND POWER CONTROL ON THE FORWARD CHANNEL MODEL

In Chapter III, the performance of the DS-CDMA cellular system in a Nakagami fading environment including Lognormal Shadowing for different values of the Nakagami-*m* parameter was analyzed. This analysis assumes that the intended user was in the least optimum position within the cell, which can be any corner of the hexagon as shown in Figure 3.1. The system performance can be improved by assuming that the intended user can be anywhere in the cell, and whose position can be represented by a random variable from a specific probability density function. A revised version of bit error probability can be defined by incorporating this probability density function in the initial formula for the bit error probability. This procedure will be examined in Section IV-A. Additionally, the analysis in Chapter III assumed that the base station was transmitting a fixed equal power to all users. In Section IV-B, the base station transmits more power to users who need it and less power to users who do not need it. System performance is thus enhanced because the co-channel interference is reduced. The analysis is similar to that given in [1]. For simplicity reasons, the hexagonal cells will be replaced by overlapping circular cells as depicted in Figure 4.1. Overlapping is used for soft-handoff reasons of mobile users between cells. Referring to Figure 4.1, the center base station is located at the origin of the polar coordinate system, with the intended mobile user's position in the center cell to be defined by (r,θ) where $0 < r < 1$ and $-\pi < \theta \leq \pi$.

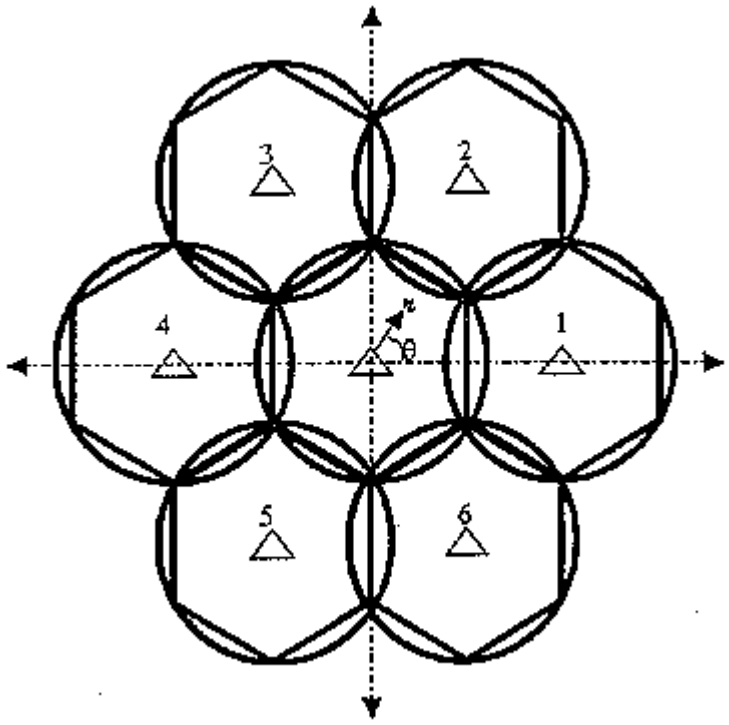

Figure 4.1. Circular Seven-Cell Cluster from [1].

Based on the previous analysis in Chapter III, it is known that the distance between the base station in the center cell to each of the adjacent base stations is $\sqrt{3}$ since $\boldsymbol{d} = 1$ is normalized. The distance D_i from each adjacent base station to the mobile user in the center cell as a function of r and θ is given in [1] as follows:

$$D_i = \begin{cases} \sqrt{r^2 - 2\sqrt{3}r\cos\theta + 3}, & i = 1 \\ \sqrt{r^2 - \sqrt{3}r\cos\theta - 3r\sin\theta + 3}, & i = 2 \\ \sqrt{r^2 + \sqrt{3}r\cos\theta - 3r\sin\theta + 3}, & i = 3 \\ \sqrt{r^2 + 2\sqrt{3}r\cos\theta + 3}, & i = 4 \\ \sqrt{r^2 + \sqrt{3}r\cos\theta + 3r\sin\theta + 3}, & i = 5 \\ \sqrt{r^2 - \sqrt{3}r\cos\theta + 3r\sin\theta + 3}, & i = 6 \end{cases}$$

These distances D_i are used in order to calculate the path loss for the intended information signal and the co-channel interference. Since these distances D_i are

randomized, it is too difficult and complicated to use the Hata model in order to predict the path loss. A more convenient and practical formula to compute the path loss is as follows:

$$\bar{L}_n(d) \propto \left(\frac{\boldsymbol{d}}{d_0} \right)^n \tag{4.1}$$

where $n = 4$ is the path loss exponent.

Following the notation as in [1], and assuming that the intended mobile user's position is fixed and exactly defined using the parameters r and θ as r_f and θ_f respectively, (3.3) can be revised to

$$\begin{aligned} \tilde{a} &= \frac{\exp\left(\frac{\lambda^2 \sigma_{dB}^2}{2} \right)}{3N} \sum_{i=1}^{6} \sum_{j=0}^{K_i - 1} \frac{f_{ij}}{f_1} \frac{\bar{L}_n\left(r_f\right)}{\bar{L}_n\left(D_i\right)} + \frac{N_o}{2E_c} \\ &= \frac{\exp\left(\frac{\lambda^2 \sigma_{dB}^2}{2} \right)}{3N} \sum_{i=1}^{6} \sum_{j=0}^{K_i - 1} \frac{f_{ij}}{f_1} \frac{r_f^n}{D_i^n} + \frac{N_o}{2E_c} \end{aligned} \tag{4.2}$$

where E_c is given as

$$E_c = \frac{f_1 P_t T_{cc}}{\bar{L}_n\left(r_f\right)} = \frac{f_1 P_t T_{cc}}{r_f^n} \tag{4.3}$$

The use of $\tilde{a}$ instead of α in (3.4) gives similar results for bit error probability as depicted in [1] in the case of equal transmitting power for all user channels.

A. USER DISTRIBUTION IN THE CELL

As mentioned at the beginning of Chapter IV, it is possible to enhance the performance of the DS-CDMA cellular system, assuming that the users are physically distributed in the cell following a specific probability distribution function rather than the intended mobile user being placed in the worst case position in the cell. In the case that the user density is uniform and assuming that the probability density function $p_\theta(\theta)$ for

the angular positions of a user is uniformly distributed, the first event error probability is developed in [1] and is given as follows:

$$\tilde{P}_2(d) = \int_{-\pi}^{\pi} \int_{o}^{1} \int_{-\infty}^{\infty} \frac{r}{\pi} Q\left[\sqrt{\frac{z_d}{\frac{\exp\left(\frac{\lambda^2\sigma_{dB}^2}{2}\right)}{3N}\sum_{i=1}^{6}\sum_{j=0}^{K_i-1}\frac{f_{ij}}{f_1}\frac{r^n}{D_i^n}+\frac{N_o r^n}{2E_c r_f^n}}}\right] p_{Z_d}(z_d)\, dz_d\, dr\, d\theta \quad (4.4)$$

where z_d is the value of the random variable Z_d which is the sum of d Nakagami-square-Lognormal random variables.

Substituting (4.4) in (3.5), an upper bound on the bit error probability for the Nakagami-*m*-Lognormal fading channel is obtained. The integral in (4.4) was simulated using 95,000 Monte Carlo trials for different values of the Nakagami-*m* parameter with 60º antenna sectoring. Figures 4.2 through 4.6 indicate how the system performs compared to the worst case user position analyzed in Chapter III in different fading conditions with a Lognormal Shadowing value of $\sigma_{dB} = 7$.

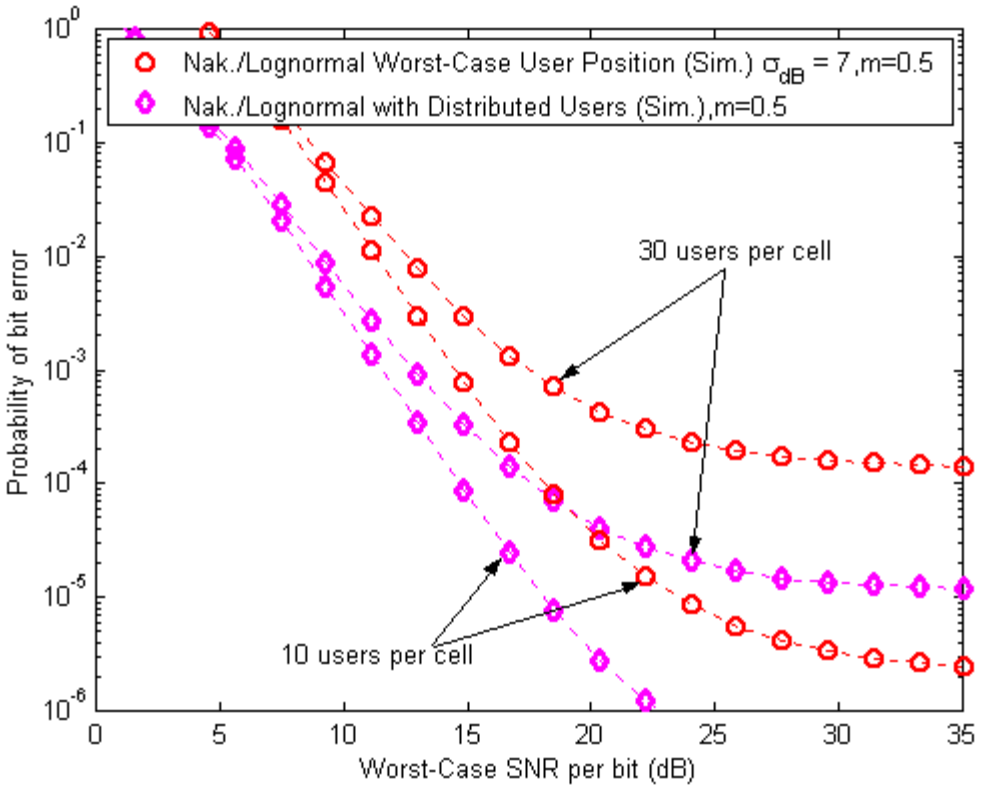

Figure 4.2. Probability of Bit Error for DS-CDMA with Nakagami Fading (m = 0.5) and Lognormal Shadowing (σ_{dB} = 7) Applying Linear User Distribution with 60º Sectoring and FEC Using a Rate 1/2 Convolutional Encoder with v = 8.

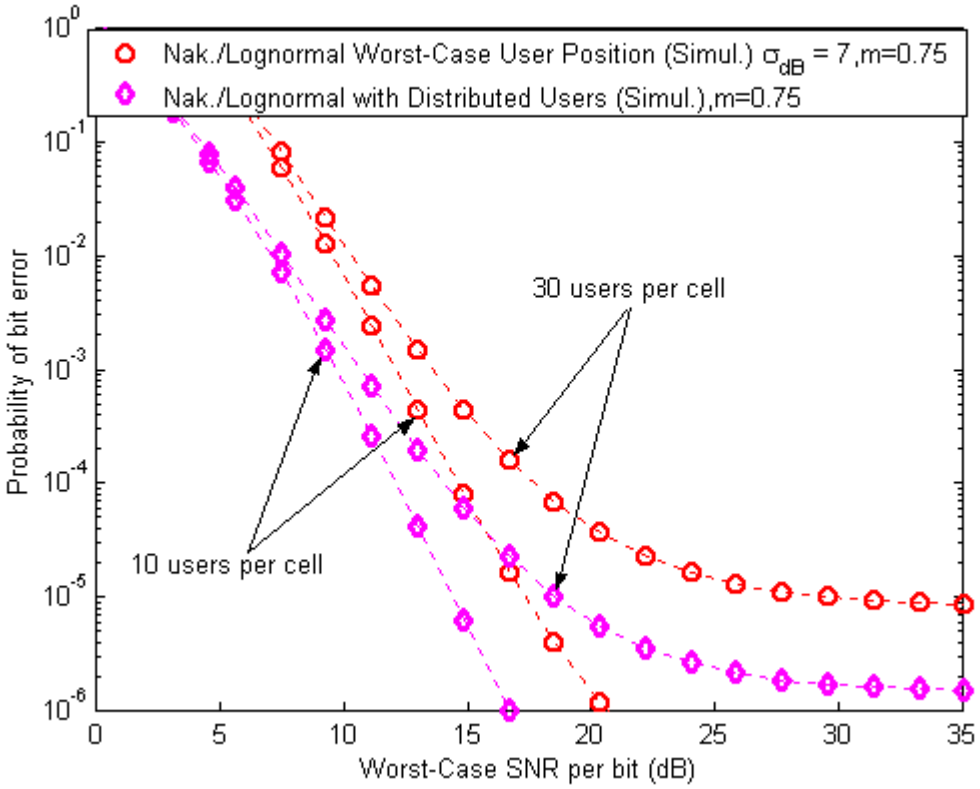

Figure 4.3. Probability of Bit Error for DS-CDMA with Nakagami Fading (m = 0.75) and Lognormal Shadowing (σ_{dB} = 7) Applying Linear User Distribution with 60º Sectoring and FEC Using a Rate 1/2 Convolutional Encoder with v = 8.

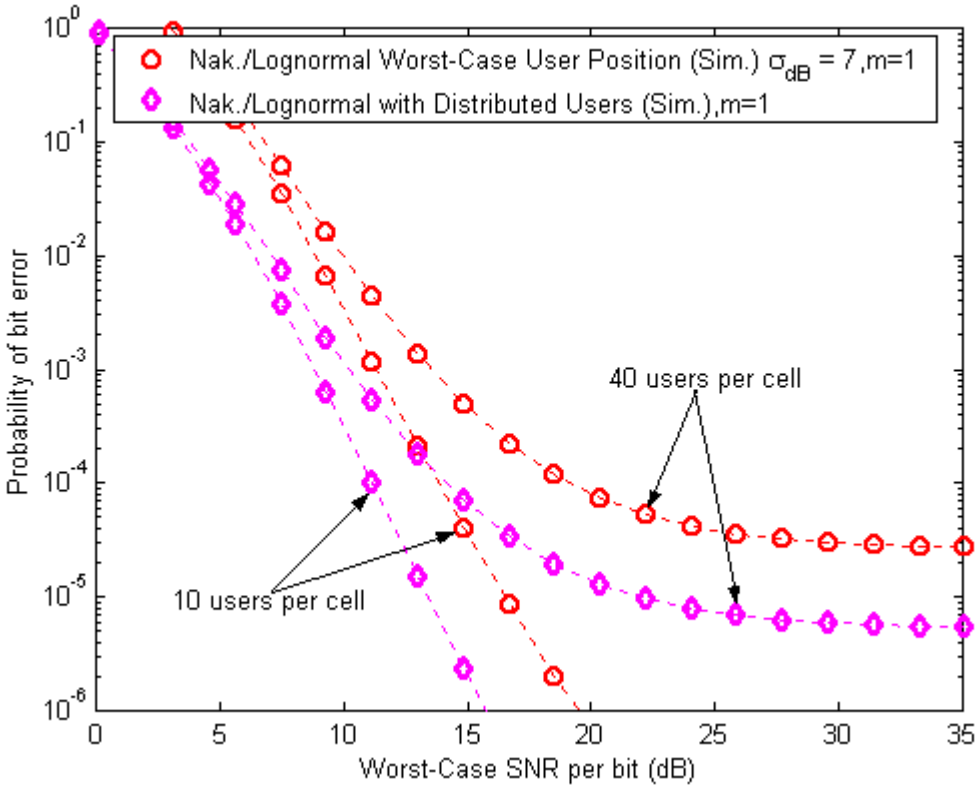

Figure 4.4. Probability of Bit Error for DS-CDMA with Nakagami Fading (m = 1) and Lognormal Shadowing (σ_{dB} = 7) Applying Linear User Distribution with 60º Sectoring and FEC Using a Rate 1/2 Convolutional Encoder with v = 8.

.

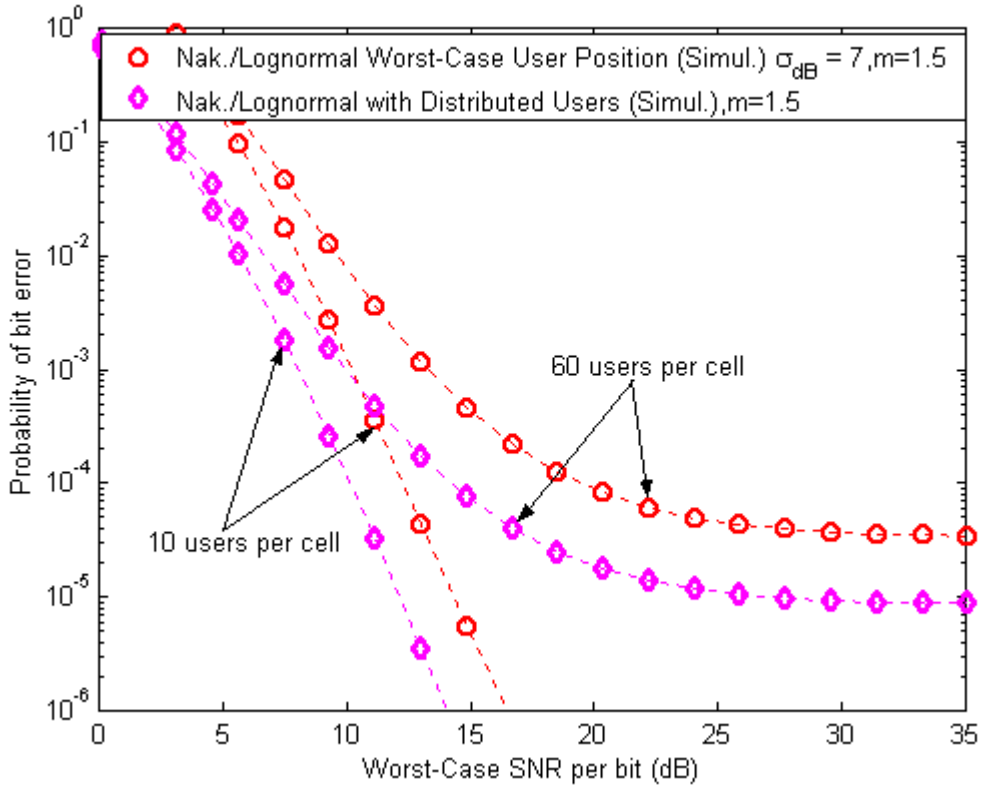

Figure 4.5. Probability of Bit Error for DS-CDMA with Nakagami Fading (m = 1.5) and Lognormal Shadowing (σ_{dB} = 7) Applying Linear User Distribution with 60º Sectoring and FEC Using a Rate 1/2 Convolutional Encoder with v = 8.

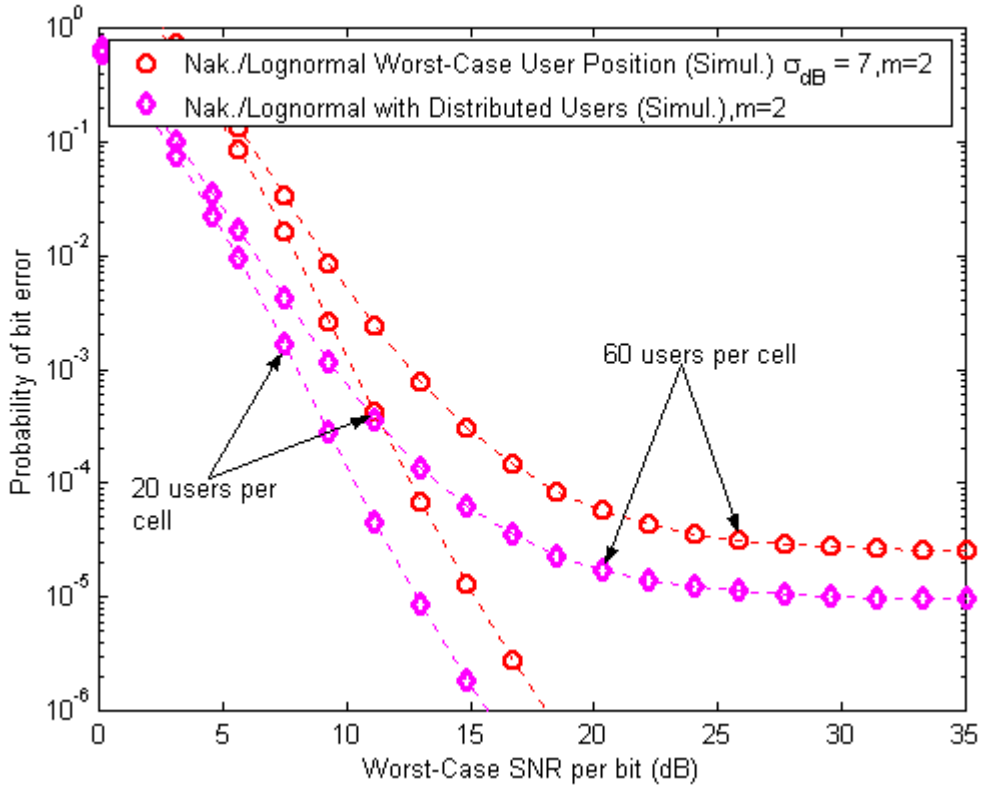

Figure 4.6. Probability of Bit Error for DS-CDMA with Nakagami Fading (m = 2) and Lognormal Shadowing (σ_{dB} = 7) Applying Linear User Distribution with 60º Sectoring and FEC Using a Rate 1/2 Convolutional Encoder with v = 8.

.

Observing Figures 4.2 through 4.6, it is obvious that the system performs better (3 to 4 dB) in various fading environments when the linear user distribution compared to the worst-case position of the user is incorporated.

B. POWER CONTROL ON THE FORWARD CHANNEL

In Section A the user distribution in the performance analysis was incorporated and better results were obtained compared to those in the previous chapter. The system performance can be enhanced even more if, in addition to user distribution, the power received by each user is adjusted to be equal. Working in this manner, the transmitting

power to non-intended users is reduced, which leads to a reduction of co-channel interference from users located in other cells.

In previous chapters, the baseline transmit power was defined as P_t. Assume that:

$$P = \frac{P_t}{a} \tag{4.5}$$

is the target level power which each user should receive and a is an attenuation factor. The values in (4.5) are constant for all users in all cells. Each mobile user, when receiving the information signal, measures the actual power received and reports it back to the base station. From that point on, the received power for each mobile user is not a random variable as mentioned in (2.12). It can stated that it is a realization of the random variable as described in [1]:

$$P_k = \frac{P_{t,k}}{\bar{L}_n(\boldsymbol{d}_k)x_k} = \frac{f_k P_t}{\bar{L}_n(\boldsymbol{d}_k)x_k} = \frac{f_k aP}{\boldsymbol{d}_k^n x_k} \tag{4.6}$$

where $\boldsymbol{d}_k$ is the user's actual distance and x_k is the shadowing experienced by the specific user. In order for each user to receive the same target power level P, the base station has to adjust the power factor as follows:

$$f_k = \frac{\boldsymbol{d}_k^n x_k}{a} \tag{4.7}$$

Substituting (4.7) into (4.6) implies:

$$P_k = P \tag{4.8}$$

Adjusting the power factor to achieve the target power level P for all users makes it possible to overcome the Lognormal Shadowing effect on the information signal.

Thus, [1] gives the first event error probability $P_2(d)$ conditioned or r_l, r, θ as follows:

$$\hat{P}_2(d)\Big|_{\eta,r,\theta} = Q\left[\sqrt{\frac{\sum_{l=1}^{d} r_l^2}{\frac{\exp\left\{\lambda^2\sigma_{dB}^2\right\}}{3N}\sum_{i=1}^{6}\sum_{j=0}^{K_i-1}\frac{\mathrm{E}\left\{r_{ij}^n\right\}}{D_i^n}+\frac{N_o}{2E_c}}}\right] \tag{4.9}$$

where r_l^2 is the value of the Nakagami-square random variable and r_{ij} as in [1] is the random variable representing the distance between mobile user *j* in adjacent cell *i*, with the same pdf as the random variable *r*. Recalling the probability density function of the sum of *d* Nakagami-*m* square random variables from (3.9) and the fact that $p_{R,\theta}(r,\theta)=\frac{r}{\pi}$, the dependency on r_l, r, θ can be removed as follows:

$$\hat{P}_2(d) = \int_{-\infty}^{\infty}\int_{-\pi}^{\pi}\int_{o}^{1} Q\left[\sqrt{\frac{u}{\frac{\exp\left\{\lambda^2\sigma_{dB}^2\right\}}{3N}\sum_{i=1}^{6}\sum_{j=0}^{K_i-1}\frac{\mathrm{E}\left\{r_{ij}^n\right\}}{D_i^n}+\frac{N_o}{2E_c}}}\right] p_U(u) \tag{4.10}$$
$$\times\, p_{R,\theta}(r,\theta)\,dr\,d\theta\,du$$

where $u=\sum_{l=1}^{d} r_l^2$ is the value of the sum of *d* Nakagami-square random variables. A closed form solution for $\hat{P}_2(d)$ is given as follows:

$$\hat{P}_2(d) = \int_{-\pi}^{\pi}\int_{o}^{1} \frac{r}{\pi}\sqrt{\left(\frac{\Omega}{2\hat{\alpha}m+\Omega}\right)}\,\frac{\Gamma(md+\frac{1}{2})}{2\sqrt{\pi}\,\Gamma(md+1)\left(\frac{2\hat{\alpha}m+\Omega}{2\hat{\alpha}m}\right)^{md}} \tag{4.11}$$
$$\times\sum_{k=0}^{\infty}\frac{(md+\frac{1}{2})_k\left(\frac{2\hat{\alpha}m}{2\hat{\alpha}m+\Omega}\right)^k}{(md+1)_k}\,dr\,d\theta$$

where $\hat{\alpha} = \dfrac{\exp\left\{\lambda^2\sigma_{dB}^2\right\}}{3N}\sum_{i=1}^{6}\sum_{j=0}^{K_i-1}\dfrac{\mathrm{E}\left\{r_{ij}^n\right\}}{D_i^n} + \dfrac{N_o}{2E_c}$

Analytical computation of the closed form solution can be found in Appendix IV-A. Substituting (4.10) or (4.11) in (3.5) it is possible to compute an upper bound on the probability of bit error. The integral in (4.10) was simulated using 95,000 Monte Carlo trials for different values of the Nakagami-*m* parameter with 60º antenna sectoring. The average received SNR per bit for the Nakagami-Lognormal channel with perfect power channel is from [1] as follows:

$$\overline{\gamma}_b = \mathrm{E}\left\{\frac{R^2 f_1 P_t T}{N_o d_k^n x_k}\right\} = \mathrm{E}\left\{R^2\right\}\frac{PT}{N_o} = \frac{E_b}{N_o} \tag{4.12}$$

As shown in Figure 4.7, in the case of ten users per cell, the power-controlled system works better than the system with fixed power (~6 dB). However, in the case of thirty users per cell, the power controlled system works better than the fixed power system for $\overline{\gamma}_b < 17$ dB which is the point where the interference floor seems to be developed. This phenomenon is explained analytically in [1] and in a few words means that by increasing the received power for all users in order to overcome the Lognormal Shadowing effect, the co-channel interference is simultaneously increased. Furthermore, in the case of *m* = 0.5, the system seems to be able to accommodate up to 30 users with a bit error probability of $\sim 10^{-4}$ in the region $10 \text{ dB} < \overline{\gamma}_b < 17 \text{ dB}$.

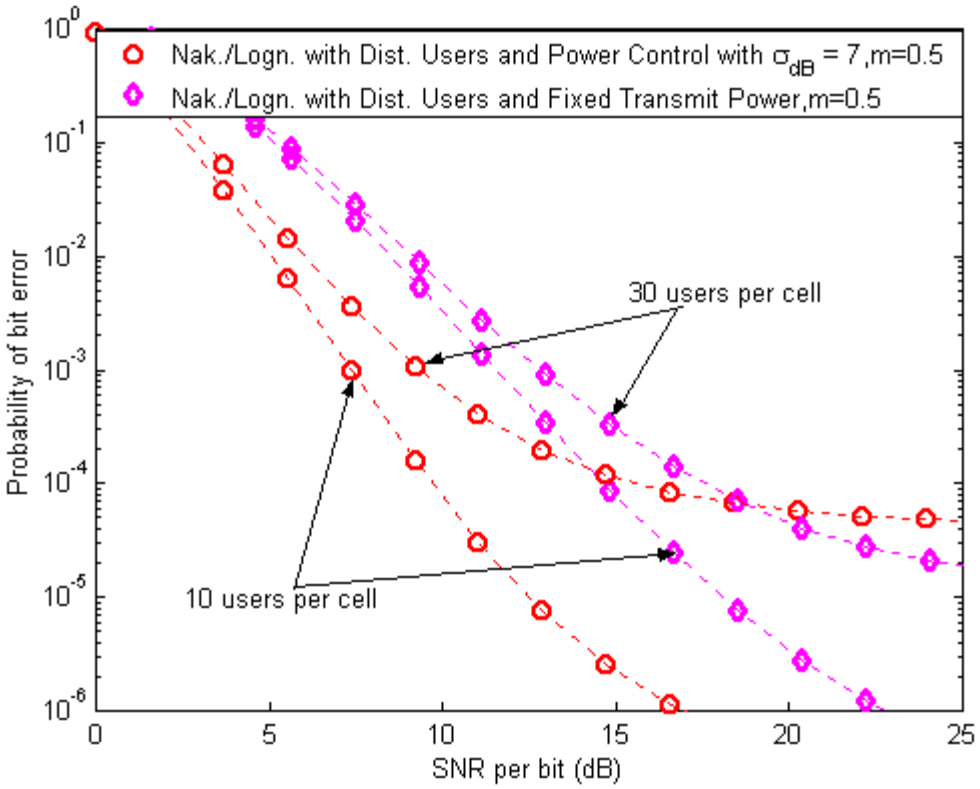

Figure 4.7. Probability of Bit Error for DS-CDMA with Nakagami Fading (m = 0.5) and Lognormal Shadowing $(\sigma_{dB} = 7)$ Applying Forward Power Control and Linear User Distribution with 60º Sectoring and FEC Using a Rate 1/2 Convolutional Encoder with v = 8.

Similar results are obtained when changing from m = 0.5 to m = 1.5 as seen in Figure 4.8. In that case, the system accommodates up to 60 users per cell with a bit error probability of $\sim 10^{-4}$ when $\overline{\gamma}_b < 16$ dB.

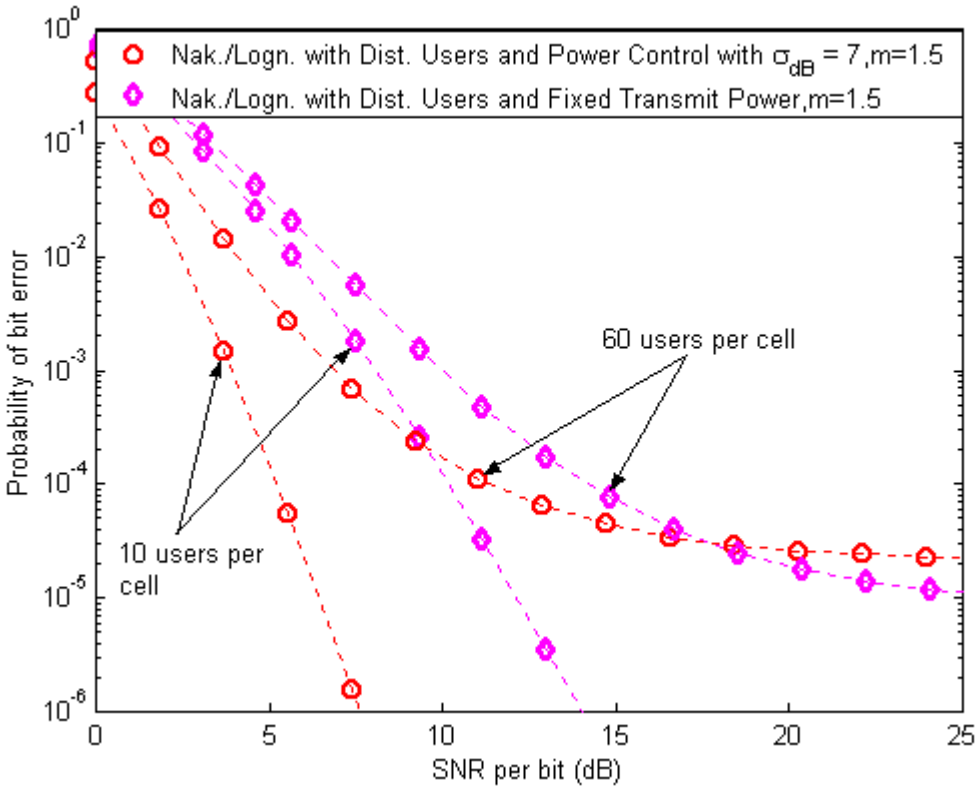

Figure 4.8. Probability of Bit Error for DS-CDMA with Nakagami Fading (m = 1.5) and Lognormal Shadowing $(\sigma_{dB} = 7)$ Applying Forward Power Control and Linear User Distribution with 60º Sectoring and FEC Using a Rate 1/2 Convolutional Encoder with v = 8.

When the system operates in more lightly shadowing environments $(\sigma_{dB} < 6)$, the power-controlled system outperforms the fixed power system as depicted in Figure 4.9 for the case of 140 users per cell.

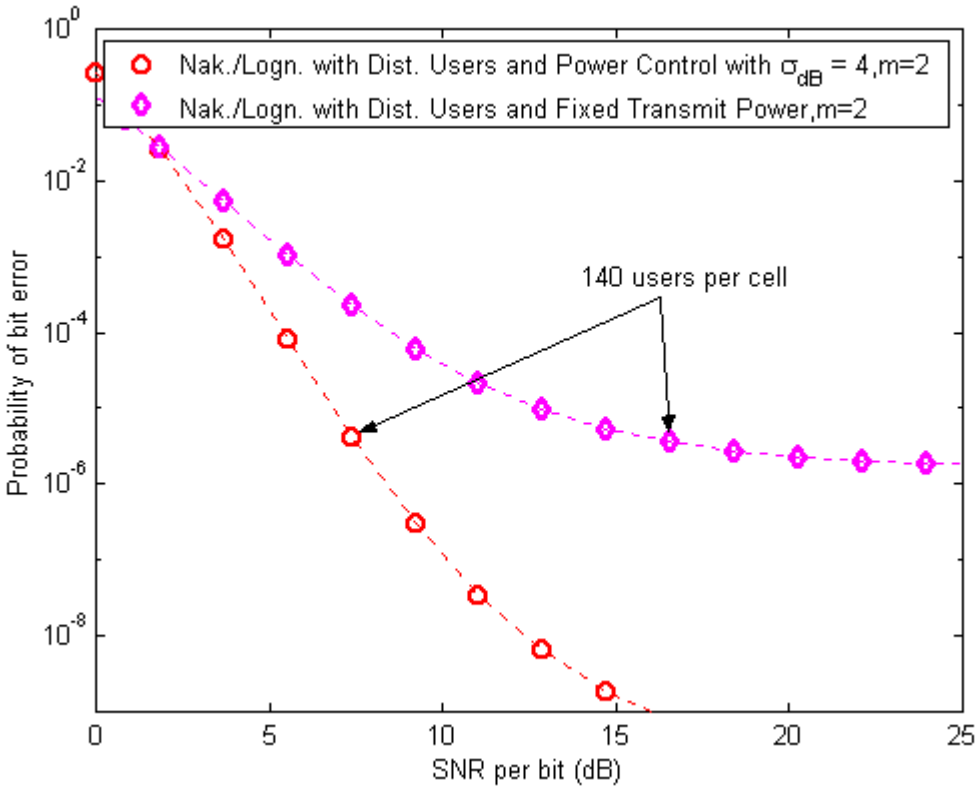

Figure 4.9. Probability of Bit Error for DS-CDMA with Nakagami Fading ($m = 2$) and Lognormal Shadowing $(\sigma_{dB} = 4)$ Applying Forward Power Control and Linear User Distribution with 60º Sectoring and FEC Using a Rate 1/2 Convolutional Encoder with $v = 8$.

In these circumstances, the benefits of eliminating the Lognormal Shadowing of the signal overcomes the increase to co-channel interference.

Additionally, system designers must be very careful when the system operates in heavily Lognormal Shadowing environments $(\sigma_{dB} > 6)$ in order for the power controlled system to operate out of the interference-limited region even when using 60º sectoring.

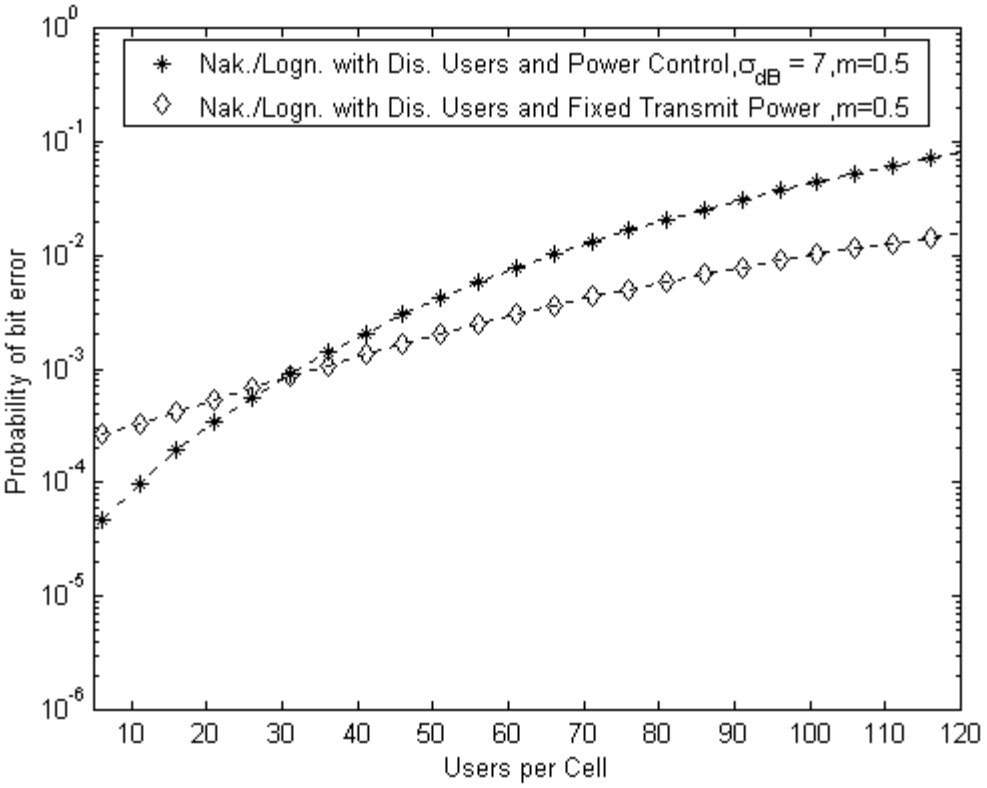

Figure 4.10. Probability of Bit Error for DS-CDMA with Nakagami Fading (m = 0.5) and Lognormal Shadowing $(\sigma_{dB} = 7)$ vs. Users per Cell Applying Forward Power Control and Linear User Distribution with 60º Sectoring and FEC $(R_{cc} = 1/2$ and $v = 8)$, $\overline{\gamma_b} = 15$ dB.

In the case of m = 0.5 and $\sigma_{dB} = 7 > 6$, the power controlled system roughly accommodates up to 35 users per cell, for $\overline{\gamma}_b = 15$ dB.

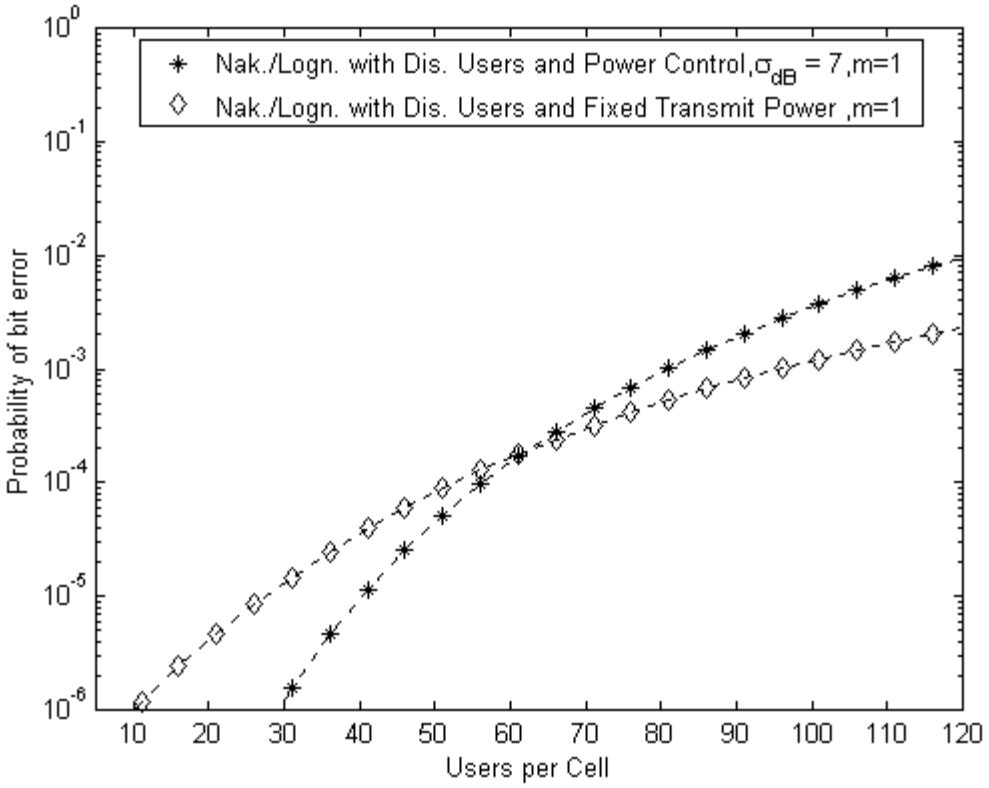

Figure 4.11. Probability of Bit Error for DS-CDMA with Nakagami Fading (m = 1) and Lognormal Shadowing $(\sigma_{dB} = 7)$ vs. Users per Cell Applying Forward Power Control and Linear User Distribution with 60º Sectoring and FEC $(R_{cc} = 1/2$ and $v = 8)$, $\overline{\gamma_b} = 15$ dB.

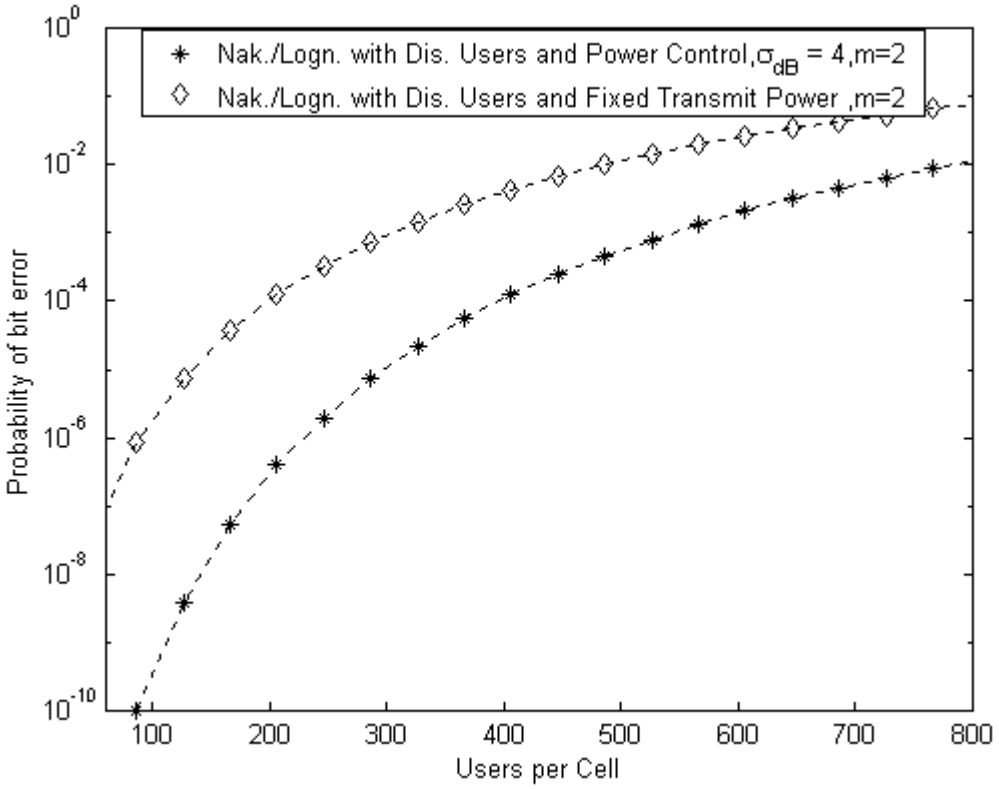

Figure 4.12. Probability of Bit Error for DS-CDMA with Nakagami Fading (m = 2) and Lognormal Shadowing $(\sigma_{dB} = 4)$ vs. Users per Cell Applying Forward Power Control and Linear User Distribution with 60º Sectoring and FEC $(R_{cc} = 1/2$ and $v = 8)$, $\overline{\gamma_b} = 12$ dB.

By increasing the value of the Nakagami-m parameter to m = 1, the severity of the fading is decreased and thus the power-controlled system can accommodate up to 64 users per cell for $\overline{\gamma}_b = 15$ dB as shown in Figure 4.11. When m = 2 and $\sigma_{dB} = 4$ the power controlled system outperforms the one with fixed power.

If instead of six sectors, 120º sectoring or no sectoring is used, the amount of co-channel interference will be increased by a factor of two and six respectively which will result in the worst performance of the power controlled system. In that case, the number of users per cell that the system can accommodate in the no interference-limited region will decrease.

Figures similar to the aforementioned figures can be found in Appendix IV-B for

Lognormal Shadowing $\sigma_{dB} = 4$ and $\sigma_{dB} = 9$, which reinforce the previous comments. Especially when $\sigma_{dB} = 9$ and m = 0.5, m = 0.75, m = 1 the fixed power system outperforms the one with power control as depicted in Figures 4.21, 4.22 and 4.23 of Appendix IV-B. That means in heavy shadowing and severe fading environments system designers must use fixed power system and not the power controlled one.

Accordingly, it can be stated that by carefully adding power-control to the forward channel, it is possible to enhance the system performance operating in a lightly shadowed and not severe fading Nakagami-Lognormal channel.

C. SUMMARY

In this chapter, the system performance was enhanced by considering that the user's positions in the cell are randomly distributed following a linear distribution. That assumption is more realistic compared to the worst-case position of the intended user located at the corner of the hexagon. Given the revised version of the first event error probability referring to the more realistic case, it was possible to compute an upper bound on the probability of bit error by simulating the integral of (4.4) by using 95,000 Monte Carlo trials. The system performance was improved by 3 to 4 dB for $\sigma_{dB} = 7$.

Furthermore, in Section IV-B, a power control technique was applied. Thus, all users received the same amount of power. This technique overcomes the effects of Lognormal Shadowing and distance dependent path loss. Simulating the integral of (4.10) by using 95,000 Monte Carlo trials, an upper bound on the probability of bit error was computed. By properly using the power control technique, it was possible to greatly increase system performance and user capacity in the forward channel operating in a Nakagami-Lognormal Shadowing environment. As mentioned previously, system designers must be very careful when incorporating power control in heavily shadowed environments in order for the system to operate in the no interference limited region.

THIS PAGE INTENTIONALLY LEFT BLANK

APPENDIX IV-A. ANALYTICAL COMPUTATION OF A CLOSED FORM SOLUTION FOR THE FIRST EVENT ERROR PROBABILITY IN THE CASE OF FORWARD POWER CONTROL

Equation (4.10) gives that:

$$\hat{P}_2(d) = \int_{-\infty}^{\infty} \int_{-\pi}^{\pi} \int_{o}^{1} Q\left[\sqrt{\frac{u}{\frac{\exp\left\{\lambda^2\sigma_{dB}^2\right\}}{3N}\sum_{i=1}^{6}\sum_{j=0}^{K_i-1}\frac{\mathrm{E}\left\{r_{ij}^n\right\}}{D_i^n}+\frac{N_o}{2E_c}}}\right] p_U(u)$$

$$\times\, p_{R,\theta}(r,\theta)\,dr\,d\theta\,du$$

Substituting $p_{R,\theta}(r,\theta)=\frac{r}{\pi}$ and $\hat{\alpha}=\frac{\exp\left\{\lambda^2\sigma_{dB}^2\right\}}{3N}\sum_{i=1}^{6}\sum_{j=0}^{K_i-1}\frac{\mathrm{E}\left\{r_{ij}^n\right\}}{D_i^n}+\frac{N_o}{2E_c}$ we get for $\hat{P}_2(d)$ the following:

$$\hat{P}_2(d) = \int_{-\infty}^{\infty} \int_{-\pi}^{\pi} \int_{o}^{1} Q\left[\sqrt{\frac{u}{\hat{\alpha}}}\right]\frac{r}{\pi}\, p_U(u)\,dr\,d\theta\,du \tag{4.13}$$

Equation (3.9) gives:

$$p_U(u) = \left(\frac{m}{\Omega}\right)^{md}\frac{u^{md-1}}{\Gamma(md)}\exp\left(-\frac{mu}{\Omega}\right) \tag{4.14}$$

Applying (4.14) to (4.13) we get for $\hat{P}_2(d)$ the following:

$$\hat{P}_2(d) = \int_{-\infty}^{\infty} \int_{-\pi}^{\pi} \int_{o}^{1} Q\left[\sqrt{\frac{u}{\hat{\alpha}}}\right]\frac{r}{\pi}\left(\frac{m}{\Omega}\right)^{md}\frac{u^{md-1}}{\Gamma(md)}$$

$$\times\, \exp\left(-\frac{mu}{\Omega}\right)dr\,d\theta\,du \tag{4.15}$$

From [9] we have the following equality:

$$\frac{{\alpha_3}^{\beta}}{\Gamma(\beta)}\int_0^{\infty}\exp(-\alpha_3 t)t^{\beta-1}Q\left(\sqrt{ct}\right)dt=\sqrt{\frac{\psi}{1+\psi}}\frac{\Gamma\left(\beta+\frac{1}{2}\right)}{2\sqrt{\pi}\Gamma(\beta+1)(1+\psi)^{\beta}} \tag{4.16}$$
$$\times\ {}_2F_1\left(1,\beta+\frac{1}{2};\beta+1;\frac{1}{1+\psi}\right)$$

where ${}_2F_1$ is the Gaussian hypergeometric function defined as follows:

$${}_2F_1\left(1,\beta+\frac{1}{2};\beta+1;z\right)=\sum_{k=0}^{\infty}\frac{\left(\beta+\frac{1}{2}\right)_k z^k}{(\beta+1)_k} \tag{4.17}$$

$$\psi=\frac{2}{\alpha_3},\ z=\frac{1}{1+\psi}\ \text{and}$$

$$(g)_k=\frac{\Gamma(g+k)}{\Gamma(g)}$$
$$=g(g+1)...(g+k-1)$$

$$(g)_0=1$$

Comparing now the variables of Equations (4.15) and (4.16) and noting the random variable U takes only positive values we get that: $\alpha_3=\frac{m}{\Omega},\ \beta=md,\ t=w,\ c=\frac{1}{\hat{\alpha}}$ and $\psi=\frac{\Omega}{2\hat{\alpha}m}$. Applying these last five equations to (4.14) and making use of (4.15) we get for $\hat{P}_2(d)$ the following:

$$\hat{P}_2(d)=\int_{-\pi}^{\pi}\int_o^1\frac{r}{\pi}\sqrt{\left(\frac{\Omega}{2\hat{\alpha}m+\Omega}\right)}\frac{\Gamma(md+\frac{1}{2})}{2\sqrt{\pi}\Gamma(md+1)\left(\frac{2\hat{\alpha}m+\Omega}{2\hat{\alpha}m}\right)^{md}} \tag{4.18}$$
$$\times\ {}_2F_1\left(1,md+\frac{1}{2};md+1;\frac{2\hat{\alpha}m}{2\hat{\alpha}m+\Omega}\right)drd\theta$$

Substituting ${}_2F_1$ by its definition, we finally get for $\hat{P}_2(d)$ the following close form solution:

$$\hat{P}_2(d) = \int_{-\pi}^{\pi} \int_{o}^{1} \frac{r}{\pi} \sqrt{\left(\frac{\Omega}{2\hat{\alpha}m + \Omega}\right)} \frac{\Gamma(md + \frac{1}{2})}{2\sqrt{\pi}\Gamma(md+1)\left(\frac{2\hat{\alpha}m + \Omega}{2\hat{\alpha}m}\right)^{md}} \times \sum_{k=0}^{\infty} \frac{(md + \frac{1}{2})_k \left(\frac{2\hat{\alpha}m}{2\hat{\alpha}m + \Omega}\right)^k}{(md+1)_k} dr d\theta \tag{4.19}$$

THIS PAGE INTENTIONALLY LEFT BLANK

APPENDIX IV-B. PROBABILITY OF BIT ERROR FOR THE NAKAGAMI-LOGNORMAL CHANNEL USING FORWARD CHANNEL POWER CONTROL

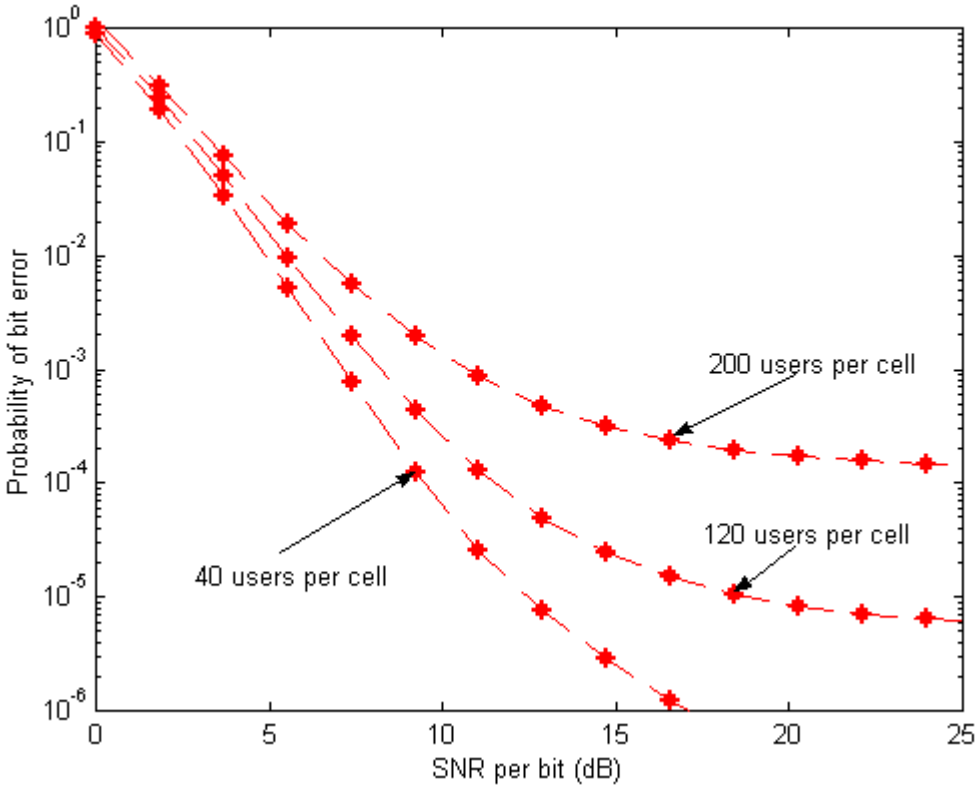

Figure 4.13. Probability of Bit Error for DS-CDMA with Nakagami Fading (m = 0.5) and Lognormal Shadowing $(\sigma_{dB} = 4)$ Applying Forward Power Control and Linear User Distribution with 60º Sectoring and FEC Using a Rate 1/2 Convolutional Encoder with v = 8.

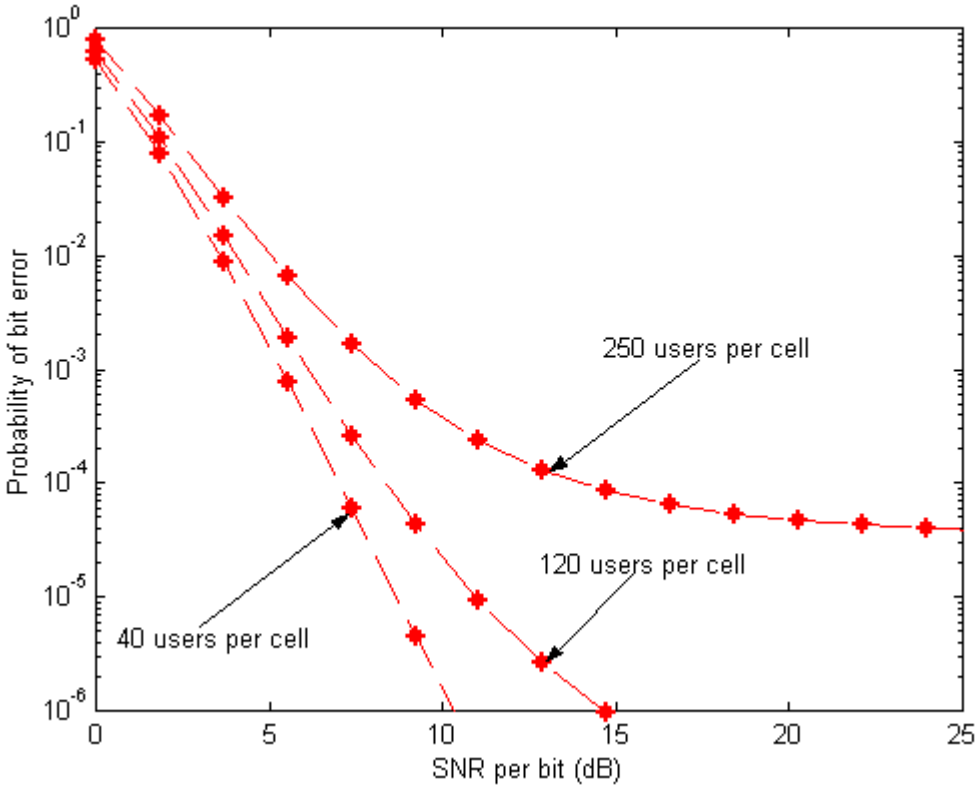

Figure 4.14. Probability of Bit Error for DS-CDMA with Nakagami Fading ($m = 0.75$) and Lognormal Shadowing $(\sigma_{dB} = 4)$ Applying Forward Power Control and Linear User Distribution with 60º Sectoring and FEC Using a Rate 1/2 Convolutional Encoder with $v = 8$.

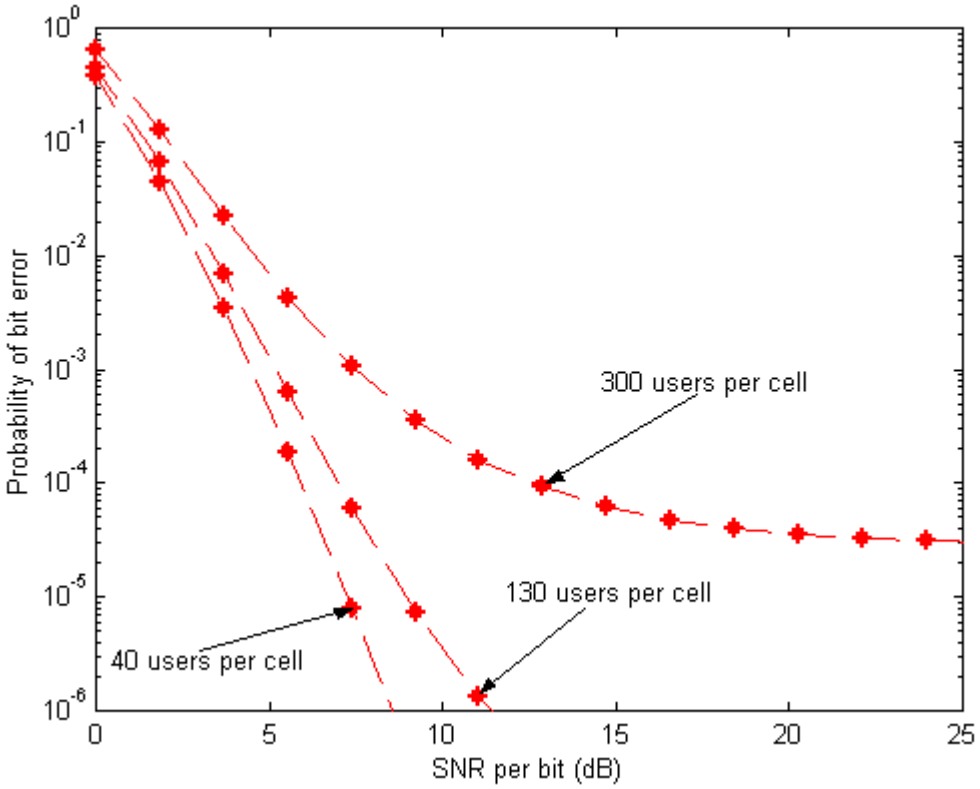

Figure 4.15. Probability of Bit Error for DS-CDMA with Nakagami Fading (m = 1) and Lognormal Shadowing $(\sigma_{dB} = 4)$ Applying Forward Power Control and Linear User Distribution with 60º Sectoring and FEC Using a Rate 1/2 Convolutional Encoder with v = 8.

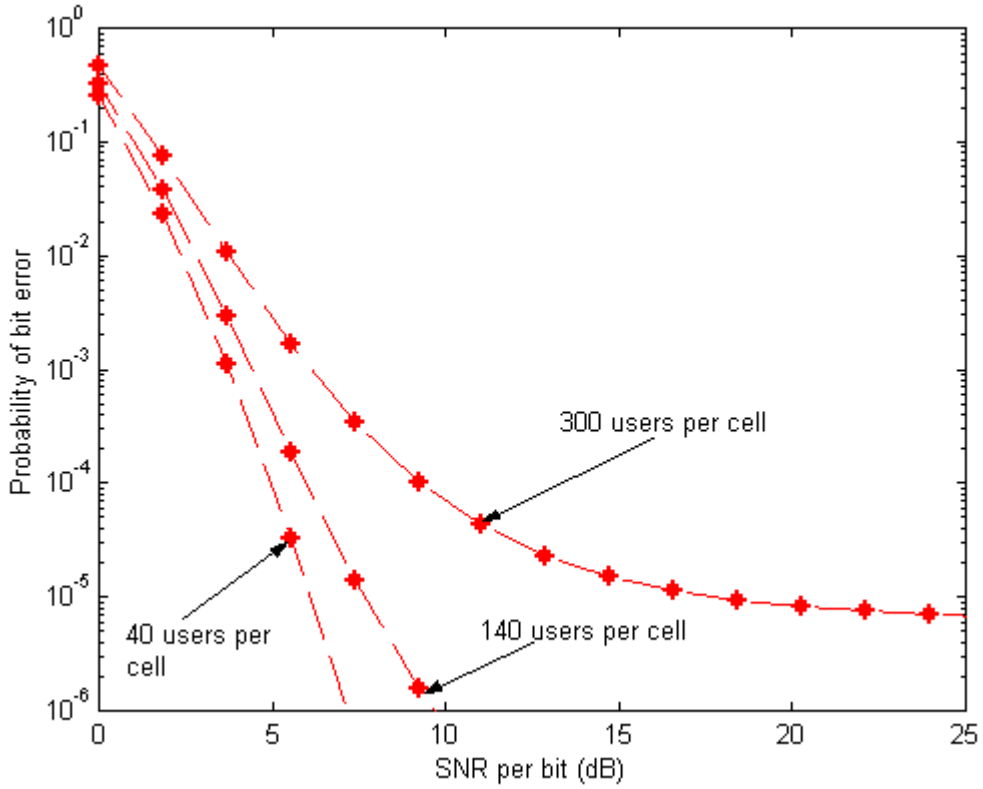

Figure 4.16. Probability of Bit Error for DS-CDMA with Nakagami Fading (m = 1.5) and Lognormal Shadowing $(\sigma_{dB} = 4)$ Applying Forward Power Control and Linear User Distribution with 60º Sectoring and FEC Using a Rate 1/2 Convolutional Encoder with v = 8.

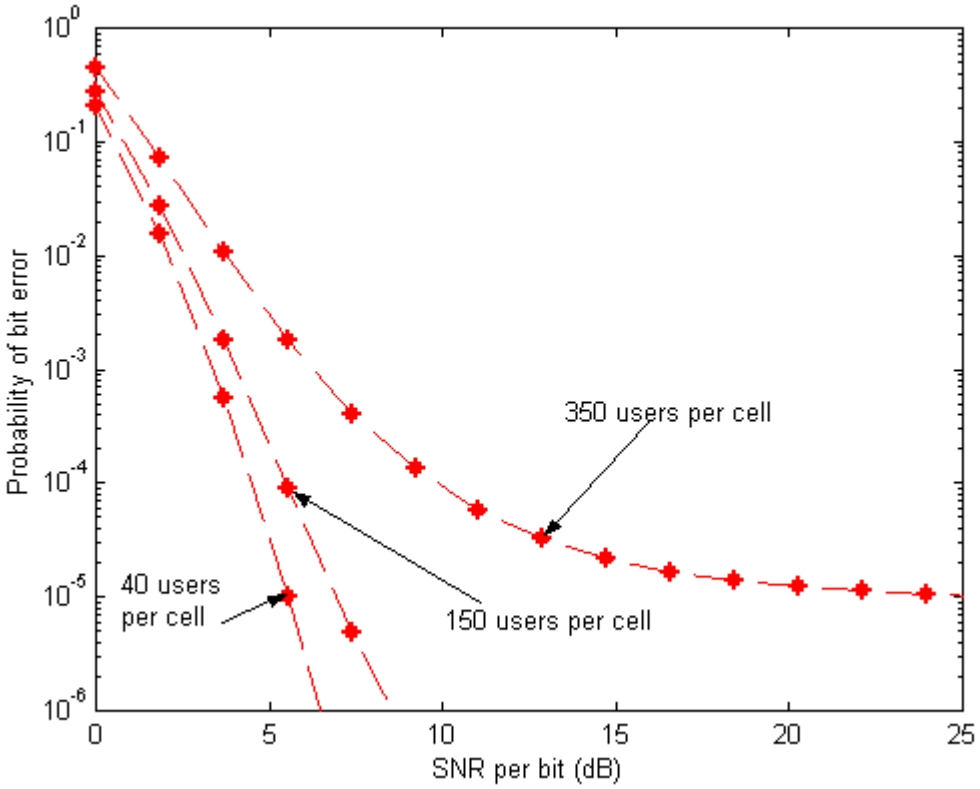

Figure 4.17. Probability of Bit Error for DS-CDMA with Nakagami Fading (m = 2) and Lognormal Shadowing $(\sigma_{dB} = 4)$ Applying Forward Power Control and Linear User Distribution with 60º Sectoring and FEC Using a Rate 1/2 Convolutional Encoder with v = 8.

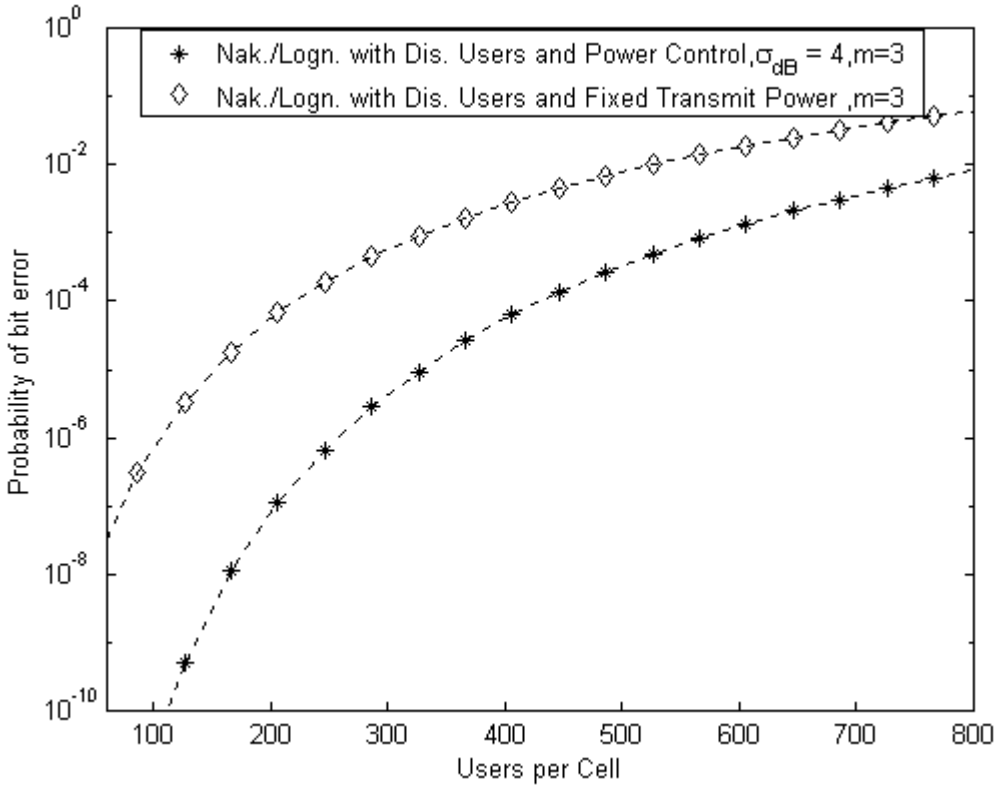

Figure 4.18. Probability of Bit Error for DS-CDMA with Nakagami Fading (m = 3) and Lognormal Shadowing $(\sigma_{dB} = 4)$ vs. Users per Cell Applying Forward Power Control and Linear User Distribution with 60º Sectoring and FEC $(R_{cc} = 1/2$ and $v = 8)$, $\overline{\gamma_b} = 12$ dB.

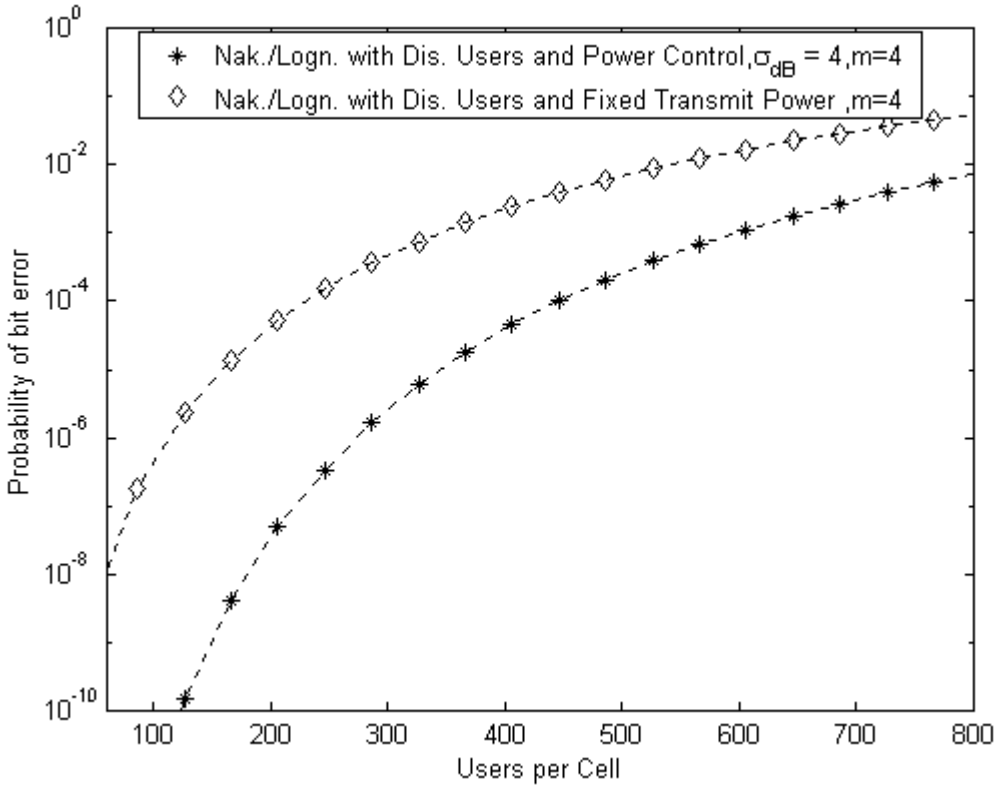

Figure 4.19. Probability of Bit Error for DS-CDMA with Nakagami Fading (m = 4) and Lognormal Shadowing $(\sigma_{dB} = 4)$ vs. Users per Cell Applying Forward Power Control and Linear User Distribution with 60º Sectoring and FEC $(R_{cc} = 1/2$ and $v = 8)$, $\overline{\gamma_b} = 12$ dB.

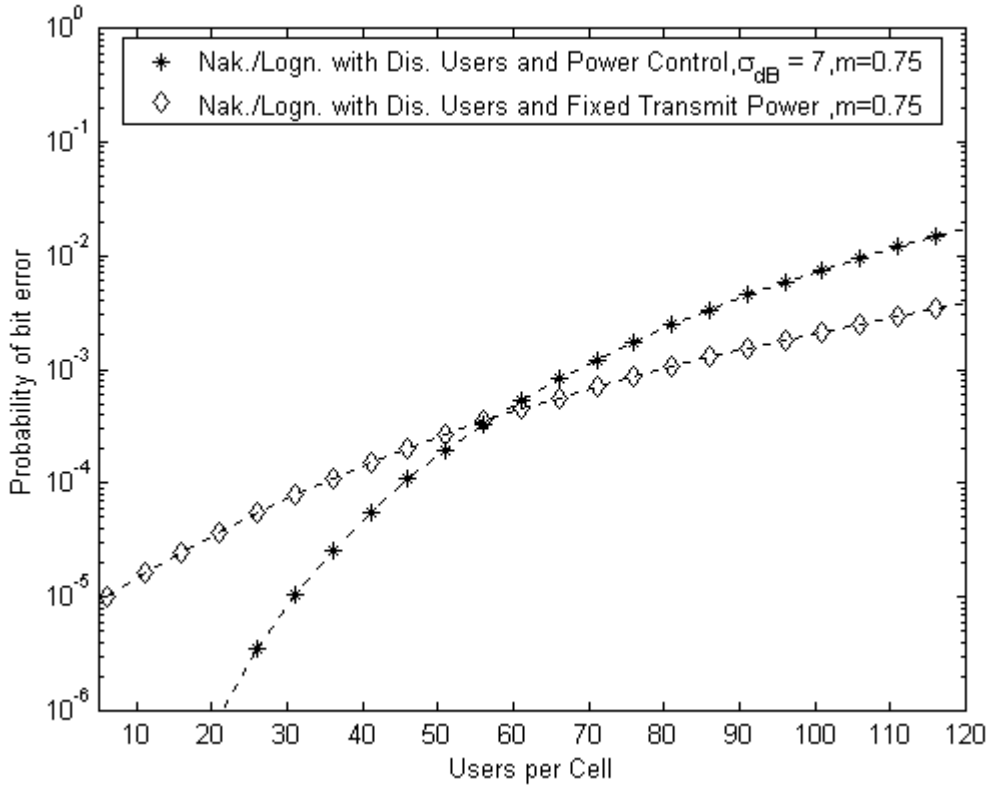

Figure 4.20. Probability of Bit Error for DS-CDMA with Nakagami Fading (m = 0.75) and Lognormal Shadowing $(\sigma_{dB} = 7)$ vs. Users per Cell Applying Forward Power Control and Linear User Distribution with 60º Sectoring and FEC $(R_{cc} = 1/2$ and $v = 8)$, $\overline{\gamma_b} = 15$ dB.

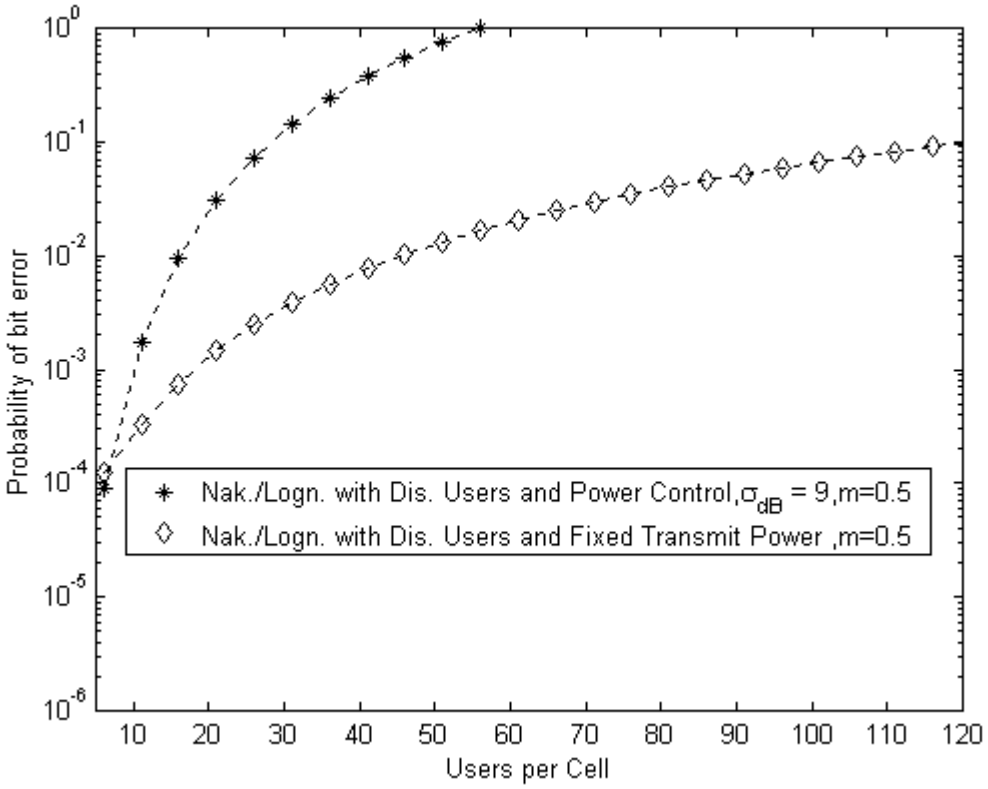

Figure 4.21. Probability of Bit Error for DS-CDMA with Nakagami Fading (m = 0.5) and Lognormal Shadowing $(\sigma_{dB} = 9)$ vs. Users per Cell Applying Forward Power Control and Linear User Distribution with 60º Sectoring and FEC $(R_{cc} = 1/2$ and $v = 8)$, $\overline{\gamma_b} = 20$ dB.

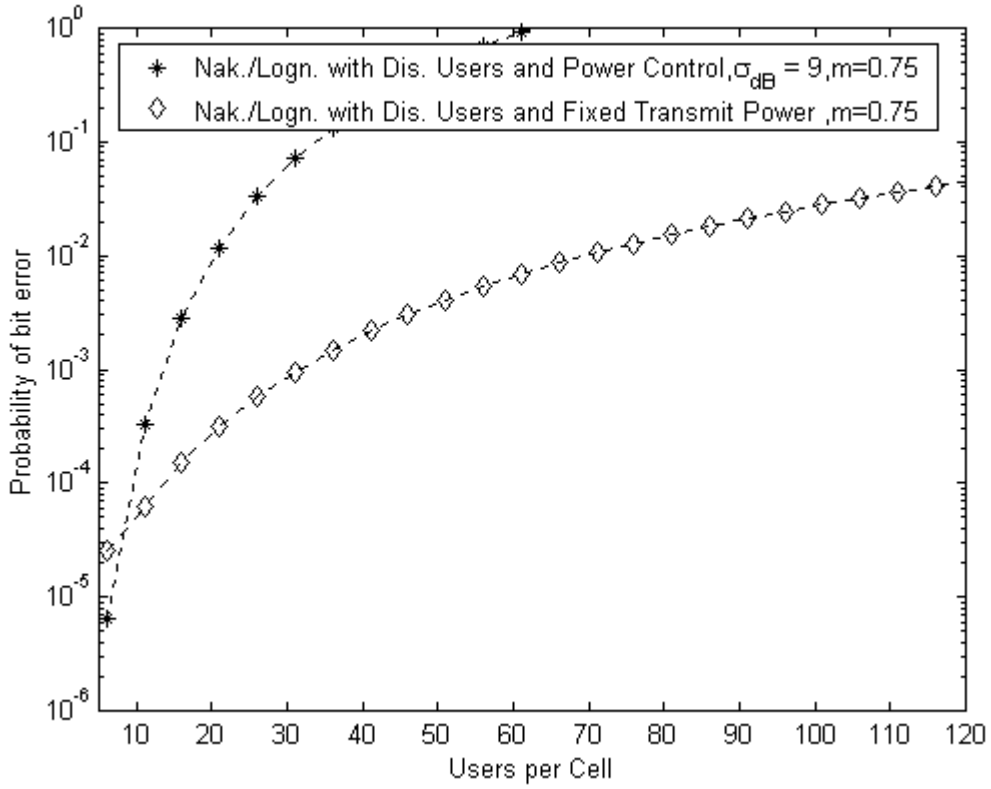

Figure 4.22. Probability of Bit Error for DS-CDMA with Nakagami Fading (m = 0.75) and Lognormal Shadowing $(\sigma_{dB} = 9)$ vs. Users per Cell Applying Forward Power Control and Linear User Distribution using with 60º Sectoring and FEC $(R_{cc} = 1/2$ and $v = 8)$, $\overline{\gamma_b} = 20$ dB.

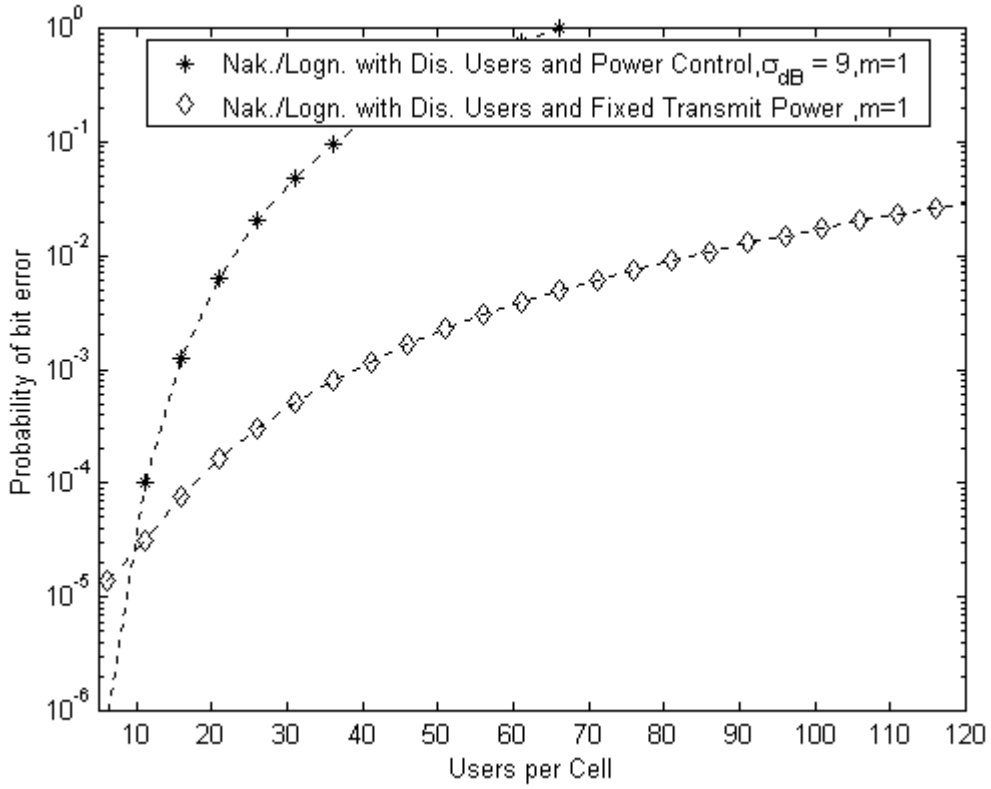

Figure 4.23. Probability of Bit Error for DS-CDMA with Nakagami Fading (m = 1) and Lognormal Shadowing $(\sigma_{dB} = 9)$ vs. Users per Cell Applying Forward Power Control and Linear User Distribution with 60º Sectoring and FEC $(R_{cc} = 1/2$ and $v = 8)$, $\overline{\gamma_b} = 20$ dB.

THIS PAGE INTENTIONALLY LEFT BLANK

V. CONCLUSIONS AND FUTURE WORK

In this thesis, it was possible to look at the performance on the forward channel of a six-sectored DS-CDMA cellular system with FEC operating in a Nakagami fading and lognormal shadowing environment. Attempts were made to enhance the performance of the system by using different techniques such as linear user distribution and power control.

A. CONCLUSIONS

In Chapter II, a forward channel for the DS-CDMA cellular system was created. By taking into account all the appropriate losses predicted by the extended Hata model and using Nakagami fading in order to include small-scale propagation effects, the model for the transmitted signal for the forward channel was built. Additionally, Lognormal Shadowing was incorporated. The result for a model that included all the aforementioned characteristics of the propagation channel was a closed formula, which describes the received signal to a mobile user's receiver.

In Chapter III, given the expression for the upper bound on the probability of bit error by using Forward Error Correction (FEC) in the form of convolutional encoding with soft-decision decoding, the performance of the cellular system was analyzed in two ways. A statistical model $\tilde{Z}_d$ was created in order to approximate the sum of d multiplicative Nakagami-square-Lognormal random variables as a multiplicative Nakagami-square-Lognormal random variable. By using this statistical model, it was possible to compute an upper bound of the probability of bit error in different fading environments varying the Nakagami-m parameter from 0.5 to 2. These results were compared with the Monte Carlo simulated results. This model was accurate in the SNR per bit range from $\overline{\gamma}_b = 10$ to 15 dB for all values of m. Specifically, the model was tested for $m = 0.5$, $m = 0.75$, $m = 1$, $m = 1.5$ and $m = 2$. These specific values of m vary the severity of the fading channel from one-sided Gaussian fading ($m = 0.5$) to Ricean fading ($m = 2$). The analysis in this chapter took into account the intended user was at the

worst-case position in the corner of the center cell. The model is a very helpful tool for system designers, which can be used quickly and effectively for analyzing the performance of DS-CDMA cellular systems operating in a Nakagami-Lognormal channel.

Also in this chapter, the decrease in the system's performance was mentioned when using three sectors instead of six, or the no sectoring case. Furthermore, the system's performance was examined with different values of users per adjacent cell and for Lognormal Shadowing 7 dB and 4 dB. The enhancement in the system's performance from 7 dB to 4 dB was very obvious. (Lightly shadowing environment.)

In Chapter IV, the performance analysis in Chapter III was modified by incorporating user distribution within the cell and assuming that the user's position is random following a specified distribution. Using a modified formula for the upper bound on the probability of bit error for the DS-CDMA cellular system with FEC in Nakagami-Lognormal channel in order to incorporate the user's distribution, the performance of the system was analyzed with the new assumption included. It is worth mentioning that in this specific case, the system performance was 3 to 4 dB better than predicted in Chapter III, the worst-case scenario, using the results predicted by the Monte Carlo simulations in both cases. Additionally, power control was implemented in the forward traffic channel in a way that each user received the same amount of power. That fact overcame the effects of Lognormal Shadowing and distance dependent path loss. Once again using Monte Carlo trials, it was discovered that by properly using the power control technique, the system performance was greatly improved. On the other hand however, system designers must be very careful when incorporating power control in the forward channel in order for the system to operate in the no interference limited region especially in heavy shadowing environments.

B. FUTURE WORK

It is possible to further analyze the performance of DS-CDMA cellular systems operating in a Nakagami fading and lognormal shadowing channel. For example, FEC

can be used with Serially Concatenated Convolutional Codes (SCCC), which is a more sophisticated type of coding in order to improve system performance.

Furthermore, an error at the pilot tone recovery can be introduced which may yield more realistic results. Additionally, in Chapter IV, different types of user distributions can be used which may produce better results.

Finally, a similar statistical model can be applied to the reverse channel of a DS-CDMA cellular system in a Nakagami fading and Lognormal Shadowing environment.

THIS PAGE INTENTIONALLY LEFT BLANK

LIST OF REFERENCES

[1] J. E. Tighe, "Modeling and Analysis of Cellular Forward System," Ph. D. Dissertation, Naval Postgraduate School, Monterey, California, March 2001.

[2] N. Panagopoulos, "Performance Analysis of Pilot-Aided Forward CDMA Cellular Channel," Thesis, Naval Postgraduate School, Monterey, California, September 2001.

[3] T. S. Rappaport, *Wireless Communications: Principles and Practice*, Upper Saddle River, New Jersey: Prentice Hall PTR, 1996.

[4] R. Janaswamy, *Radiowave Propagation and Smart Antennas for Wireless Communications*, Kluwer Academic Publishers, Boston, Dordrecht, London, 2001.

[5] J. S. Lee, L. E. Miller, *CDMA Systems Engineering Handbook*, Boston, London, Artech House, 1998.

[6] J. G. Proakis, *Digital Communications*, Boston, Massachusetts, WCB, McGraw-Hill, 1993.

[7] A. A. Abu-Dayya, N. C. Beaulieu, P. J. McLane "Comparison of Methods of Computing Lognormal Sum Distributions and Outages for Digital Wireless Applications," *IEEE International Conference in Conf. Rec. SUPERCOMM'94*, vol. 3, pp. 1270-1275, May 1994.

[8] P. Kontodios, "Performance Analysis of Noncoherent Binary Frequency Shift Keying Using Equal Gain Combining and Post Detection Selection Combining over a Nakagami Fading Channel," Thesis, Naval Postgraduate School, Monterey, California, September 1998.

[9] Thomas Eng and Laurence B. Milstein, "Coherent DS-CDMA Performance in Nakagami Multipath Fading," *IEEE Trans. Comm*., vol. 43, pp. 1134-1143, 1995.

THIS PAGE INTENTIONALLY LEFT BLANK

INITIAL DISTRIBUTION LIST

1. Defense Technical Information Center
   Ft. Belvoir, Virginia

2. Dudley Knox Library
   Naval Postgraduate School
   Monterey, California

3. Chairman, Department of Electrical of Computer Engineering
   Naval Postgraduate School
   Monterey, California

4. Chairman, Department of Information Sciences
   Naval Postgraduate School
   Monterey, California

5. Professor Tri T. Ha, Code EC/Ha
   Department of Electrical and Computer Engineering
   Naval Postgraduate School
   Monterey, California

6. CDR Jan E. Tighe
   Naval Information Warfare Activity
   Ft. Meade, Maryland

7. Professor David Jenn
   Department of Electrical and Computer Engineering
   Naval Postgraduate School
   Monterey, California

8. Professor Jovan Lebaric, Code EC/Lb
   Department of Electrical and Computer Engineering
   Naval Postgraduate School
   Monterey, California

9. Embassy of Greece, Naval Attaché
   Washington, DC

10. Ioannis Karagiannis
    Megistis 39 Kallithea,17673
    Athens, Greece